

**The Effect of Stress Reductions During Steady State Creep  
In High Purity Aluminum**

by

**Iris Ferreira**

**Doctor of Philosophy**

**University of Washington**

**1978**

The Effect of Stress Reductions During Steady State Creep  
In High Purity Aluminum

by

Iris Ferreira

A dissertation submitted in partial fulfillment  
of the requirements for the degree of

Doctor of Philosophy

University of Washington

1978

Approved by

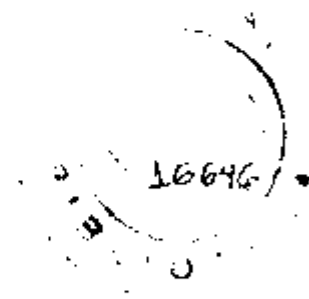
Robert G. Stang

Program Authorized  
to Offer Degree

Metallurgical Engineering

Date

November 28, 1978



Doctoral Dissertation

In presenting this dissertation in partial fulfillment of the requirements for the Doctoral degree at the University of Washington, I agree that the Library shall make its copies freely available for inspection. I further agree that extensive copying of this dissertation is allowable only for scholarly purposes. Requests for copying or reproduction of this dissertation may be referred to University Microfilms, 300 North Zeeb Road, Ann Arbor, Michigan 48106, to whom the author has granted "the right to reproduce and sell (a) copies of the manuscript in microform and/or (b) printed copies of the manuscript made from microform."

Signature

A handwritten signature in black ink, appearing to be "J. J. ...", written over a horizontal line.

Date

Dec. 28, 1978

#### ACKNOWLEDGMENTS

The author wishes to acknowledge the assistance of his many associates at the University of Washington and the staffs of the Departments of Mining, and Metallurgical and Ceramic Engineering.

The author is especially indebted to his advisor, Professor Robert G. Stang, for continued encouragement and invaluable guidance during all phases of this investigation. He also wishes to thank Professors Thomas G. Stoebe and Thomas F. Archbold for their interest and support during this investigation.

The author would especially like to thank his wife, Izis, for her help in preparing the first draft and, more importantly, for her untiring support and encouragement.

Finally, the author gratefully acknowledges the financial support of the Instituto de Energia Atomica and Fundacao de Amparo a Pesquisa do Estado de Sao Paulo, Brasil.

University of Washington

Abstract

THE EFFECT OF STRESS REDUCTIONS DURING STEADY STATE CREEP  
IN HIGH PURITY ALUMINUM

by Iris Ferreira

Chairman of Supervisory Committee: Dr. Robert G. Stang  
Assistant Professor  
Division of Metallurgical  
Engineering

The relationship between the strain-time behavior after stress reductions and accompanying changes in internal dislocation structure has been the subject of considerable discussion in recent literature. In an attempt to resolve this controversy, constant stress creep tests and stress reduction experiments were conducted in high purity aluminum at stresses between 3.44 MPa and 15 MPa and at test temperatures between 523K and 623K. All experiments were conducted in a region of stress and temperature in which creep deformation is believed to be due to the diffusion-controlled motion of dislocations. The stress sensitivity  $n$ , which describes the steady state creep rate, was found to be  $n = 4.6 \pm 0.2$ , and the activation energy for steady state creep  $Q = 1.43 \pm 0.05$  eV/at., in excellent agreement with data reported in the literature.

The transient creep behavior was analysed following reductions in stress performed at a true strain of 0.16, which is well into the steady state region. The transient creep curves obtained after the decrease in stress exhibit the following features:

- for strains smaller than  $4 \times 10^{-3}$ , the creep rate was positive

and decreased as a function of time. The corresponding time interval was called Stage I.

- for true strains greater than  $4 \times 10^{-3}$ , the creep rate was positive, but increased as a function of time to the steady state creep rate at the reduced stress. The corresponding time interval was called Stage II.
- incubation periods immediately after the stress reduction in which the creep rate is zero were not detected.

Microscopic observations of the sample microstructure, performed at several strains in the transient period (during Stages I and II), revealed that during Stage I, the dislocation density inside the subgrains is rapidly decreased. Also, during Stage I the subgrain size maintained a nearly constant value. Stage II is generally characterized by an increase in subgrain size.

Stress reduction experiments in which the stress was reduced from 8.35 MPa, 15 MPa and 6.23 MPa to 3.44 MPa at 573 K, with simultaneous observations of the subgrain size, showed that it is possible to correlate the instantaneous creep rate during Stage II to the square of the subgrain size present in the specimen.

The same analysis was made at a constant initial stress of 15 MPa and at reduced stresses of 8.35 MPa and 6.23 MPa. Using these data it was possible to express the instantaneous creep rate at constant subgrain size by a power function of the applied stress.

A phenomenological equation describing the steady state creep rate and the instantaneous creep rate during Stage II, involving the subgrain size, was developed, giving

$$\dot{\epsilon} = 1.1 \times 10^9 (D/b^2) (\lambda/b)^p (\sigma/E)^N.$$

where  $N$  and  $p$  satisfy the relation  $N - p = n$ , and  $n$  is the stress sensitivity coefficient of the steady state creep rate. Here  $p = 2$  and  $N = 6.6 \pm 0.2$ .

The theoretical background for the subgrain size dependence term,  $\lambda^2$ , and for the high stress sensitivity coefficient,  $N = 7$ , is discussed in terms of current theories. It is shown that the network recovery theory cannot explain the results obtained. The results are discussed in terms of the internal stress theory.

The activation energy determined for the processes responsible for Stages I and II is found to equal the activation energy for steady state creep. This suggests that the recovery processes following stress reductions are controlled by diffusion and have the same character as those responsible for steady state creep.

## TABLE OF CONTENTS

	<u>Page</u>
List of Figures .....	iv
List of Tables .....	ix
Chapter I: Introduction .....	1
Chapter II: Literature Survey .....	4
2.1 Introduction .....	4
2.2 Phenomenological Aspects of High Temperature Creep .....	4
2.2.1 Temperature Dependence .....	8
2.3 Microstructural Aspects of the Creep Process .....	17
2.4 Steady State Creep Theories .....	22
Chapter III: Experimental Procedures and Techniques .	39
3.1 Constant Stress Creep Apparatus .....	39
3.2 Specimen Preparation .....	41
3.3 Test Procedure .....	53
3.3.1 Determination of Effective Gage Length ...	53
3.4 Optical and Electron Microscopy .....	55
3.4.1 Dislocation Density Measurement.....	57
3.4.2 Subgrain Size Measurement .....	59
Chapter IV: Steady State Creep Behavior .....	60
4.1 Introduction .....	60
4.2 Results and Discussion.....	61
4.2.1 Strain - Time Data .....	61
4.2.2 Stress and Temperature Dependence of the Steady State Strain Rate .....	61
4.2.3 Stress Dependence of the Subgrain Size ...	71
4.3 Summary and Conclusions .....	77
Chapter V: Transient Creep Experiments .....	78
5.1 Introduction .....	78
5.2 Results and Discussion .....	78
5.3 Theoretical Analyses of the $\lambda^2$ and $\sigma^2$ Terms .....	100
5.4 Summary and Conclusions .....	104



TABLE OF CONTENTS

(Continued)

	<u>Page</u>
Chapter VI: Transient Creep - Incubation Period .....	107
6.1 Introduction .....	107
6.2 Results .....	108
6.2.1 Influence of Temperature and Stress .....	108
6.2.2 Recovery of the Transient Strain After Stress Reduction .....	115
6.2.3 Dislocation Density Measurements .....	120
6.3 Discussion .....	123
6.4 Summary and Conclusions .....	136
Chapter VII: Summary of Results and Conclusions .....	138
Chapter VIII: Suggestions for Further Work .....	140
Bibliography .....	141

LIST OF FIGURES

	<u>Page</u>
Figure 2.1 Schematic creep curve for constant stress and temperature showing the three stages of creep.	5
Figure 2.2 The relation between the activation energy for creep ( $Q_c$ ) and the activation energy for self diffusion ( $Q_{SD}$ ) for several pure metals near $0.5 T_m^{SD}$ (Sherby and Burke (1968)).	9
Figure 2.3 Steady-State creep rates of nominally pure fcc metals correlated by equation 2.9 (Ref. 22)	16
Figure 3.1 Schematic diagram of the load system employed a) Zero strain	40
Figure 3.1 (b) Strain $\epsilon$	41
Figure 3.2 Calibration curve of the load system of the creep machine for $W = 4.200$ Kg.	44
Figure 3.3 Schematic diagram of the grip assembly used.	45
Figure 3.4 Schematic diagram of the strain measuring device.	47
Figure 3.5 Circuit diagram of the power supply and rectifying circuit for the LVDT.	49
Figure 3.6 Circuit diagram for the automatic voltage step-backing circuit.	50
Figure 4.1 Typical creep curves at an applied stress of 15 MPa. The true strain is plotted versus fraction of time to fracture at 573 K.	62
Figure 4.2 The effect of stress on the steady state strain rate of 99.999% aluminum at 573K. The data of Ahlquist and Nix (122) at 573 K for 99.99% aluminum is shown for comparison.	65

	<u>Page</u>
Figure 4.3	68
The effect of temperature on the steady state creep rate of 99.999% aluminum tested at 6.23 MPa.	
Figure 4.4 (a)	73
Transmission electron micrograph of a sample deformed at 573 K and 9.01 MPa to a true strain of 0.16. An illustration of the typical subgrain structure observed. The sample was quenched to room temperature under load to maintain the high temperature structure. Magnification = 3500 X.	
Figure 4.4 (b)	74
Optical Micrograph obtained using polarized light for a sample deformed at 573 K and 9.01 MPa to a true strain of 0.16 and etched to reveal the subgrain structure (same specimen as Figure 4.4.(a)). Magnification = 210 X	
Figure 4.5	76
The variation of subgrain size in the steady state stage as a function of applied stress. The error bars shown for the data obtained in this study indicate 95% confidence limits.	
Figure 5.1	80
Typical transient creep curve obtained at 573 K after a stress reduction from 6.23 MPa to 3.44 MPa	
Figure 5.2	81
Strain-time curves illustrating typical behavior after stress reductions from 15 MPa, 8.35 MPa and 6.23 MPa to 3.44 MPa. The stress was reduced at a true strain of .16 in each case.	
Figure 5.3	82
The variation in strain rate as a function of time after a stress reduction for initial stresses of 15 MPa, 8.35 MPa and 6.23 MPa reduced to 3.44 MPa at a true strain of 0.16 in each case.	
Figure 5.4	83
Macrograph of the specimens at several stages of creep strain	
Figure 5.5	85
The variation of subgrain size as a function of time for initial stresses of 15 MPa, 8.35 MPa and 6.23 MPa reduced to 3.44 MPa at a true strain of 0.16. The error bars indicate 95% confidence limits.	

- Figure 5.6 Strain rate vs subgrain size for samples which have been subjected to a stress reduction from 15 MPa, 8.35 MPa and 6.23 MPa to 3.44 MPa and allowed to deform at the reduced stress for differing time intervals. The strain rate is measured just before the test is interrupted for subgrain size measurements. The data for a sample deformed well into the steady state region at 3.44 MPa and not subjected to a stress reduction is shown for comparison. 86
- Figure 5.7 Strain-time curves illustrating typical behavior after stress reduction for an initial stress of 15 MPa and reduced stresses of 8.35 MPa, 6.23 MPa and 3.44 MPa at 573 K. 91
- Figure 5.8 The variation of strain rate as a function of time after stress reduction for an initial stress of 15 MPa and reduced stresses of 8.35 MPa, 6.23 MPa and 3.44 MPa. 92
- Figure 5.9 (a) Optical micrographs of etched high purity aluminum deformed at 573 K and 15 MPa to a true strain of 0.16 at which the stress  
Magnification = 290 X 93
- Figure 5.9 (b) 28 minutes after the reduction in stress  
Magnification = 240 X 94
- Figure 5.9 (c) 55 minutes after the reduction in stress  
Magnification = 147 X 95
- Figure 5.10 The variation of the subgrain size as a function of time after stress reduction for an initial stress of 15 MPa reduced to 8.35 MPa, 6.23 MPa at a true strain of 0.16. The error bars indicate 95% confidence limits. 96

	<u>Page</u>
Figure 5.11	97
Strain rate vs subgrain size for samples which have been subjected to a stress reduction from a certain initial stress to a reduced stress and allowed to deform at the reduced stress for differing time intervals. The strain rate is measured just before the test is interrupted for subgrain size measurement.	
Figure 5.12	98
Creep strain rate vs the reduced stress at constant subgrain size $\lambda$ .	
Figure 6.1	109
Strain time curves illustrating the effect of temperature. The stress was reduced at a true strain of .16 in each case.	
Figure 6.2	112
The effect of temperature on the time $\theta$ required to reach the transient strain $\epsilon$ . The stress is reduced from 6.23 MPa to 3.44 MPa at a true strain of .16.	
Figure 6.3	113
Strain-time curves illustrating typical behavior after stress reductions from 15 MPa, 8.35 MPa and 6.23 MPa to 3.44 MPa. The stress was reduced at a true strain of .16 in each case.	
Figure 6.4	116
Strain-time curves illustrating typical behavior after stress reductions from 15 MPa to several reduced stresses.	
Figure 6.5	116
The variation of the interval of time $\Delta t$ involved in stage I, as a function of $(\sigma_I - \sigma_R)/G$ . ( $\sigma_I$ = initial stress, $\sigma_R$ = reduced stress, $G$ shear modulus)	
Figure 6.6	118
Examples of transient creep obtained on reloading, after steady state deformation at 8.35 MPa and at 5 min. and 8 hours at a reduced stress of 3.44 MPa.	
Figure 6.7	119
Transient strain recovered as a function of the time the specimen is allowed to recover at the reduced stress.	

	<u>Page</u>
Figure 6.8 Strain rate and dislocation density as a function of time after a stress reduction for initial stress of 8.35 MPa reduced to 3.44 MPa	122
Figure 6.9 (a) Schematic diagram showing the measurement of recovery time.	125
Figure 6.9 (b) Reproduction of chart trace showing effect of stress reduction for nickel 650°C; initial stress 10-.55 Kg/mm <sup>2</sup> ; stress reduction 0.45 Kg/mm <sup>2</sup> (88).	125
Figure 6.10 Schematic variation of the internal and effective stresses as a function of time after the stress reduction.	132

## CHAPTER I

### INTRODUCTION

The current energy shortage caused by depletion of world reserves of oil, natural gas and coal makes it imperative that we reduce our use of these increasingly valuable materials. Energy can be saved by improving the thermal efficiency of heat engines which consume these fuels. One apparently simple way to increase the efficiency of these devices is to increase the input temperature of the operating fluid. This creates a problem because increased operating temperatures generally reduce the strength of the materials used in these engines. This problem has not been completely solved by currently available high temperature technologies.

One of the most important problems to be solved in the development of high temperature technologies concerns the occurrence of time dependent plastic deformation, or creep. Creep occurs when working temperatures are greater than  $0.4 T_m$ , where  $T_m$  is the melting temperature in degrees K. An improvement of high temperature systems will certainly be obtained when a better understanding of the creep phenomena is achieved.

A general description of the creep process has been developed during the past fifty years. It is now generally accepted that creep deformation is due to thermally activated processes: motion of dislocations, grain boundary sliding or the diffusional transport of matter. Many theoretical models, either phenomenological in nature or based on dislocation theory have been proposed to explain the creep phenomena.

However, the suggested theories have not been completely successful for a number of reasons. Many of these reasons will be described in subsequent chapters but it is worth mentioning a few here to clarify the focal point of this study. Most of the theories are concerned with creep processes occurring at a constant rate of deformation, i.e., steady state creep. These theories neglect or fail to describe the transient deformation generally observed when a sample is initially loaded or when stress is changed. These theoretical descriptions of the creep process use very simple and idealized microstructural features (dislocation configurations) which bear little relationship to the true observed creep microstructures. Consequently, most creep theories can explain the available data only by making "ad hoc" assumptions not truly confirmed by experiments. One of the most important shortcomings of these theories, as will be shown, is the lack of consideration of the deformed structure which develops while the sample is being strained. For example, it is well established that subgrains are formed during high temperature deformation in a large number of materials and that their presence can influence a number of material properties. There seems to be no reason to justify the omission of this important microstructural feature in the description of the creep phenomena.

The influence of the subgrains on the creep phenomena is an area in which knowledge is lagging behind the general understanding of creep process. A study of this aspect of the creep process is urgently needed, and will certainly contribute to an improvement



in the comprehension of the high temperature mechanical properties of materials.

This dissertation is an attempt to define the influence of subgrains on the rate controlling creep mechanisms at high temperatures. Structural observations will be presented as a function of temperature, stress and strain to clarify the effects of subgrain size on the steady state creep and transient creep following reductions in stress. Substructural observations will be combined with information concerning the creep kinetics to test the possibility of expressing the steady state creep rate and the instantaneous creep rate following reductions in stress in terms of the subgrain size, as suggested by Sherby and coworkers (1,2,3). A significant aspect of this study is that the approach used, that is, to correlate the instantaneous creep rate following a reduction in stress with the subgrain size present in the sample, has not been used before.

High purity aluminum (99.999% Al) has been selected for this investigation. This choice is motivated by a large number of creep studies found in the literature for this material. In addition, reliable data for several physical quantities are available for aluminum. For example, the elastic modulus as a function of temperature has been determined by Fine (4) and the self-diffusion coefficient has been measured using various techniques (5,6). Also, high purity aluminum is available at low cost. Furthermore, because aluminum is a low melting point material and the surface oxide layer very strong, the proposed work can be done in air without a highly sophisticated apparatus.

## CHAPTER II

### LITERATURE SURVEY

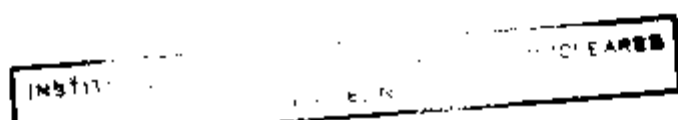
#### 2.1 Introduction

This investigation, as outlined in the previous chapter, is concerned with a study of high temperature creep deformation of high purity aluminum. This chapter will present a general review of the nature of high temperature creep. The objective of this literature review will be to provide the reader with background dealing with the experimental, structural and theoretical aspects of high temperature creep discussed in this study.

The review will be divided into three major sections. The first will be concerned with the phenomenological description of the process as influenced by stress, temperature and structural variables. The effort will focus on a description of the steady state strain rate of pure metals. In the second section, a general description of the important structural aspects of the creep process will be made. Finally, in the third section, several theoretical models which are important to this study will be described.

#### 2.2 Phenomenological aspects of high temperature creep

Time dependent deformation in many crystalline solids at elevated temperatures exhibits a rather consistent behavior. At temperatures exceeding approximately one-half the absolute melting temperature, the true strain-time relationship, shown in Figure 2.1, is generally observed for most well annealed pure materials tested at constant temperature and stress. When the load is applied, a strain



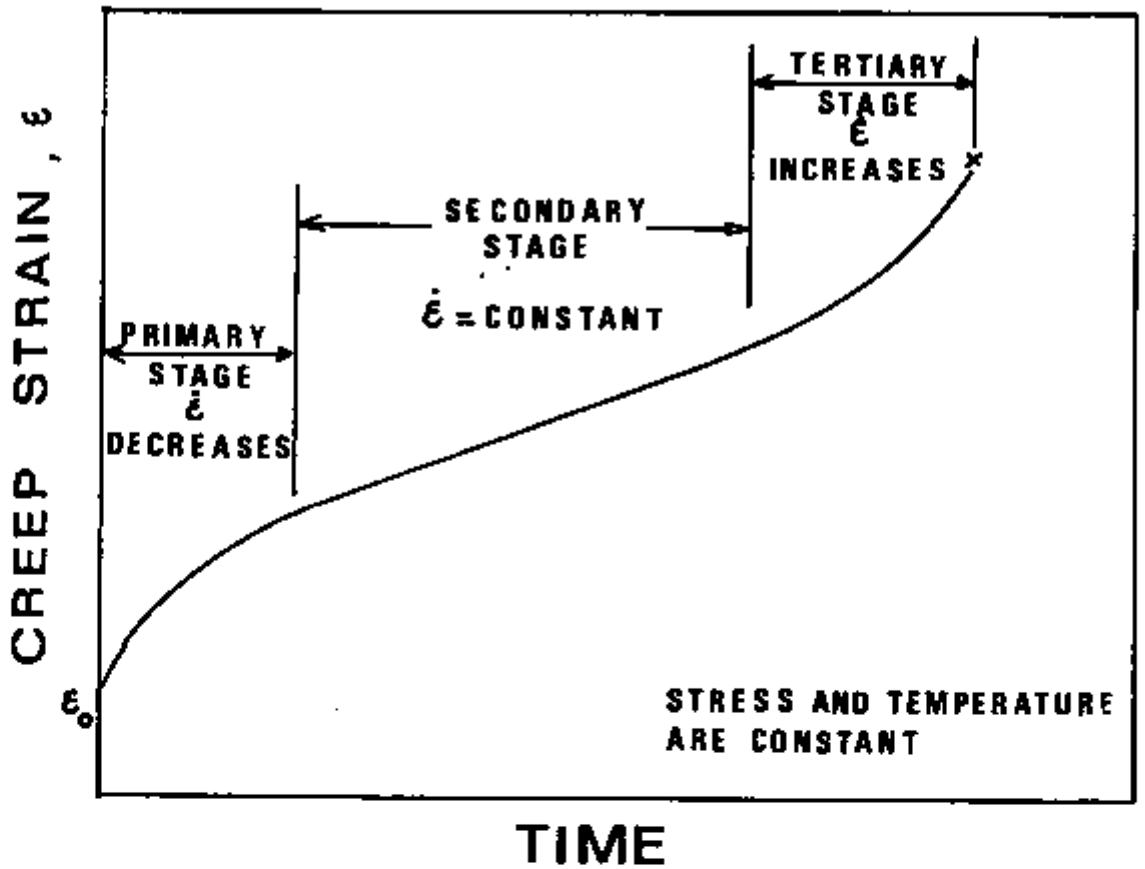


Figure 2.1 Schematic creep curve for constant stress and temperature showing the three stages of creep.

$\epsilon_0$  results. This strain  $\epsilon_0$  contains both elastic and instantaneous plastic components. As deformation proceeds, the strain rate decreases with time until a region in which the strain rate is constant is observed. The initial region in which the strain rate is decreasing is often called the primary region, while the region of constant strain rate is labeled the secondary or steady state region. The strain rate remains nearly constant in the steady state region until instabilities reduce the cross sectional area of the sample, leading to an increase in strain rate. In this third or tertiary stage, the strain rate increases until the sample fails.

There are many circumstances which lead to creep strain-time relationships which are different from that shown in Figure 2.1. Some materials do not exhibit a primary stage and steady state is attained immediately after application of a stress. This type of behavior has been observed for textured Fe-3% Si (7) and for W-5% Re alloys (8). Other materials present an inverted creep curve in which the creep rate increases during primary stage. This type of creep curve has been observed for h.c.p. single crystals (9,10) for Si (11), Cu-16% Al alloys (12), for LiF (13) and for materials subjected to a deformation prior to creep testing (14,15).

In general, the creep deformation rate  $\dot{\epsilon}$ , can be described by the relation (16):

$$\dot{\epsilon} = F(T, \sigma, \xi) \quad (2.1)$$

where  $\sigma$  is the applied stress,  $T$  is the absolute temperature and

$\xi$  describes several important material parameters. The variable  $\xi$  could include elastic modulus, crystal structure, stacking fault energy, as well as parameters which depend on the prior thermo-mechanical history of the material such as grain size, subgrain size and dislocation density. The variable  $\xi$  is generally a mild function of temperature and stress. At constant temperature and applied stress, the transient stage is associated with time dependent structural modifications, that is,  $\xi = \xi(\sigma, T, t)$  where  $t$  is time. The structure evolves until a dynamic structural equilibrium is reached leading to steady state creep. During the steady state stage, the creep rate  $\dot{\epsilon}_s$  is described by the equation

$$\dot{\epsilon}_s = F(T, \sigma, \xi_s) \quad (2.2)$$

where  $\xi_s$  characterizes the internal structure under dynamic equilibrium.

The stress, temperature and structural dependence of the creep strain rate is basic to an understanding of the creep phenomena. In the following sections, an effort will be made to demonstrate the functional contributions of each variable in equation 2.2 to the creep rate.

### 2.2.1 Temperature Dependence

The deformation behavior of metals and alloys under constant load or stress is usually separated into low- and high-temperature regions. The temperature at which the change from low to high temperature behavior occurs is generally around one-half of the melting temperature,  $0.5 T_m$  (17). For both low and high temperature regions it is found experimentally for constant stress conditions that Equation 2.2. can be written

$$\dot{\epsilon}_s \Big|_{\sigma} = K_1 \exp\left(-\frac{Q_c}{kT}\right) \quad (2.3)$$

where  $Q_c$  is the effective activation energy for creep,  $k$  is Boltzmann's constant and  $K_1$  is a slightly temperature dependent quantity. For temperatures less than  $0.5 T_m$  the activation energy decreases with temperature and is also stress dependent. The creep deformation mechanisms in this region of temperature are believed to be associated with cross slip of screw dislocations and dislocation intersection processes. This discussion will neglect the region of temperature below  $0.5 T_m$  and will focus only on the creep phenomena occurring at temperatures higher than  $0.5 T_m$ . For temperatures above  $0.5 T_m$  the activation energy does not vary with stress and is slightly temperature dependent. For temperatures near  $0.5 T_m$  good agreement between the activation energy for steady state creep and that for self diffusion,  $Q_{sd}$ , has been shown to exist for many pure metals (18). This agreement can be seen in Figure 2.2. The correspondence between these two quantities has most clearly been demonstrated in

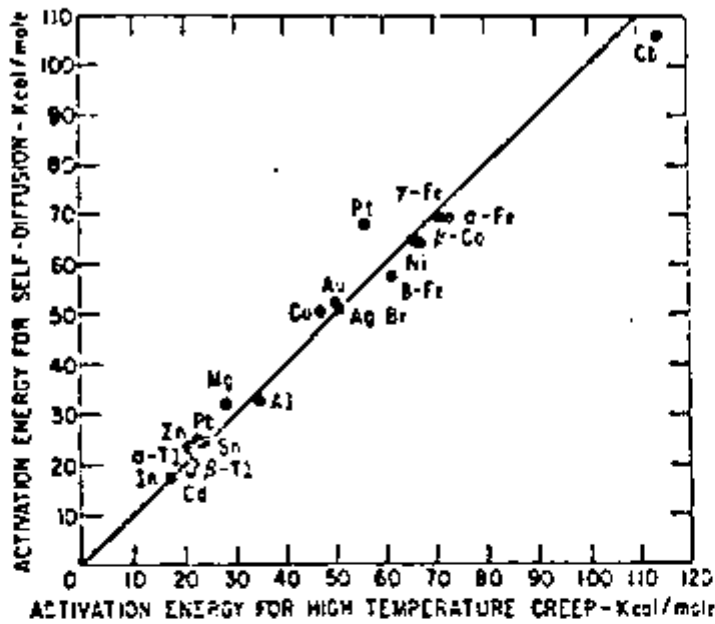


Figure 2.2 The relation between the activation energy for creep ( $Q_C$ ) and the activation energy for self diffusion ( $Q_{SD}$ ) for several pure metals near  $0.5 T_m$  (Sherby and Burke (1968)) (18).

the case of phase transitions. Sherby and Burke (18) describe a number of cases where creep rates and diffusion coefficients were measured above and below a phase transition. Parallel behavior between the strain rate and the diffusion coefficient was observed for the transitions such as the  $\alpha + \gamma$  transition in iron,  $\alpha + \beta$  in thallium, and the ferro-paramagnetic transition in  $\alpha$ Fe. In addition, Sherby et al. (19) obtained good agreement between the activation volumes  $\Delta V_c$  and  $\Delta V_{sd}$  for creep and diffusion under hydrostatic pressure, when these two quantities were measured in the same material. Based on the correlation between  $Q_c$  and  $Q_{sd}$  it is usual to rewrite Equation 2.3 in terms of the diffusion coefficient  $D$ , thus

$$\dot{\epsilon}_s|_{\sigma} = K_2 D \quad (2.4)$$

where  $D = D_0 \exp(-Q_{sd}/kT)$  and  $K_2$  is a slightly temperature dependent quantity.

### 2.2.2 Stress Dependence

The relation between the steady state creep rate of metals at constant temperature and the applied stress,  $\sigma$ , generally assumes one of two forms depending on the magnitude of the applied stress. At low and intermediate stresses,  $\sigma/G \leq 10^{-3}$ , where  $G$  is the shear modulus, this relation is given by

$$\dot{\epsilon}_s|_T = K_3 \sigma^n \quad (2.5)$$



where  $K_3$  is a constant. In general, the exponent  $n$  is constant over a wide range of stress and temperature. For fine grained materials tested at temperatures close to the melting point ( $T > 0.9 T_m$ ) and at low applied stresses,  $n$  is usually found to equal 1. This type of creep is generally referred to as Nabarro-Herring creep (20,21) and will not be the subject of further discussion in this study. At intermediate stresses,  $10^{-5} < \sigma/G < 10^{-3}$ , and at temperatures  $0.5 < T/T_m < 0.9$ ,  $n$  assumes values between 3 and 7 for many solid solution alloys and pure metals. In general, a value of  $n$  in the range  $4.2 < n < 6.9$  is found for most pure metals. This result suggests an average value of  $n = 5$  (22). At high stresses the power relationship in equation 2.5 breaks down. Creep rates for these high stresses are greater than those predicted by extrapolation of the intermediate stress data.

Empirical relations have been proposed to describe the behavior of the steady state creep strain rate at high stresses. Zurkov and Sanfirova (23) suggested an expression of the form

$$\dot{\epsilon}_s = A \exp(\beta \sigma) \quad (2.6)$$

where  $A$  contains the temperature dependence and  $\beta$  is a quantity not depending on  $\sigma$  but is a function of  $T$  and structural variables.

Garofalo (24) proposed an empirical relation of the form

$$\dot{\epsilon}_s = K_4 \sinh(\beta \sigma)^n \quad (2.7)$$

which breaks down to

$$\dot{\epsilon}_s = K_5 \sigma^n$$

at low stresses, and becomes

$$\dot{\epsilon}_s = K_6 \exp(\beta \sigma)$$

at high stresses, which is a form similar to that proposed by Zurkova and Sanfirova. Similar expressions have been suggested by Weertman (25) and by Barrett and Nix (26).

The incorporation of terms describing structural variables has been a very difficult task. The fact that  $\xi$  in Equation 2.1 depends on  $T$  and  $\sigma$  introduces an additional complication when a separation of variables is attempted. The following discussion will show that a definitive description has not been achieved yet.

Among the various variables included in  $\xi$ , known for its important influence on the steady state creep rate, is the modulus of elasticity. Phenomenologically, it has been shown (27) that the steady state creep rate of pure polycrystalline metals can be represented by

$$\dot{\epsilon}_s = K_7 (\sigma/G)^n \quad (2.8)$$

where  $K_7$  is a quantity which includes the temperature dependence,  $G$  is the shear modulus and  $\sigma$  and  $n$  have the previously cited meaning.

The influence of the grain size on the steady state creep rate has been the subject of a serious controversy. Early investigations of this aspect of the creep phenomena led to inconclusive results; while some data suggested that the creep rate decreased when the grain size was increased, others indicated the opposite behavior. Bird et al. (22) showed, using recent data, that the creep rate is influenced by the grain size only below a certain critical size. Above this critical size, for some pure metals, the steady state creep rates obtained for single crystals are nearly equal those obtained for polycrystals in a wide range of grain sizes. They suggested that the increasing creep rate obtained for grain sizes smaller than the critical size could be due to an increasing contribution of grain boundary sliding to the over all creep deformation at very small grain sizes.

The general aspects of the creep process briefly described above were reviewed in great detail by Sherby and Burke (18) in 1968, later by Bird et al. (22) (1969) and most recently by Takeuchi and Argon (28) (1976). Bird et al. (22) have shown that much of the steady state creep data available in the literature can be described by an expression of the form:

$$\dot{\epsilon}_s = A_0 \frac{Gb}{kT} (\sigma/G)^n D \quad (2.9)$$

where  $G$  is the shear modulus,  $b$  is the Burgers' vector,  $D = D_0 \exp(-H_{sd}/kT)$  is the diffusion coefficient,  $H_{sd}$  is the enthalpy of diffusion,  $D_0$  is a quantity related to the crystal structure and

the atomic frequency, and  $A_0$  and  $n$  are dimensionless quantities. Because of the inclusion of  $G$  and  $T$  in Equation 2.9, the apparent activation energy for creep is always slightly different from the activation enthalpy of diffusion. It is possible to circumvent this problem by defining an activation enthalpy for creep, which is not temperature dependent according to the equation (29)

$$\dot{\epsilon}_s = K \frac{G}{T} (\sigma/G)^n \exp(-H_c/kT) \quad (2.10)$$

where  $K$  is a constant and  $H_c$  is the enthalpy for creep.

Bird et al. (22) examined the data for several metals to determine the value of the constants  $A_0$  and  $n$  in Equation 2.9. The extent of these values, obtained for various metals, is listed in Table 2.1.

TABLE 2.1\*

Summary of Values of the Parameters  $n$  and  $A_0$ .

<u>Material</u>	<u>n</u>		<u><math>A_0</math></u>	
fcc	4.4 - 5.3	(5)	$10^5 - 10^8$	$(10^7)$
bcc	4.0 - 7.0	(5)	$10^5 - 10^{15}$	$(10^9)$
hcp	4.0 - 6.0	(5)	$10^3 - 10^8$	$(10^6)$
Class II alloys	4.5 - 6.0	(5)	$10^5 - 10^9$	$(10^6)$
Class I alloys	3.0 - 4.0	(3.5)	$10^{-2} - 10^4$	(10)

\*typical values are shown in parentheses

As an illustration of how structural variables, included in  $\xi$ , might affect the steady state strain rate equation, consider the following. In Figure 2.3, the correlation with Equation 2.9 is shown for fcc metals. If all the factors that are pertinent to steady state creep were correctly incorporated in Equation 2.9, the reliable reported data in fcc metals should be packed around a single straight line, within the accuracy of  $\sigma$ ,  $T$ ,  $D$  and  $G$ . Figure 2.3 clearly shows that such a correlation is not obtained. This implies that other factors that are important in the creep process have not been included in Equation 2.9. For fcc metals, it has been suggested that the major influence could come from the effects of stacking fault energy  $\gamma$ . Barrett and Sherby (30) suggested that the constant  $A$  in Equation 2.9 should be dependent on  $\gamma$ . This approach assumes  $n$  to be the same constant for all pure metals. An alternative possibility was considered by Bird et al. (22), in which  $A_0$  was assumed to be an universal constant and the remaining parameter,  $n$ , was assumed to be dependent on the dimensionless quantity  $Gb/\gamma$ . They, in fact, have shown that when an appropriate value of  $n$  for each metal is selected from a  $n$  vs  $\gamma$  diagram, all the creep data are well represented within a factor of two by setting the constant  $A_0 = 2.5 \times 10^6$ .

The approach used by Bird et al. (22) has an important limitation; it is restricted mainly to pure metals and simple alloys. No effort was made to include creep data of more widely used alloys. In a series of recent papers (31,32,33) Wilshire and his colleagues presented a new effort to solve this aspect of the creep phenomena. They introduced the idea of a "friction stress",  $\sigma_0$ , to characterize

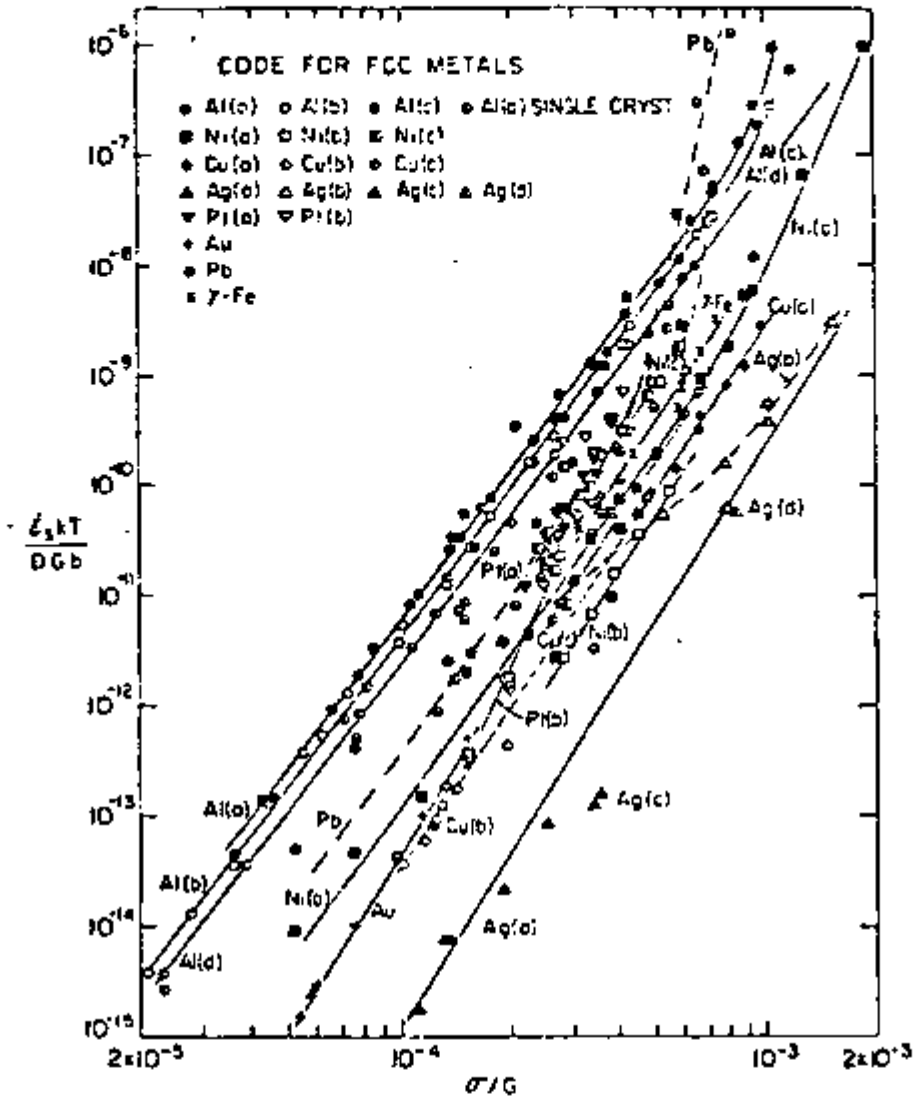


Figure 2.3 Steady-State creep rates of nominally pure fcc metals correlated by equation 2.9 (Ref. 22)

the steady state creep substructure. By incorporating this concept into the normal power law creep expression, Equation 2.5, where the stress exponent may vary from 4, for pure metals, to values ~40, for certain dispersion strengthened alloys, the steady state creep rate may be expressed by a relationship

$$\dot{\epsilon}_s = B'(\sigma - \sigma_0)^4 \quad (2.11)$$

where  $B'$  is a temperature dependent quantity. In this way the stress exponent,  $n$ , which may be both large and variable, is replaced by a universal exponent of 4. This approach, however, has been strongly criticized (34,35).

### 2.3 Microstructural Aspects of the Creep Process

The experimental evidence now shows that the decrease in creep rate during the primary stage reflects microstructural changes in the material (22,28,36). Barrett et al. (37) showed that load application causes a large increase in dislocation density. Later in the primary region, subgrains start to form. At this point, the dislocation density must be described by two quantities, the dislocation density in the subgrain wall and the dislocation density which is not associated with subgrain boundaries, sometimes called free dislocation density. As deformation proceeds, the free dislocation density and average subgrain size change continuously until steady state creep is attained. In the steady state region, both quantities maintain nearly constant values (22,28,36).

In 1935 Jenkins and Mellor (38) were the first to observe the development of subgrains after high temperature deformation of iron. They referred to these changes as subcrystallization or grain fragmentation. In the early fifties, after the work of Wood and his colleagues on aluminum (39,40,41), an explanation for the process was proposed. They suggested that these subgrains were due to accumulation of edge dislocations by climb (polygonization) leading to the development of low angle boundaries. Since then, the terms "subgrain" and "substructure" have gained wide acceptance.

Subgrains have been observed to form in most single crystalline as well as polycrystalline pure metals (22). In the alloy Fe-4% Mo (42), which exhibits steady state creep behavior virtually immediately after application of a stress, subgrains have also been observed. However, a W-5% Re (8) alloy and Al-3.1% Mg (43) which also exhibit this behavior, do not form a subgrain structure.

If the grain size of the test specimen is large, the initial formation of the subgrains may begin near the grain boundaries (44) and if the material is heavily textured, it is usually confined to such regions and is not extensive (7).

Subgrain boundaries in polycrystals after high temperature creep are composed of two and three dimensional networks consisting of complex mixtures of tilt and twist components (22,45,46,47). In an investigation of the creep of molybdenum single crystals, Clauer, Wilcox and Hirth (46) demonstrated that tilt boundaries predominate, suggesting a climb-polygonization mechanism in that material.



The subgrain size has been observed to be independent of grain size by a number of investigators (47,48,49). The nature of the total substructure may, however, be dependent on the grain size. For example, Barrett, Nix and Sherby (37) found equiaxed substructures in small grain-size (50 micrometers) Fe-3% Si and banded substructures in large grain-size material (0.3 mm), tested at the same temperature and stress.

It is believed that the rate at which subgrains form during creep is dependent upon the relative ease of the processes of cross slip and dislocation climb (50). The ease of these processes depends strongly on the distance between partial dislocations, that is, the stacking fault energy. As the stacking fault energy  $\gamma$  is lowered, the separation between partials increases and cross slip and dislocation climb become more difficult. This conception is based on experimental evidence that metals with high stacking fault energy ( $\gamma \sim 150 \text{ ergs/cm}^2$ ) such as Al,  $\alpha$ -Fe, Mg, Sn, Ta and Mo show pronounced tendencies for subgrain formation (17,46,51,52,53). Copper, a metal of intermediate stacking fault energy ( $\gamma \sim 80 \text{ ergs/cm}^2$ ), exhibits a low tendency toward a subgrain formation (54), and Pb, which has a low stacking fault energy ( $\gamma \sim 25 \text{ ergs/cm}^2$ ) does not seem to form subgrains (55).

The character of the subboundary also seems to depend on the stacking fault energy. Metals with high stacking fault energy form subgrains with well defined subboundaries consisting of planar arrays of dislocation networks (46,47,56). Copper forms rather diffuse

subboundaries consisting of complex dislocation tangles (57,58) at normal strain rates but can form well-defined subgrain boundaries when the rate of deformation is very low (59).

The subgrain size  $\lambda$ , which develops early in the steady state region has been measured as a function of stress (37,47,60-64), temperature (47,63,64) and strain (37,63,65). These observations showed that  $\lambda$  is a function of stress and is only slightly temperature dependent. In addition, these observations have also shown that the stress dependence of  $\lambda$  is invariant over a large range of stress and can be expressed by

$$\lambda = B \sigma^{-m} \quad (2.12)$$

where  $B$  and  $m$  are constants (18,22). The value of  $m$  is usually of the order of unity; other values have been also reported (63,66,67). Young and Sherby (68) and Sikka et al. (69) have shown that the stress dependence is modified above a critical value of the stress, changing from  $m = 1$  to  $m = 2$  dependence. They have also noted that at these stress levels, the subgrain boundaries are characterized by dislocation cell boundaries.

The dislocation density inside subgrains at steady state,  $\rho_s$ , has been correlated with the applied stress for many materials. It has been shown that the dislocation density is stress dependent and can be expressed by (22):

$$\rho_s = (\tau/a_1 G b)^2 \quad (2.13)$$

where  $\tau$  is the shear stress,  $\tau = G/2$ ,  $\alpha_1$  is a constant of the order of unity, and  $b$  and  $G$  have the previously cited meanings.

The general features of the process of substructure development during transient creep at temperatures above  $0.5 T_m$  can be summarized (28) as:

1. After the instantaneous deformation, the dislocation structure is essentially the same as in low temperature deformation;
2. The dislocation structure at the beginning of the primary stage is quite heterogeneous. As the strain increases, subgrains start to form in a non-homogeneous fashion; regions with dense parallel subgrains and regions with coarse subgrains or totally depleted of subgrain boundaries are distributed alternately;
3. The dense substructure region gradually becomes coarser and simultaneously the coarser region denser, leading finally to a homogeneous substructure at the steady state. At this point, the total dislocation density is made up of dislocations in the subgrain boundaries and dislocations inside the subgrains.

It has to be noted that the steady state creep substructure is steady only in a time average. In fact, it is continuously changing and corresponds to a dynamic equilibrium between the rate of formation of new subgrains and the rate of decomposition of the old ones (16,28,70).

During creep of polycrystalline metals at elevated temperature, deformation may also occur by the relative translation or shear of

one grain with respect to another. This aspect of the creep process is usually referred to as grain boundary sliding. Quantitative measurements of grain boundary sliding in a number of polycrystalline metals and alloys are now available (52,71-75). McLean and Farmer (52) have shown that the average grain boundary displacement in aluminum is directly proportional to the total elongation of the specimen. The proportionality constant is strongly dependent on the applied stress and to a much less extent on temperature and impurity concentration. Gifkins (76) has tabulated values of the proportionality constant for various metals and alloys and found that values range from 0.027 to 0.93 depending on the material and test conditions. In general, the proportionality constant decreases sharply with stress for a large number of pure metals and alloys. Tests in which the stress was maintained constant showed that the contribution of grain boundary sliding to the total strain is decreased as the grain size is increased and does not depend on temperature (76).

#### 2.4 Steady State Creep Theories

The attempts to describe the creep phenomenology in terms of microscopic processes are numerous. Bailey and Orowan (77,78) were the first to view creep as a competition between two processes: strain-hardening and recovery. A consequence of this point of view is that steady state creep represents a state in which strain-hardening is dynamically balanced by recovery. Later, after dislocation

theory was developed, these concepts were incorporated to form several creep models. It is important to note that a link between these different approaches exists if dislocation multiplication, glide and interaction are regarded as hardening processes, and climb and annihilation are regarded as recovery processes.

The theoretical models for creep are currently divided into three main groups: the first includes theories based on a mechanism which assumes that the creep rate is controlled by recovery (climb and/or annihilation); a second group of theories is based on the assumption that dislocation glide is the rate controlling mechanism; and finally a group of theories in which the simultaneous effects of dislocation glide, driven by the effective stress, and recovery, driven by the internal stress, are assumed to be the rate controlling mechanisms. A general discussion of these theories follows.

Weertman (25,79) has developed an expression for the steady state creep rate at intermediate stresses based on a dislocation mechanism. In both of his theories he assumes that dislocation loops are generated at Frank-Reed (F-R) sources and these loops pile up against obstacles in the lattice. In his first theory (1955) he assumes that Lomer-Cottrell locks are obstacles and in the 1957 theory the obstacles are believed to be the stress fields due to the edge components of the leading loops on parallel slip planes. The pile up generates back stresses which stop the F-R sources. The leading dislocation must then climb the obstacle to relieve the back stress on the source and, in doing so, it absorbs or emits vacancies.

A gradient of vacancies is established. The creep rate is then controlled by the escape rate of the leading dislocation by means of diffusion of vacancies to or away from the dislocation pile up at the obstacles. Later, in 1968, Weertman (80) improved this theory by using a model developed by Hazzledine (81). Hazzledine proposes that as groups of dislocations, created at two sources on neighboring slip planes, move toward one another they will become interlaced into groups of dislocation dipoles. The resulting equation obtained by Weertman after this procedure is

$$\dot{\epsilon}_s = \frac{\alpha DG \Omega}{b^{3.5} M^{0.5} kT} (\sigma/G)^{4.5} \quad (2.14)$$

where M is the number of active dislocation sources per unit of volume, G is the shear modulus,  $\Omega$  is the atomic volume and  $\alpha$  is a constant whose value is in the range  $0.015 < \alpha < 0.33$ .

This model is successful in predicting the stress exponent for the power law. However, this is only so if it is assumed that M is independent of stress. This aspect of the model has been criticized by Bird et al. (22). These authors pointed out that dislocation pile-ups are not observed in creep tested materials.

A different model, based on climb of dislocations as the rate controlling mechanism, has been proposed by Nabarro (82). He assumed a special type of regular array of edge dislocations; the creep rate has been calculated by assuming a steady climb motion of these dislocations and by neglecting any glide. A third power dependence of the creep rate on stress is obtained in this formulation. This

model has been modified by Weertman (80) by introducing a different expression for the climb velocity of dislocations. Dupouy (83) modified the theory, taking the effect of internal stress into consideration, and has shown that the stress exponent can be very large.

Recently, interest has focused on a somewhat different dislocation climb model of creep proposed by Ivanov and Yanushkevich (84). In this model the subgrain boundary is assumed to act as a site at which dislocations annihilate. Isolated dislocations or groups of piled-up dislocations that may have been created at sources inside the subgrain, or at other subgrain boundaries, approach the subgrain boundary and interaction occurs. If the approaching dislocation has the same character as those forming the boundary, it will climb to one of the nearest dislocations in the subgrain boundary. Otherwise, if it is opposite in character, annihilation will occur after climbing. This model yields an equation for the steady state creep rate of the form

$$\dot{\epsilon}_s = \frac{\alpha_1 D G \Omega}{b^3 k T} (\sigma/G)^3 \quad (2.15)$$

where  $\alpha_1$  is a dimensionless constant,  $\alpha_1 \approx 0.5$ , and the other terms have the usual meaning.

A modification of the Ivanov and Yanushkevich theory by Blum (85) yields a stress dependence of 4. This is based on additional assumptions that the subgrain walls have finite width and this width is not stress dependent. The final expression obtained in this approach is

$$\dot{\epsilon}_s = \frac{\alpha_2 D G \Omega}{k T} (\sigma/G)^4 \quad (2.16)$$

where  $\alpha_2$  is a dimensionless constant,  $\alpha_2 = \alpha_1$ , and  $a$  is the subgrain wall thickness. The remarkable aspect of the subgrain recovery model is that the subgrain size included in the theory drops out of the final expression. Weertman (86) has extended the models described above to allow for interactions of dislocation pile-ups with the subgrain boundaries. The model gives a final expression for the creep strain rate

$$\dot{\epsilon}_s = \alpha \left(\frac{D}{b}\right)^2 \left(\frac{\lambda}{b}\right)^3 \left(\frac{\sigma}{G}\right)^6 \left(\frac{G\Omega}{kT}\right) \quad (2.17)$$

where  $\lambda$  is the subgrain size and  $\alpha$  is a constant. When the stress dependence of the subgrain size during steady state,  $\lambda \propto \sigma^{-1}$ , is included in Equation 2.17, a third power stress dependence is again obtained.

Exell and Warrington (87) suggested a model in which dislocation annihilation occurs by the meeting of migrating subgrain boundaries containing dislocations of opposite sign, after observing subgrain boundary migration during steady state deformation. A quantitative estimate of the contribution of this mechanism to recovery has not yet been made.

Another group of recovery theories are based on the strain-hardening-recovery mechanism proposed by Bailey and Orowan (77,78). In these lines are the models proposed by Mitra and McLean (88), McLean



(89), Davies and Wilshire (90) and Lagneborg (36). In agreement with direct observations, these authors assume the dislocations inside the subgrains to be arranged in a three dimensional network. The creep process is treated as consisting of consecutive events of recovery and strain hardening. The strength is provided by the attractive and repulsive junctions of the network. Some of these junctions will break as a result of thermal fluctuations; those connected with the longest dislocations break more frequently. The released dislocations move a certain distance until they are held up by the network and thereby give rise to a strain increment and the material strain hardens. Simultaneously, recovery of the dislocation network takes place. The model assumes that recovery occurs by a gradual growth of the larger meshes and the shrinkage of the smaller ones, in analogy with grain growth. The driving force for dislocation motion in the recovery process is due to the line tension of the curved dislocation mesh. This recovery process tends to increase the average mesh size of the network, that is, to decrease the dislocation density. Eventually some links will be sufficiently long for their junction to break under the influence of the thermal fluctuations and of the applied stress, and the consecutive events of recovery and strain hardening can repeat themselves. The treatment by Lagneborg (36) makes use of the following equations for the transient stage:

$$\dot{\epsilon}(t) = \dot{\epsilon}_0 \exp \left\{ -\frac{bA[\alpha Gb \rho(t)]^{1/2} - \sigma}{kT} \right\} \quad (2.18)$$

and

$$\frac{d\rho}{dt} = \frac{1}{bL} \frac{d\epsilon(t)}{dt} - 2M\tau\rho^2(t) \quad (2.19)$$

where  $\dot{\epsilon}_0$  is a parameter related to the mobile dislocation density,  $A$  is the activation area for creep,  $\alpha$  is a constant,  $\rho$  is the total dislocation density,  $L$  is the mean free path of dislocation motion,  $\tau$  is the dislocation line tension and the other quantities have the usual meanings.

During the steady state stage, the dislocation density  $\rho_s$  is constant. Assuming that the growth of the average dislocation mesh,  $R_m$ , obeys the equation

$$\frac{dR_m}{dt} = M\tau/R_m \quad (2.20)$$

the steady state strain rate,  $\dot{\epsilon}_s$ , is expressed as

$$\dot{\epsilon}_s = 2bLM\rho_s^2 \quad (2.21)$$

where  $M$  is the mobility of climbing dislocations. These recovery models stand in direct contrast to the subgrain boundary recovery models: in the subgrain recovery models (84,85,86), the rate controlling recovery event is localized in the subgrain interior, while

in the network models (36,89,90) it is localized at subgrain boundaries.

The models described thus far assume that the strain rate is controlled by the recovery of dislocations. Another point of view assumes that glide of dislocations is the rate controlling mechanism. In general, the glide models use the microscopic equation for the strain rate in terms of dislocation density and velocity as a starting point. This equation, called the Taylor-Orowan equation, has the form:

$$\dot{\epsilon} = \alpha \rho_m b v \quad (2.22)$$

where  $\rho_m$  is the density of mobile dislocations,  $v$  is the velocity of dislocations and  $\alpha$  is a constant. By making additional assumptions, the dislocation density is calculated and substituted into Equation 2.21.

Hirsch and Warrington (91), using an idea initially proposed by Mott (92) formulated a model based on the non conservative motion of jogged screw dislocations. Screw dislocations, with jogs which do not lie in the slip plane, can move only when the jogs absorb or emit vacancies or interstitials. Dorn and Mote (93) formulated the thermally activated motion of jogged screw dislocation under the condition of an equilibrium concentration of vacancies near the jogs. Barrett and Nix (26) improved the model by formulating the dislocation velocity in terms of the diffusion controlled flow of vacancies to and from the jogs. The result obtained by Barrett and

Nix for the creep strain rate is:

$$\dot{\epsilon}_s = C \rho_m D \sinh (\eta b^2 / 2 kT) \quad (2.23)$$

where  $\eta$  is the spacing between jogs,  $\rho_m$  is the density of dislocations that are mobile and  $C$  is a constant which is possibly temperature dependent. This model has been criticized by Weertman (80) and some modifications have been introduced by Levitin (94).

All the models referred to above use a relation between the dislocation velocity and stress for single dislocations. The mobile dislocation density has to be determined from other conditions. One of the weaknesses of the glide theories is the difficulty in deriving a  $\rho_m$  versus  $\sigma$  relationship which gives the correct observed stress dependence of  $\dot{\epsilon}_s$ .

The theories described above express the steady state creep rate in terms of the independent action of dislocation glide or dislocation climb. Attention is now shifted to a different approach used by Ahlquist, Gascaneri and Nix (95). They suggested that neither the dislocation glide nor recovery of dislocations can be identified as the only rate controlling creep process. According to their theory the creep rate can be described by any one of these processes, i.e., dislocation glide driven by the effective stress or recovery driven by the internal stress. The internal stress,  $\sigma_i$ , has its origin in the elastic interaction between dislocations; the effective stress,  $\sigma^*$ , is then defined as the difference between the applied stress,  $\sigma$ , and the internal stress.

In this model, the separation of the applied stress into two different components has permitted the analysis of the steady state creep rate in terms of three independent equations. One is based on the Bailey-Drowan (77,78) concept which states that steady state creep is determined by a balance between strain hardening and recovery, or

$$\dot{\epsilon}_s = r/h \quad (2.24)$$

where  $r = - \left( \frac{\partial \sigma_i}{\partial t} \right)_{\sigma, \epsilon, T}$  is the rate of recovery and  $h = \left( \frac{\partial \sigma_i}{\partial \epsilon} \right)_{\sigma, T, t}$  is the strain hardening rate. Another equation for the steady state creep rate is Equation 2.22, in which  $\rho_m$  is expressed in terms of  $\sigma_i$  and  $V$  is expressed in terms of  $\sigma^*$ . The third equation used in the formulation of the model is a form of phenomenological equation developed by Sherby and Burke (18)

$$\dot{\epsilon}_s = K(T) \sigma^n \quad (2.25)$$

The phenomenological description of the steady state creep rate is then obtained by combining the three equivalent equations in a compatible manner. By doing so they found that the exponent,  $n$ , is given by

$$n = \left( \frac{\sigma^*}{\sigma_i} + 1 \right)^m / \left( \frac{m-1}{p} \cdot \frac{\sigma^*}{\sigma_i} + 1 \right) \quad (2.26)$$

where the parameters  $p$ ,  $n$ ,  $l$  and  $m$  are defined as:

$p$  is the stress sensitivity coefficient for the dislocation velocity,  $l$  is the internal stress sensitivity coefficient for  $\sigma^*$ , and  $\rho_m$  the mobile dislocation density

$$m + 1 = \left( \frac{\partial \ln \dot{\epsilon}_s}{\partial \sigma} \right) \quad \text{and} \quad n = \left( \frac{\partial \ln \dot{\epsilon}_s}{\partial \sigma} \right) \quad (2.27)$$

These parameters are determined using the transient strain dip test (96) and the stress transient dip test techniques (97). In both of these methods,  $\sigma_i$  is determined by reducing the applied stress to a level at which the plastic strain rate is momentarily zero. The most attractive feature of this phenomenological theory is its ability to qualitatively predict the stress and temperature dependencies of the creep rate without resorting to detailed mechanistic models.

The experimental measurements and observations of high temperature creep available at present are by no means sufficiently extensive to make it possible to rule out all proposed theories except the operative one. The theories in their present stage are too crude to permit such a selection. Furthermore, some of them are complementary to one another rather than alternative. Lagneborg (36) noted that the current theories suffer from several deficiencies:

1. Failure to separate the applied stress into its thermal ( $\sigma^*$ ) and athermal ( $\sigma_i$ ) components (recovery theories (25,79,82,84, 86,88,89,90) and glide theories (26,91));
2. Lack of consideration of changes occurring during primary creep

- and the transition to steady state (most of the theories);
3. Failure to take into account the stress dependence of the activation area (glide theories (26,91));
  4. The arbitrariness introduced by the unknown mobile dislocation density or the number of activatable dislocation sites (recovery theories and glide theories);
  5. Failure to include the subgrain structure (in most of the theories).

A discussion involving item 5 above follows:

Historically, creep theories have not related subgrain size to subprocesses controlling the creep rate, and, as reviewed above, even now most theories do not attribute any significant role in the creep process to subgrains. This is because initial evidence obtained in the 1950s indicated that a true substructural steady state in which dislocation density, subgrain size and subgrain misorientation were constant, did not exist. For instance, the work of McLean (38,71,98) and McLean and Farmer (99) suggested that the subgrain misorientation was strain dependent. Subsequent studies of hot extrusion of aluminum (67) have shown that the subgrain size, misorientation and shape remain essentially constant to strains of 3.7. Bird et al. (22) cite a number of cases in which limiting subgrain misorientations seem to be reached during hot working. Nevertheless, they conclude that this does not imply a steady state substructure misorientation during creep, since creep stresses are much less than hot working stresses. However, in a number of recent creep

studies using transmission electron microscopy (47,60,63), the constancy of subgrain size and misorientation during the steady state stage has been confirmed.

There is, at present, considerable evidence that the occurrence of a subgrain structure in a deformed material may influence a number of its properties. It has been suggested that subgrain boundaries may be preferred paths for fatigue crack propagation (100,101). The presence of a subgrain structure is also associated with the increase in current carrying capacity of deformed type II superconductors (102).

The presence of a subgrain structure is also believed to alter the creep properties. Early investigations performed by Hazzlett and Hansen (14) on aluminum showed that prior plastic straining at low temperatures, followed by a recovery annealing treatment, that is, the previous introduction of a cell structure, causes an increase in creep strength. They also observed an increase in the room temperature flow stress measured in a tensile test. Similar results were obtained by Ancker et al. (15) and Azhaska et al. (103,104) on nickel and Hasegawa et al. (12,105) on Cu-Al alloys. These observations suggest that the cell boundaries may act as barriers to dislocation glide.

The importance of subgrains on the creep process has also been suggested by observations of the creep rate after stress-change experiments. Sherby, Trozera and Dorn (106) reported that aluminum containing fine subgrains (obtained by deformation at high stress)



was stronger in creep than the same material containing coarse subgrains (obtained by deformation at relatively low stresses). Stang et al. (7), studying the creep properties of subgrain forming (random oriented material) and non-subgrain forming (textured material) Fe 3% Si, observed that the transient behavior of these materials is widely different, indicating that the presence of subgrains can affect the creep process.

In a study of high temperature mechanical behavior of polycrystalline tungsten, Robinson and Sherby (1) observed that the stress dependence of  $\dot{\epsilon}_s$  depends on whether or not subgrains form. They proposed a phenomenological equation to describe the steady state creep behavior of tungsten. The relationship proposed was that

$$\dot{\epsilon}_s = S \lambda^2 D (\sigma/E)^7 \quad (2.28)$$

where  $\dot{\epsilon}_s$  is the creep rate, either instantaneous or steady state, S is a structure constant equal to about  $3 \times 10^4 \text{ cm}^{-4}$ ,  $\lambda$  the subgrain or grain size, D is the diffusion coefficient,  $\sigma$  the creep stress and E the average unrelaxed elastic modulus. The equation contains a number of unusual features, but particularly unique are the two terms,  $\lambda^2$  and  $(\sigma/E)^7$ . They suggested that the  $\lambda^2$  term represented either subgrain size in subgrain forming materials, or grain size in materials which do not form subgrains. As the subgrain size stress dependence is usually of the form  $\lambda = B \sigma^{-1}$  or  $\lambda = B' (\sigma/E)^{-1}$ , the introduction of the subgrain size stress dependence into Equation

2.28 leads to the equation

$$\dot{\epsilon} = 3 \times 10^{40} B^2 \left( \frac{\sigma}{E} \right)^5 D \quad (2.29)$$

for the creep rate of subgrain forming materials. If subgrains do not form in creep, it was hypothesized that the grain size,  $L$ , should be substituted into equation 2.28 for  $\lambda$ , in which case the creep rate becomes

$$\dot{\epsilon} = 3 \times 10^{40} L^2 \left( \frac{\sigma}{E} \right)^7 D \quad (2.30)$$

Both forms of behavior were observed in the creep deformation of tungsten (1): Subgrain-forming tungsten exhibited a five power law stress dependence, whereas non-subgrain forming tungsten showed a seven power law stress dependence.

Robinson and Sherby (1) also observed that a normal power law breakdown at  $\frac{\dot{\epsilon}}{D} \sim 10^9 \text{ cm}^{-2}$  occurred in the subgrain forming tungsten but normal power law breakdown did not occur within the range of test condition for non-subgrain forming tungsten, which extended to  $\frac{\dot{\epsilon}}{D}$  values of about  $10^{-11} \text{ cm}^{-2}$ .

Later, Young, Robinson and Sherby (2) using subgrain size values available in the literature with results of constant strain rate tests at high temperature observed a behavior similar to that of tungsten in high purity aluminum.

Recently, Sherby, Klundt and Miller (3), using results available in the literature for 99.99% aluminum, obtained in tests at

constant stress and constant structure conditions, developed an equation which predicted the creep rate as a function of subgrain size, stress, diffusion coefficient and elastic modulus. The equation proposed is

$$\dot{\epsilon} = S \left(\frac{D}{b^2}\right) \left(\frac{\lambda}{b}\right)^p \left(\frac{\sigma}{E}\right)^N \quad (2.31)$$

where  $p = 3$ ,  $N = 8$ , and  $S$  is about equal to  $1.5 \times 10^9$ . This empirical formulation was also shown to accurately describe the creep behavior of high stacking fault materials. Equation 2.28 has the same general character as Equation 2.31 initially proposed for tungsten: both involve the subgrain size in an explicit form. However, they differ in the values of the exponents of the subgrain size and stress terms.

The approach used by Robinson and Sherby (1) and Sherby, Klundt and Miller (3) is in conflict with some recent studies; according to the ideas used to obtain equations 2.28 and 2.31, the transient period following a stress reduction, performed in the steady state region, must be accompanied by the growth of the subgrain size to a value consistent with the reduced stress. In fact, this conception is implicitly assumed during the development of Equation 2.31. Although this assumption has been used, very few microstructural observations after stress changes have been made. Mitra and McLean (107) reported that no change in subgrain size could be observed after stress reduction, but the samples were only strained 1% after stress reduction. Pontikis and Poirier (108) in a study of subgrain

sizes after stress reductions in AgCl reported that no subgrain growth occurred even in samples which were held at zero stress and at the test temperature for as long as four days. Parker and Wilshire (109) reported that no change in subgrain size could be observed following stress reductions in copper samples which were deformed until steady state creep was obtained and then subjected to a stress drop. Parker and Wilshire claimed that their data contradicted the concept that the creep rate depends explicitly on the subgrain size as suggested by Robinson and Sherby (1).

The review presented above has shown that several aspects of the creep phenomena are not well understood. In particular, the influence of subgrains on the creep controlling mechanisms has not been determined in a clear way. Data on this aspect of the creep process are still lacking. This point will form the major feature of this dissertation, to be described in the following chapters.

## CHAPTER III

### EXPERIMENTAL PROCEDURES AND TECHNIQUES

#### 3.1 Constant Stress Creep Apparatus

Determination of the relation between applied stress, observed strain rate and the internal structure in a material, deformed under creep conditions, is simplified if apparatus capable of maintaining a constant stress while the sample is being deformed is used. A system of apparatus was designed and constructed for this investigation to maintain a constant tensile creep stress by means of a contoured lever arm originally proposed by Andrade and Chalmers (110).

A schematic diagram of this load system is shown in Figure 3.1. A flexible steel strip carries the load and is forced, by the applied weight,  $W$ , to stay vertically tangent to the contoured lever arm. The arm rotates about its fulcrum point on a self aligning bearing. The load is transmitted to the specimen by another flexible strip capable of following the radius, " $d$ ", centered at the fulcrum point of the arm. The distance  $d$  remains constant during creep deformation. Two adjustable weights are placed so that the center of mass of the rotating system, without any load, coincides with the fulcrum point. As shown in figure 3.1a, at zero creep strain, the load applied to the specimen is  $(R_0 \cdot W)/d$  where  $R_0$  is the initial lever distance and  $W$  is the weight applied. In this position the steel strip lies tangent to the arm at the point  $P$ . After creep

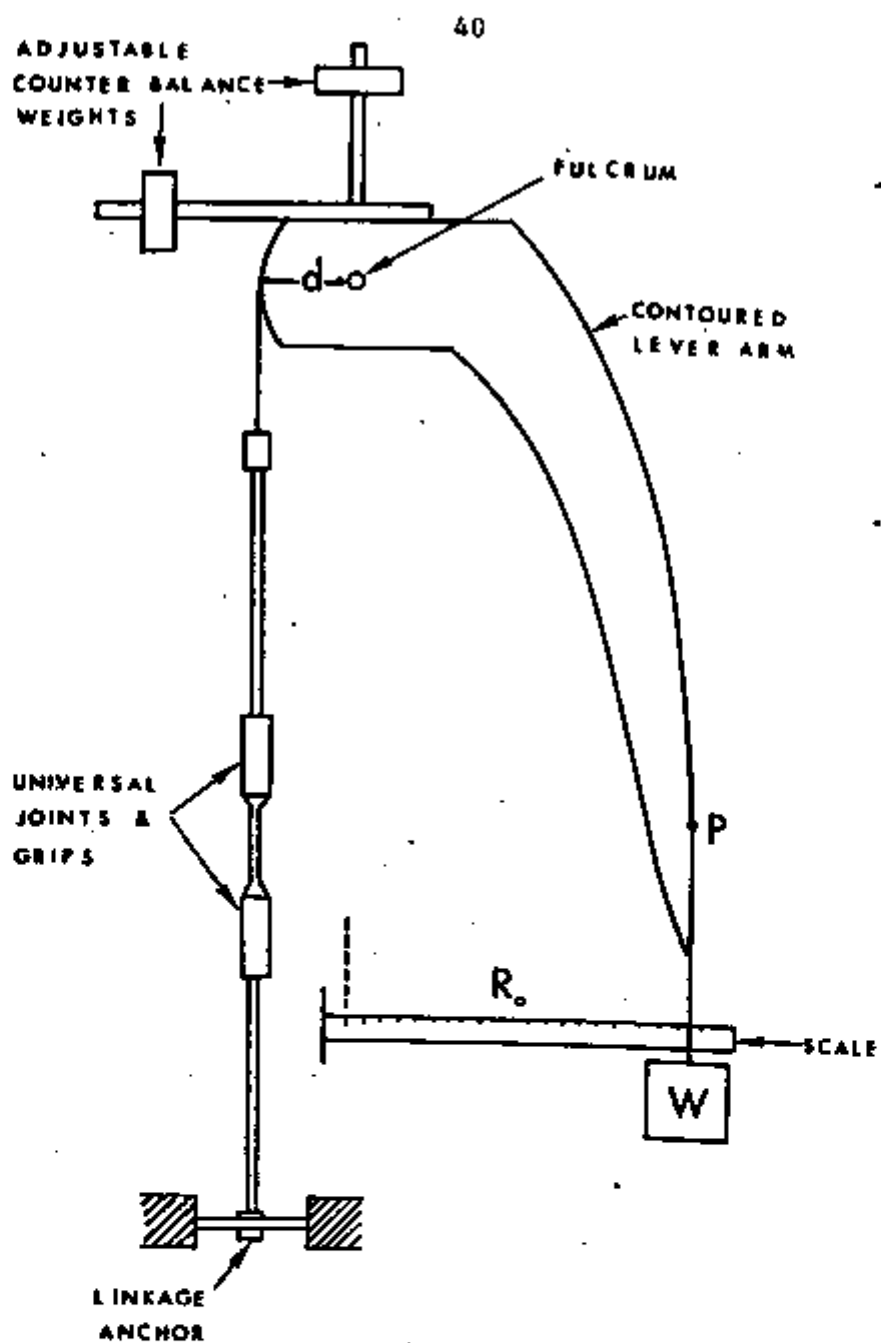
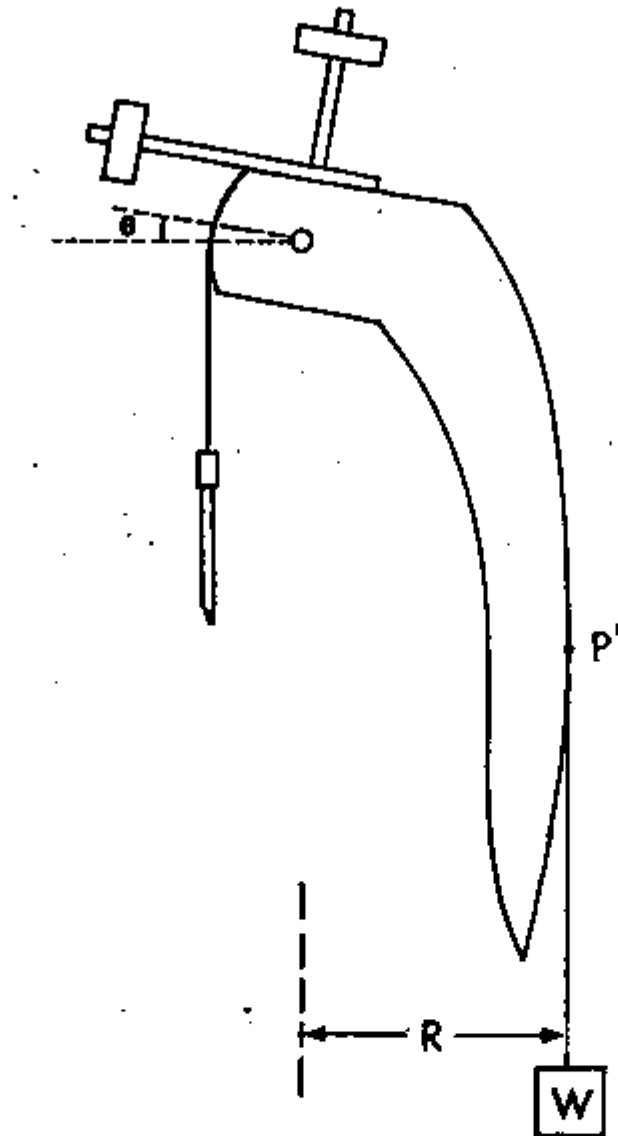


Figure 3.1 Schematic diagram of the load system employed  
a) Zero strain

Figure 3.1 (b) Strain  $\epsilon$

strain  $\epsilon$ , the arm has rotated to a new position and the tangent is now moved to the point  $P^1$ , Figure 3.1(b). With the arm in this position, the load on the specimen is  $(R.W)/d$ . The contour of the lever arm is designed so that the load on the sample is decreased as the sample elongates and the arm rotates, in a manner which maintains a constant stress on the specimen. The following equation describes the relationship between the radii and strain:

$$\epsilon = \ln (R/R_0) \quad (3.1)$$

where  $\epsilon$  is the true creep strain,  $R_0$  is the lever distance at zero strain and  $R$  is the lever distance at a true strain  $\epsilon$ .

A scale graduated in 1/64 in. was mounted with its zero directly beneath the fulcrum point of the contoured lever arm as shown in Figure 3.1(a). For any arm position, the radius  $R$  could then be obtained by observing the position of the steel load strain on this scale. The value of  $R$  corresponding to an angle of rotation  $\theta$  of the contoured lever arm and a true strain  $\epsilon$  in the specimen was determined assuming a constant volume in the gage length during creep deformation. A gage length of 4.44 cm (1.75 in.) was used. The design of the contoured lever arm was accomplished using a graphical technique. The initial lever distance  $R_0$  was 30.48 cm (12 in.) and the distance  $d = 10.16$  cm (4 in.) so that the initial lever ratio  $R_0 : d = 3:1$ .



The load system for the constant stress apparatus was calibrated with a 50 Kg Instron load cell. A turnbuckle was used to simulate the straining of the specimen and a load  $W$  was attached to the contoured lever arm. The radius  $R$  was varied using the turnbuckle and the load on the specimen,  $L$ , was then measured at the load cell. If  $R$  is known, the load  $L$  on the specimen can be calculated using the expression

$$L = \frac{W \cdot R}{d} \quad (3.2)$$

A plot of  $L(\text{calc.})$  versus  $L(\text{measured})$  was made for true strains from zero to 0.5 for several applied loads. In this plot a straight line with slope 0.99 was observed in the range between zero and 50% true strain in each case. This is shown in Figure 3.2. The straight line obtained shows that the stress on the specimen is maintained constant during deformation within 1% for strains between zero and 50%.

The grip assembly shown in Figure 3.3 was used to hold the test specimen. This assembly was constructed of AISI 316 stainless steel. To eliminate the possibility of bending the specimen during initial loading, and also to keep the stress uniaxial during the creep test, a set of universal joints was mounted on either side of the sample. The specimen ends were fastened to the linkage by means of split rectangular grips. A special alignment jig was made to facilitate the mounting and tightening of the specimen grip assembly without the risk of bending the specimen. This jig consisted of a 22.86 cm

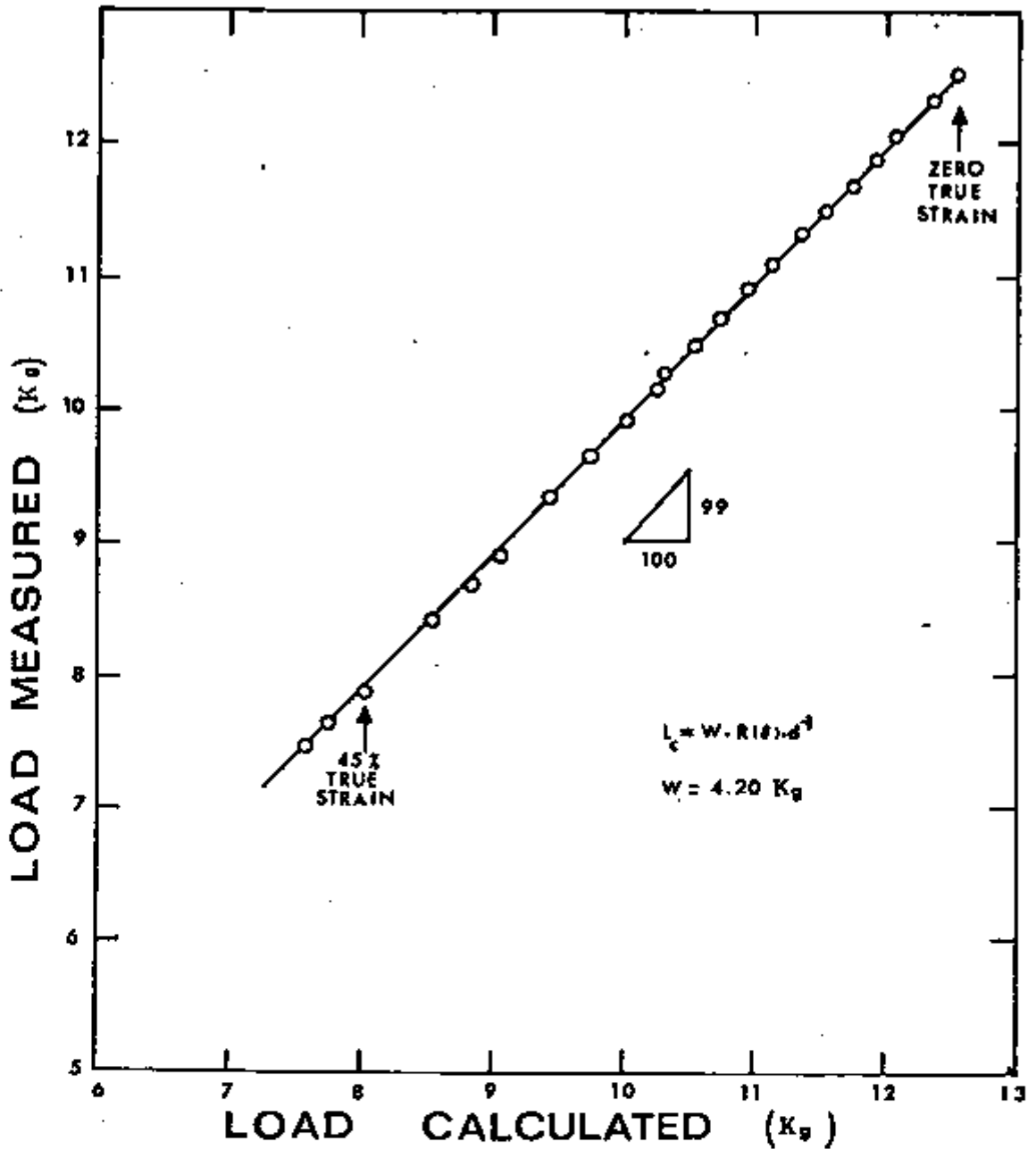


Figure 3.2 Calibration curve of the load system of the creep machine for  $W = 4.200 \text{ Kg}$ .

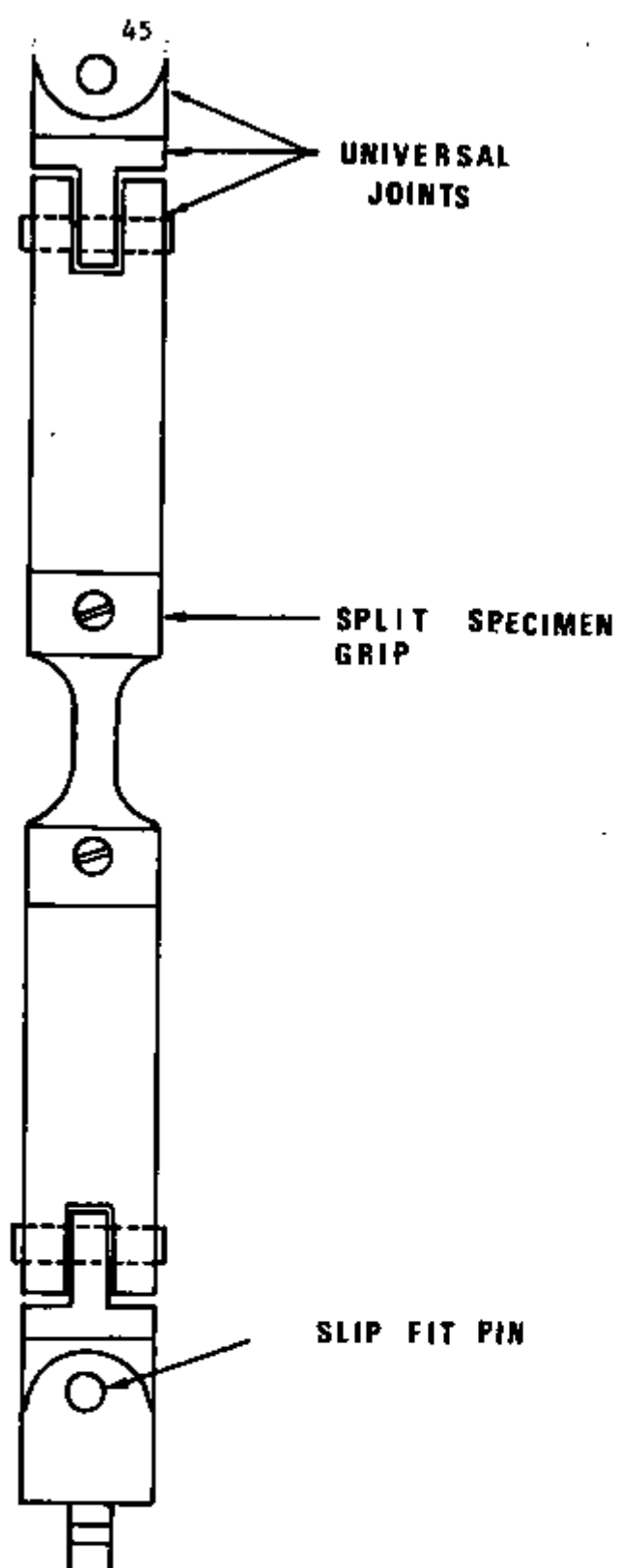


Figure 3.3 Schematic diagram of the grip assembly used.

x 5.08 cm x 3.175 cm (9" x 12" x 1.25") piece of aluminum containing a longitudinal, rectangular shaped slot. Two set screws mounted laterally in the jig were used to hold the grips fixed while the specimen was being attached. Once the specimen was tightened in the grip assembly, the upper and lower universal joints were linked to the creep machine. The jig was removed by loosening the set screws with a 2 Kg applied load. In order to prevent the grips and specimens from sintering together during the test, the grip faces and fasteners were coated with milk of magnesia.

The furnace used was a 1200 C Marshall tube unit mounted vertically in a moveable carriage which was not in physical contact with the creep machine. The furnace temperature was controlled by a Leeds and Northrup Electromax temperature controller driving a L & N SCR power package. The temperature at the center of a sample never varied by more than  $\pm 0.5^{\circ}\text{C}$  and the variation along the gage length was less than 1C measured with a test specimen with three thermocouples spot welded along its length. The measurement of the temperature of the specimen was accomplished using a chromel-alumel thermocouple with the thermocouple head in good contact with the specimen surface. A Hewlett Packard Digital Voltmeter (model 3439 A) was used to measure the thermocouple output.

Creep strain was measured using a shielded Schaevitz (model 1000 HR) linear variable differential transformer (LVDT); the LVDT core was attached to the upper pulling rod of the creep machine and the main body clamped to the creep frame as shown in Figure 3.4.

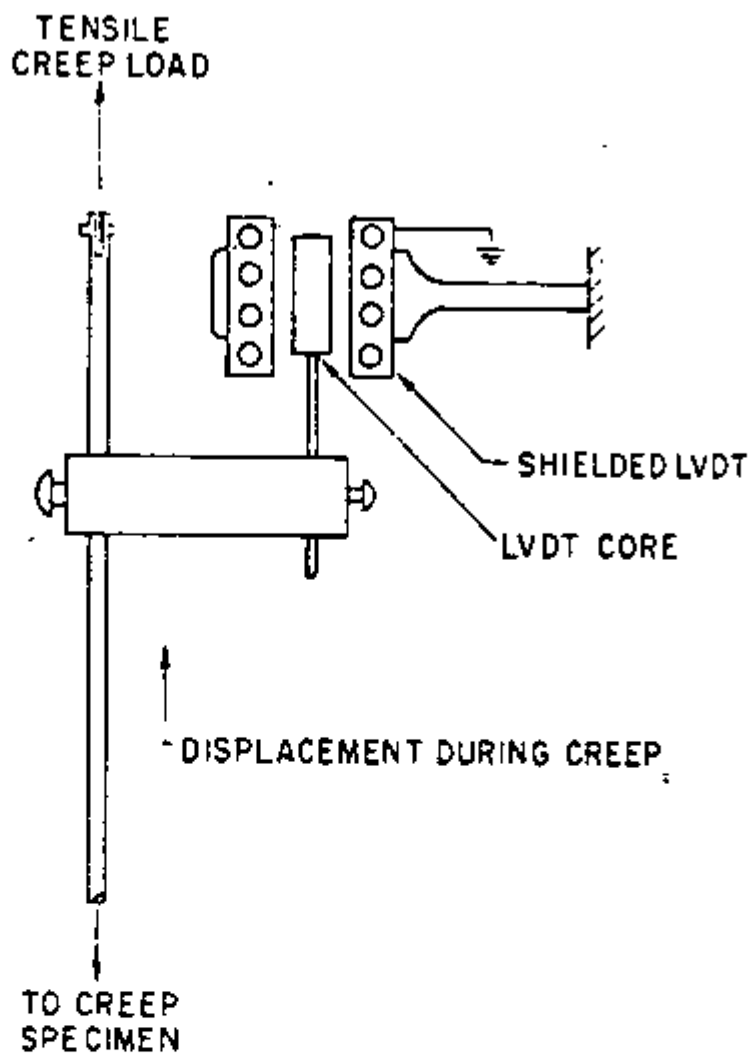


Figure 3.4 Schematic diagram of the strain measuring device.

Thus the only weight placed on the rotating lever arm system was the constant weight of the core and its support and that of the top pulling rod and top grip. The load due to the grip assembly, pulling rod and LVDT core and support was balanced out with the adjustable weights used to balance the apparatus.

The LVDT was energized by 6.3 V AC from a step-down transformer as shown schematically in the circuit diagram in Figure 3.5. Two germanium diode bridges were used to rectify the LVDT secondary outputs. The output of these bridges was balanced by a 5 K $\Omega$  variable resistor such that a zero circuit output was obtained when the core was in its null position. This system was calibrated by moving the core known distances with a micrometer head made by Wilson Mechanical Instrument Division, American Chain and Cable Company, Inc., and recording the circuit output with a Leeds and Northrup (type K 4) Universal Potentiometer. The voltage obtained at the output of the system was very linear over a LVDT range of  $\pm$  800 mV. The calibration constant of the LVDT was 26.6  $\mu$ V per micrometer of the core displacement.

The total output voltage range (0 to 800 mV) of the LVDT was measured on the 100 mV or 50 mV scale of a Honeywell Elektronik Recorder (Model 195) by cancelling part of the total output with a voltage opposite to that of the LVDT signal. This was achieved using the circuit shown schematically in Figure 3.6. At zero creep strain, the circuit was used to cancel the negative output of the LVDT and the recorder pen was set at zero. As the specimen was strained, the LVDT core raised inside the winding and the recorder pen moved

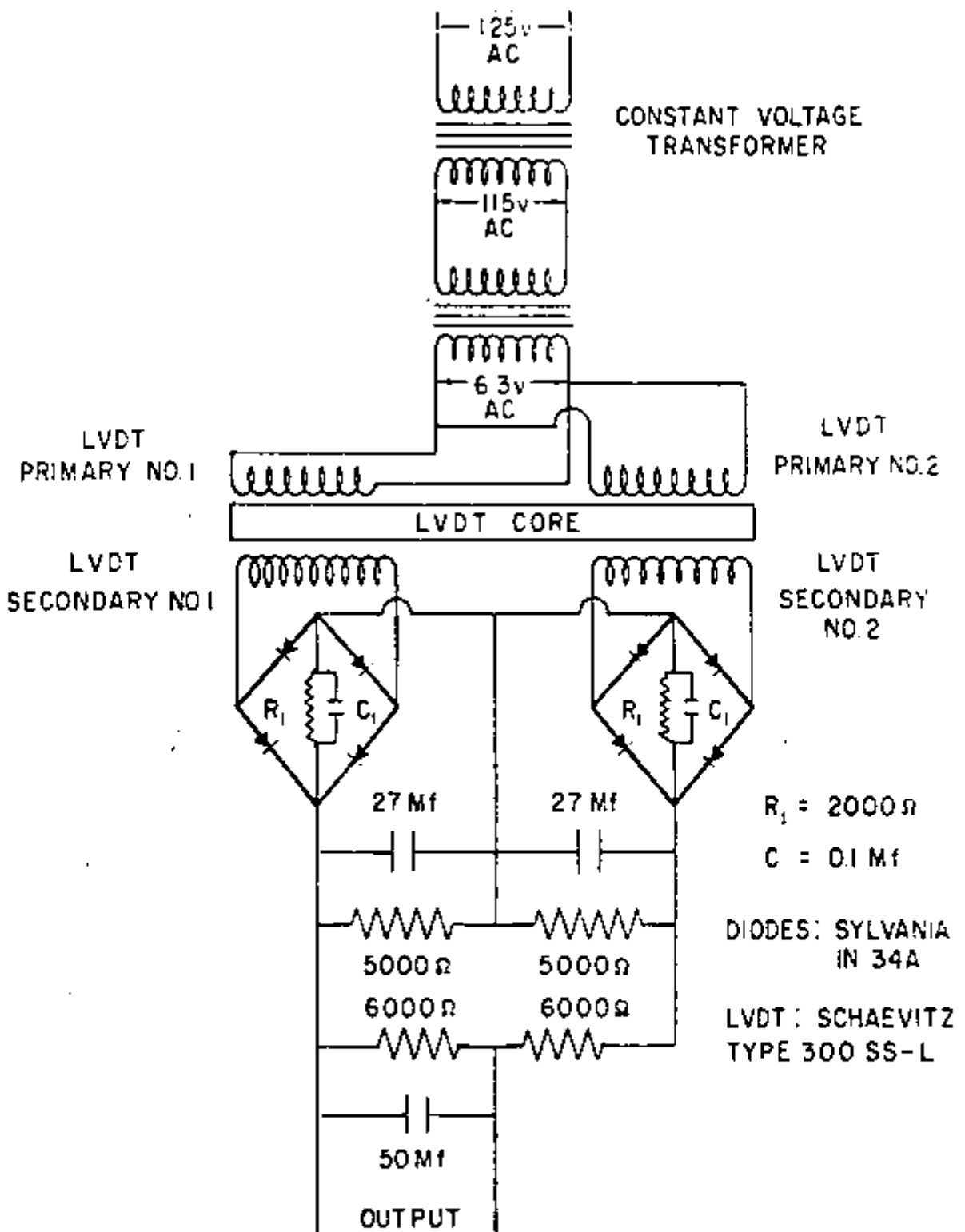


Figure 3.5 Circuit diagram of the power supply and rectifying circuit for the LVDT.

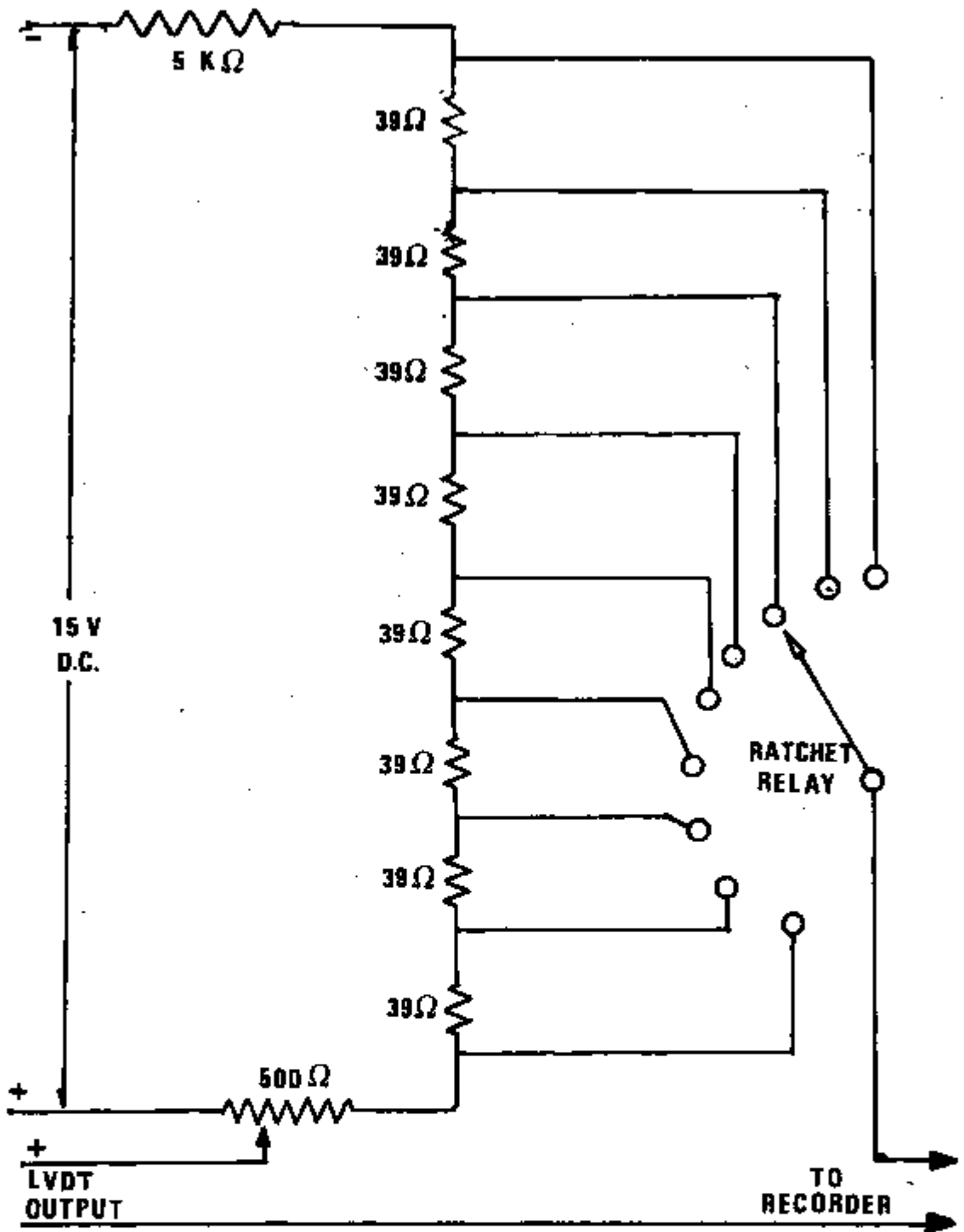


Figure 3.6 Circuit diagram for the automatic voltage step-bucking circuit.



upscale. When the recorder <sup>pen</sup> reached the end of the scale, it closed a small microswitch attached to the recorder. This microswitch activated a step relay one step and the compensation voltage decreased, thus moving the recorder pen back to zero. In this way the recorder plotted the complete displacement-time curve. Using this recorder system it was possible to measure strain changes as small as  $5 \times 10^{-4}$  and to make estimations of changes as small as  $5 \times 10^{-5}$ . In the stress change experiments a 5 mV scale was used to record the core displacement. This procedure improved the sensitivity of the strain measuring system, allowing measurements of strain changes as small as  $1 \times 10^{-4}$  and to make estimates of changes as small as  $1 \times 10^{-5}$ .

### 3.2 Specimen Preparation

High purity aluminum 99.999% Al, as specified by the supplier, was used in this investigation. The material was purchased from Atomergic Chemetals Company in the ingot form. Several pieces 2.54 cm x 2.54 cm x 10.16 cm (1" x 1" x 4") were cut from the ingots using a hacksaw; a new blade was used whenever a new set of samples was prepared. After sawing, each piece was subsequently cleaned in a 4 Molal water solution of sodium hydroxide at 70°C. This treatment removed the top layer of each surface of the piece and consequently any material embedded during preparation. After this procedure, each piece was cold rolled to its final thickness following the method described below; the rolls in the rolling mill were carefully cleaned using kerosene and fine emery paper prior to rolling.

FCC metals are known to develop a strong rolling texture that can influence the creep behavior, thus requiring the use of intermediate heat treatments. Each piece was cold rolled and subsequently heat treated. A set of cold reduction steps was used in such a way as to limit each cold reduction to less than 40%. Cook and Richards (111) have found that for copper, prior deformation of 50% leads to an almost random recrystallization texture. The data on aluminum annealing textures are more complex than for copper; in Al, the behavior depends upon purity, prior heat treatment, and the deformation history of the material. For high purity aluminum, however, the recrystallization texture behaves in a manner similar to that of copper. It has been reported that limiting cold reduction to 40% is sufficient to obtain a random structure (112). The last rolling step was chosen to give a 20% reduction to a final thickness of 1.27 mm (0.050 inches); the intermediate and final heat treatments were carried out in air at 500°C for one hour followed by furnace cooling. Prior to any heat treatment, each specimen was cleaned in acetone and rinsed in ethyl alcohol.

The creep specimens were flat reduced section tensile specimens, machined from pieces cut parallel to the rolling direction of the 1.27 mm rolled strips. Each specimen was carefully examined prior to testing; any irregularity introduced by machining was removed with emery paper. The dimensions of the creep specimens used are shown in Figure 3.7. After machining and prior to creep testing, the final specimen was heat treated as described earlier for one

hour at 500°C in air. The average grain size at the end of the specimen preparation process was 0.5 mm as measured by the line intercept method to be described later.

### 3.3 Test Procedure

#### 3.3.1 Determination of Effective Gage Length

The strain measuring apparatus described in Section 3.1 can be used to evaluate true specimen creep strain only after the determination of the effective length over which deformation is occurring. This effective length was determined by scribing two parallel lines of known separation,  $X_0$ , on the surface of the specimen before any testing. After the sample was strained approximately 15%, as determined by the LVDT output, the test was interrupted. The effective length was then calculated by measuring the distance,  $x$ , between the scribed lines after this creep deformation, using the relation

$$e = \frac{x - x_0}{x_0} = \frac{\Delta l}{l_{ef}} \quad (3.3)$$

where  $\Delta l$  is the core displacement during the strain  $e$ , as determined from the LVDT output and  $l_{ef}$  is the effective gage length. Using several specimens, it was found that the effective gage length was 4.38 cm (1.90") for the creep specimen configuration of Figure 3.5.

### 3.3.2 Test Setup Procedure

The following setup procedure was used:

1. Measure the specimen cross sectional area
2. Mount sample in the alignment jig and tighten the grips
3. Attach the alignment jig containing the specimen to the machine frame
4. Remove the alignment jig
5. Set the furnace in place

The alignment jig was removed (step 4) with a 2 Kg load applied to the specimen to reduce the risk of introducing spurious deformation. The 2 Kg load corresponds to an applied stress of 4.9 MPa; this stress is of the order of 40% of the yield stress for annealed high purity aluminum at room temperature (the yield strength is 11.7 MPa in tension). The 2 Kg load was replaced by a small 341 g preload and the furnace turned on. When the temperature stabilized, the contoured lever arm was set at a value  $R'_0 > R_0$  to compensate for the elastic strains and thermal expansion strains associated with the machine parts. The  $R'_0$  values had previously been calibrated as a function of the applied load using a thick steel strip in place of the specimen. The entire system was allowed to stabilize for two to three hours before any test was started.

The weights corresponding to the total load were separated into two cans that were connected by a thin wire whenever stress reduction tests were to be performed. Reduction of the applied stress was accomplished by cutting the thin wire using a gas torch. This procedure gives a rapid rate of unloading.

### 3.4 Optical and Electron Microscopy

Specimens intended for optical and transmission electron microscopy of the dislocation substructure generated during creep were deformed as described in the previous section to a specific preselected strain. When this preselected strain was reached, the specimen was water quenched under load in an attempt to preserve the existing creep substructure. The cooling period from the testing temperature to 50°C took five minutes. It is believed that this rapid quenching rate of the specimen was sufficient to freeze the dislocation substructure developed during testing. This assumption is supported by results of an investigation of the substructure during creep deformation of pure nickel by Richardson et al. (113). These investigators found no detectable difference in the structure retained, after high temperature creep, by either water quenching (fast cooling) or by slow (3 hours) cooling under load.

Optical microscopy was used to investigate the subgrain size. To reveal the subgrains, two different techniques were used; in both cases, a mechanical polishing followed by electrolytic polishing of the specimen was used as a starting procedure. The techniques employed are described below.

Technique A: The specimens, prepared as described above, were subsequently etched in the DeLacombe-Beaujard (114) solution maintained at 0°C for a period of approximately 3 minutes. The specimens were then washed in water and rinsed in ethyl alcohol. After drying, the specimens were optically observed using a Reichert Universal Camera Microscope (Model MEF) at magnifications varying from

100 X to 300 X. The magnification used depended on the subgrain size of the samples, the higher magnification being used for the smaller subgrains.

Technique B: After the initial preparation, the specimens were electropolished in a solution of 60 ml orthophosphoric acid ( $H_3PO_4$ ) and 40 ml concentrated sulfuric acid ( $H_2SO_4$ ). The electrolyte was heated to 70 - 80°C and operated for fifteen minutes with a current density of 0.78 A/cm<sup>2</sup> (5 A/inch<sup>2</sup>) at 18 VDC. This electrolytic polishing operation removes a large quantity of metal (a few micrometers) and results in a shiny, mirror-like surface. This clean surface was then anodized using the method developed by Perryman (115). The electrolyte is a solution containing

49 ml water ( $H_2O$ )

49 ml methyl alcohol ( $CH_3OH$ )

2 ml hydrofluoric acid (HF)

The anodization was performed at room temperature using 12 to 18 VDC for approximately three minutes. The different growth rates of the oxide film corresponding to different crystal orientations results in a surface with grains and subgrains clearly visible under polarized light. Observations of subgrains were performed under polarized light in the optical microscope referred to above at magnifications varying from 100 X to 200 X.

The following procedure was used for transmission electron microscopy specimen preparation:

1. Sections 15 mm in length were sheared from the gage section of the deformed samples
2. These sections were initially mechanically ground to a thickness of 300  $\mu\text{m}$  (0.012 in.)
3. Following this grinding process, the specimens were electrolytically thinned to about 250  $\mu\text{m}$  (.01 in.) in a 20% perchloric acid-80% ethanol solution maintained at  $-30^{\circ}\text{C}$  at an applied voltage of 20 VDC.
4. After this thinning process, 3 mm discs were punched out of the specimen and were electropolished in a jet thinning instrument (South Bay Technology, Inc. - J.T. Instrument model 550) in a solution of 10 to 20%  $\text{HNO}_3$  in water. The parameters found for best electrothinning were:

Jet flow	1 ml/s
Distance Nozzle-Specimen	1 mm
Applied Voltage	20 VDC
Total Current	100 mA
Solution Temperature	$-5^{\circ}\text{C}$

All transmission electron microscopy was performed with a J.E.M. 7 Electron Microscope operating at 100 KV.

#### 3.4.1 Dislocation Density Measurement

The dislocation density inside the subgrains was measured using seven to ten electron micrographs of representative areas of foils prepared from each specimen. The magnification of 20,000 X was chosen because it was high enough to resolve individual dislocations yet

was low enough such that the dislocation density in a micrograph was representative of the average dislocation density in the deformed specimen rather than a local dislocation density. Areas very close to a subgrain boundary were avoided because it was observed in many instances that a higher dislocation density was obtained at these areas.

It has been shown by Ham (116) and Hirsch et al. (117a) that, provided the dislocations are randomly oriented, the dislocation density  $\rho$  is given by:

$$\rho = \frac{2NM}{Lt} \quad (3.4)$$

where  $N$  is the number of intersections that a test line placed on a transmission electron micrograph makes with the dislocations,  $L$  is the total length of the test line,  $t$  is the thickness of the foil and  $M$  is the magnification of the micrograph.

The foil thickness was determined by counting the number of extinction contours as described by Hirsch et al. (117b). When slip traces were present, the thickness could also be determined by measuring the distance between the traces in the plane of the foil and by measuring the foil orientation (118).

It has been shown by Hirsch et al. (117b) that unless several reflections are operating, a considerable number of dislocations can be out of contrast. This leads to an underestimation of  $\rho$ . To eliminate errors due to the lack of contrast, micrographs were taken under a multibeam case, that is, at least three strong reflections operating.



It has been shown for aluminum that a considerable percentage of dislocations are either lost from foils or rearranged during foil preparation. Fujita et al. (119), using high voltage electron microscopy, have shown that when a cell structure is present in aluminum the foil thickness above which the dislocations are not lost is less than 200 nm, whereas in the absence of a cell structure, dislocations can be lost even at a thicknesses of 800 nm. In this work, areas thinner than 200 nm were avoided. The relative error in the dislocation density measurements was estimated to be of the order of 25%.

#### 3.4.2 Subgrain Size Measurement

The size of the subgrains was measured using the line intercept method proposed by Heyn (120) and recommended by the ASTM as a grain size specification (121). The number of intersections that the subgrain boundaries make with a test line was counted directly at the microscope, in at least five randomly selected areas of the specimen. The scale on a filar eye piece was used as the test line. For each specimen used, the microscope magnification was frequently measured utilizing a calibrated scale. A combination of test line length and magnification was selected to yield at least 200 intercepts for each area examined. Both optical techniques revealed the same subgrain sizes. The average subgrain intercept length and the 95% confidence limits obtained using optical microscopy are reported in the results.

## CHAPTER IV

### STEADY STATE CREEP BEHAVIOR

#### 4.1 Introduction

The main objective of this chapter is to reproduce previous work on aluminum and to show that the apparatus constructed for this study is capable of producing reliable data. The data presented in this section include the strain-time behavior obtained from constant stress tests. The influences of stress and temperature on the steady state creep deformation rate are examined. Microscopic observations of subgrains are included; also, the effect of the applied stress on subgrain size during steady state creep is discussed. A brief comparison with data published in aluminum of lower purity is also presented. The data presented in this chapter will be used to specify the conditions for investigation of the transient creep behavior after stress reductions to be described in Chapter 5.

## 4.2 Results and Discussion

### 4.2.1 Strain - time data

Constant true stress creep data are presented for stresses between 3.44 MPa and 15 MPa for the temperature range from 250°C to 350°C ( $.56 < T/T_m < .67$ , where  $T_m$  is the absolute melting temperature). Typical strain - time curves are shown in Figure 4.1, in which true plastic strain is plotted versus the fraction of time  $t_f$  to reach fracture. By plotting the data in this way, it is easy to compare the effects of stress and temperature on the shape of the creep curves. From Figure 4.1 it is seen that the creep curves obtained are all of the "normal" type, that is, a well defined primary stage is always present. The extent of primary strain increases with an increase in stress. A well established region in which the strain rate is constant exists. The strain in the tertiary stage is small when compared to the total strain.

### 4.2.2 Stress and Temperature Dependence of the Steady State Strain Rate

The results of the tests conducted in connection with the determination of the stress and temperature dependence of high purity aluminum are given in Table 4.1. Steady state creep rates were determined from the slope of the creep curve recorded. The reproducibility of steady state creep rates was usually better than  $\pm 10\%$ . Only one steady state creep rate was determined for each specimen.

To determine the stress and temperature dependence of the steady state strain rate, Equations 2.3 and 2.5 are applied to the data reported in Table 4.1.

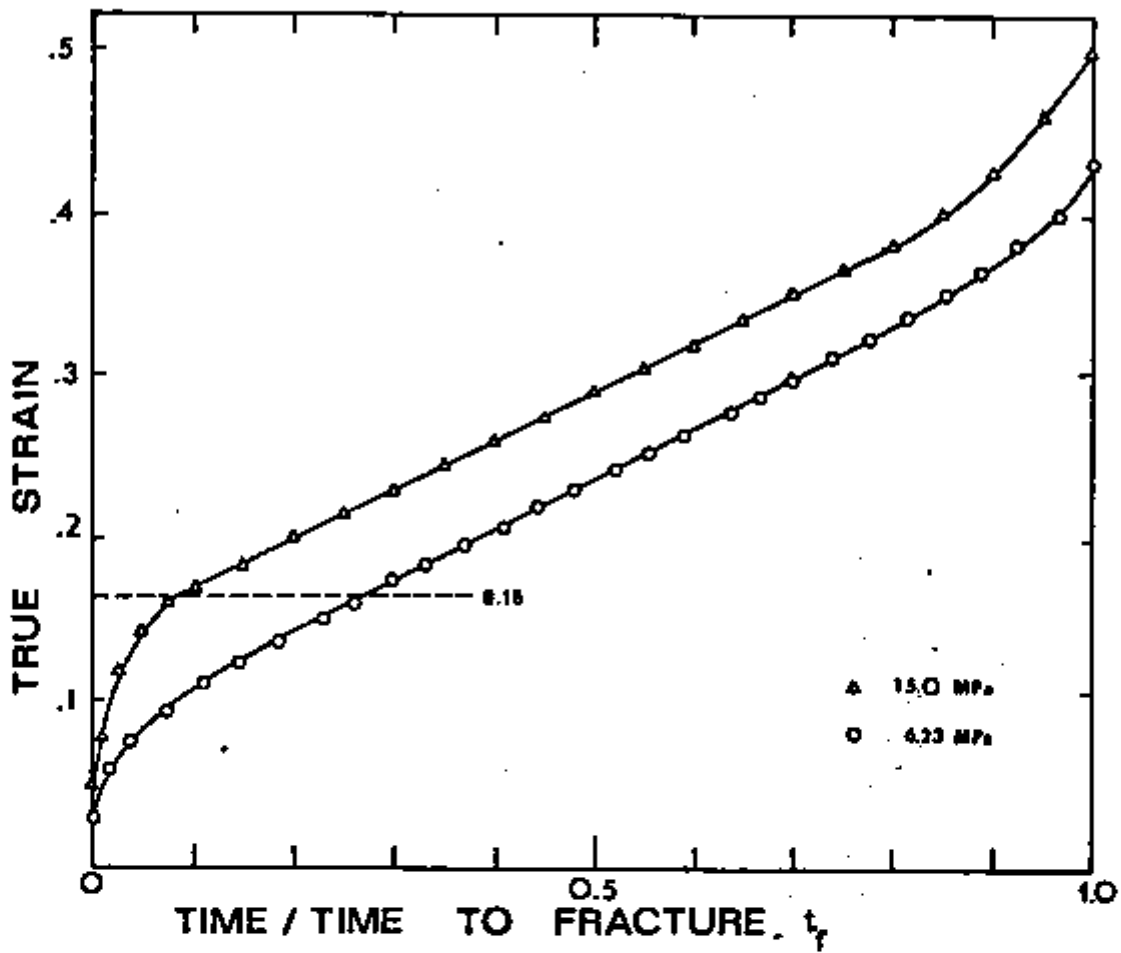


Figure 4.1 Typical creep curves at an applied stress of 15 MPa and 6.23 MPa. The true strain is plotted versus fraction of time to fracture at 573 K.

To obtain an expression for the stress sensitivity coefficient,  $n$ , Equation 2.5 is rewritten by determining the partial derivative of  $\ln \dot{\epsilon}_s$  with respect to  $\sigma$  at constant temperature. This expression is given by

$$n = \frac{\partial}{\partial \sigma} (\ln \dot{\epsilon}_s) \Big|_T \quad (4.1)$$

A log-log plot of  $\dot{\epsilon}_s$  versus  $\sigma$  yields a value for  $n$  describing the stress sensitivity of the steady state strain rate. In Figure 4.2 the values of the steady state strain rate are plotted as a function of the applied stress at 573 K. Results obtained by Ahlquist and Nix (122) at the same temperature on 99.99% Al are included for comparison. This figure shows that for strain rates less than  $5.10^{-4} \text{ s}^{-1}$ , the results can be described by a straight line with slope  $n = 4.6 \pm 0.2$  and for strain rates above  $10^{-4} \text{ s}^{-1}$  a higher value of  $n$  is obtained, that is,  $n = 6.2 \pm 0.2$ . The change in slope occurs when  $\dot{\epsilon}_s / D = 10^9 \text{ cm}^{-2}$ , where  $D_{\text{Al}} = 1.27 \exp(-1.43/kT) \text{ cm}^2/\text{s}$  (\*) is the self-diffusion coefficient for high purity aluminum (5).

(\*) The choice of diffusion coefficients for aluminum self diffusion is the subject of some controversy. Several studies of aluminum self diffusion, using void shrinkage measurements (123) and nuclear magnetic resonance techniques (6) have suggested that the enthalpy for self diffusion  $H_{\text{sd}} = 1.31 \text{ eV}$  for aluminum. Robinson and Sherby (124) discussed the coincidence of tracer diffusion measurements of  $H_{\text{sd}}$  and  $H_{\text{c}}$  obtained from creep studies. In the calculations to be performed in the present study, use will be made of the tracer diffusion value of  $D$ ,  $D_{\text{Al}} = 1.27 \exp(-1.43 \text{ eV}/kT) \text{ cm}^2/\text{s}$  (5) instead of the value  $D = 0.176 \exp(-1.31 \text{ eV}/kT)$  obtained by Volin and Baluffi (123). This choice of  $D$  will permit the comparison of the calculations performed in this study with reported calculations using  $D_{\text{Al}}$  to be described later.

TABLE 4.1

Summary of Data from Constant True Stress Creep Tests

TEST #	T (K)	$\sigma$ (MPa)	$\dot{\epsilon}_s$ ( $s^{-1}$ )	$\lambda$ ( $\mu m$ )
51	573	2.76	$4.2 \times 10^{-7}$	$110 \pm 15$
35	573	3.44	$1.1 \times 10^{-6}$	$94 \pm 10$
63	573	3.44	$1.0 \times 10^{-6}$	
30	573	4.62	$2.8 \times 10^{-6}$	
29	573	6.23	$1.5 \times 10^{-5}$	
33	573	6.23	$1.5 \times 10^{-5}$	$50 \pm 5$
39	573	6.23	$1.6 \times 10^{-5}$	$44 \pm 3$
45	573	9.01	$1.1 \times 10^{-4}$	$26 \pm 3$
37	573	11.00	$5.2 \times 10^{-4}$	$22 \pm 2$
49	573	12.00	$6.0 \times 10^{-3}$	$21 \pm 1$
50	573	15.00	$2.5 \times 10^{-3}$	$16 \pm 2$
86	573	15.00	$3.0 \times 10^{-3}$	
36	573	19.60		$13 \pm 1.5$
72	573	8.24	$6.5 \times 10^{-5}$	
78	573	8.35	$7.4 \times 10^{-5}$	$35 \pm 4$
76	623	6.23	$1.8 \times 10^{-4}$	
77	523	6.23	$1.1 \times 10^{-6}$	
82	546	6.23	$4.0 \times 10^{-6}$	

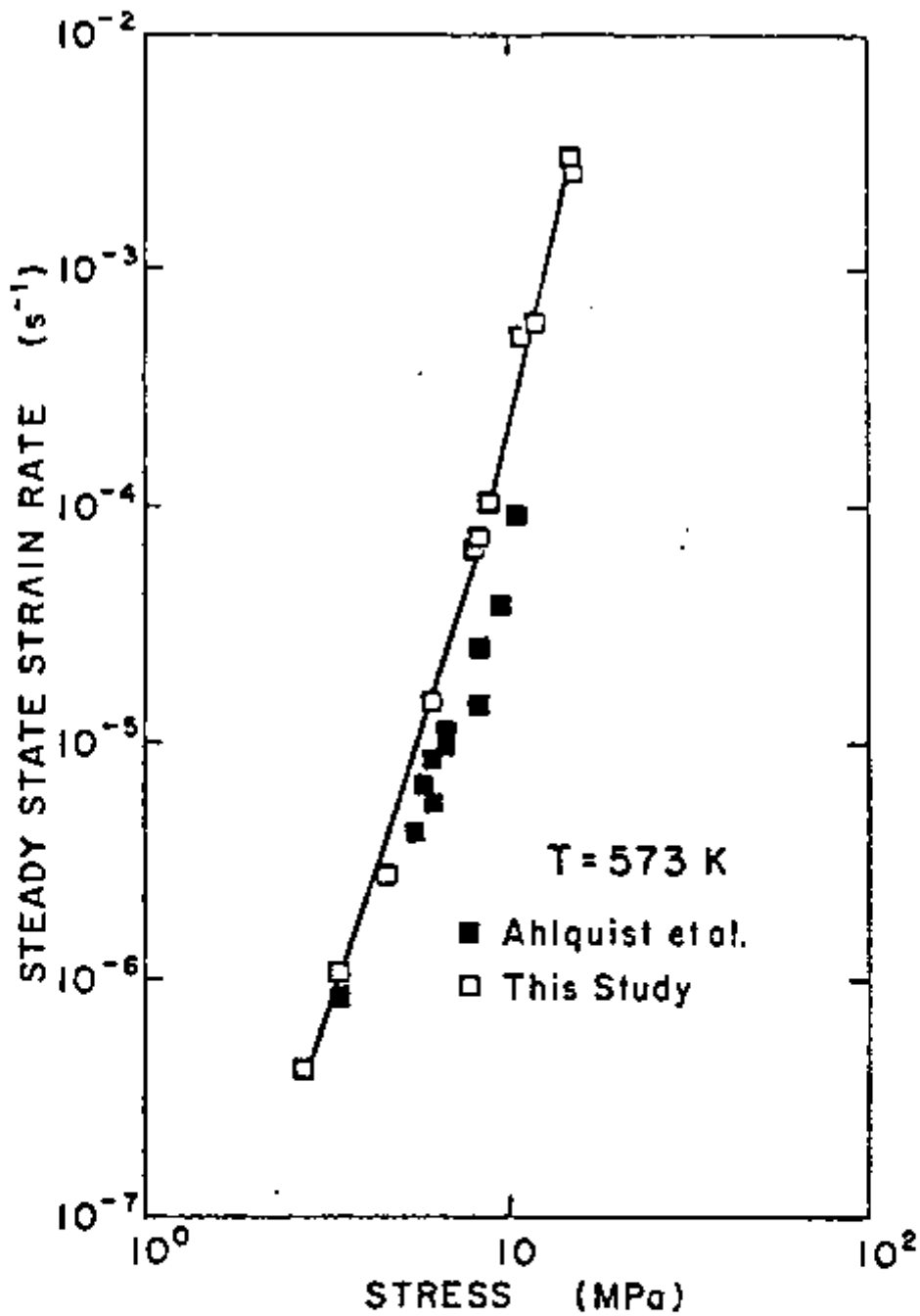


Figure 4.2 The effect of stress on the steady state strain rate of 99.999% aluminum at 573K. The data of Ahlquist and Nix (122) at 573 K for 99.99% aluminum is shown for comparison.

Sherby and Burke (18) showed that, at steady state strain rates  $\dot{\epsilon}_g \approx 10^9 D$ , most pure polycrystalline metals exhibit a change in behavior. In the region above  $\frac{\dot{\epsilon}_g}{D} \approx 10^9 \text{ cm}^{-2}$  the steady state creep rates are greater than those predicted from extrapolation of the data at lower values of  $\dot{\epsilon}_g/D$ . They also show that the beginning of the region in which the power law breakdown occurs is usually independent of the material considered. The results obtained in this study are in excellent agreement with the observations of Sherby and Burke (18). It has been suggested by Sherby and Burke that the power law breakdown is due to the presence of an excess of vacancies generated by dislocation intersection process (18). Such excess of vacancies can enhance dislocation climb and therefore make creep easier by increasing the rate of dislocation annihilation. However, Blum (125), analysing the steady state creep deformation in the presence of excess point defects, has shown that a number of difficulties are associated with Sherby and Burke's explanation. Weertman (86) explains the behavior of the creep rate in this range as due to the stress concentration effects of pile-ups of dislocations. However, quantitative agreement with experiments is obtained only if it is assumed that the pile-up size exceeds the subgrain size; pile-ups of this magnitude are improbable (126). Recently, Blum et al. (127) proposed an explanation for the power law breakdown based on the thermally activated dynamic recovery of dislocations.

To obtain a value for the activation energy for creep,  $Q_c$ , equation 2.3 is rewritten by taking the partial derivative of  $\ln \dot{\epsilon}_g$  with respect to  $1/T$  at constant stress. This procedure gives the equation:



$$Q_c = -k \frac{\partial}{\partial (1/T)} (\ln \dot{\epsilon}_s) \Big|_{\sigma} \quad (4.2)$$

A plot of  $\ln \dot{\epsilon}_s$  versus  $1/T$  at constant stress yields a value for  $Q_c$ . This is shown in Figure 4.3. The value for  $Q_c$  obtained by applying this procedure is  $Q_c = 1.43 \pm 0.05$  eV/at. To correct the apparent activation energy value for the temperature dependence of the modulus, Equation 2.9 is now rewritten:

$$\dot{\epsilon}_s = K \frac{1}{TG^{n-1}} \sigma^n \exp(-H_c/kT) \quad (4.3)$$

where  $K$  is a constant,  $T$ ,  $G$ ,  $n$ , and  $k$  have the previously cited meanings and  $H_c$  is the activation enthalpy for creep. Taking the partial derivative of  $\ln \dot{\epsilon}_s$  with respect to  $1/kT$  at constant stress leads to

$$\begin{aligned} \frac{\partial}{\partial (1/kT)} (\ln \dot{\epsilon}_s) \Big|_{\sigma} &= \frac{\partial}{\partial (1/kT)} (\ln \exp(-H_c/kT)) - (n-1) \frac{\partial}{\partial (1/kT)} \ln G \\ &+ \frac{\partial}{\partial (1/kT)} \ln(1/kT) \end{aligned} \quad (4.4)$$

$$\text{or} \quad -Q_c = -H_c - (n-1)kT^2 \frac{dG}{dT} - kT$$

$$\text{or} \quad H_c = Q_c + kT [(n-1) \cdot (T/G) \cdot \frac{G}{T} + 1] \quad (4.5)$$

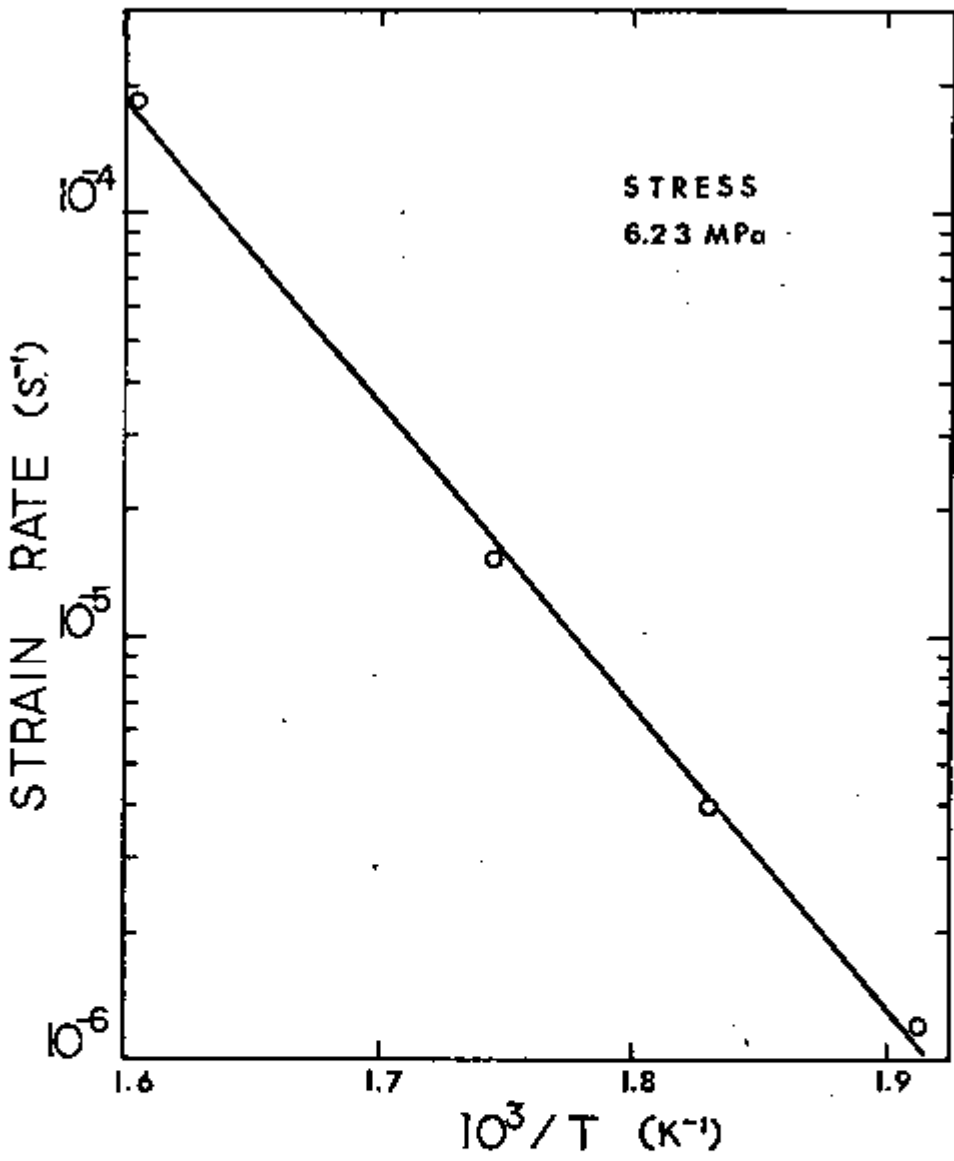


Figure 4.3 The effect of temperature on the steady state creep rate of 99.999% aluminum tested at 6.23 MPa.

Using the temperature dependence of the Youngs' modulus reported by Fine (4)

$$E \text{ (dynes/cm}^2\text{)} = 7.99 \times 10^{11} - 4.10^8 T \quad (4.6)$$

and  $G = E/2(1+\nu)$ , where  $\nu = 0.34$  is the Poissons' ratio for aluminum (147), then

$$G \text{ (dynes/cm}^2\text{)} = 2.98 \times 10^{11} - 1.49 \times 10^8 T \quad (4.7)$$

Using the values of  $G$  calculated from equation 4.7 and the value  $n = 4.6 \pm 0.2$  found previously in this section, the activation enthalpy obtained is  $H_c = 1.41 \pm 0.05$  eV/at.

In Table 4.2, the values obtained by other authors for the apparent activation energy for creep,  $Q_c$ , for the stress sensitivity coefficient,  $n$ , and for the enthalpy of self diffusion are shown. It can be seen that the results obtained for the apparent activation energy in this study are in very good agreement with values reported in the literature. The apparent activation energy for creep and the coefficient  $n$  do not seem to be strongly dependent on the purity of the aluminum. However, the absolute values of the steady state creep rate are slightly higher than the values obtained by Ahlquist and Nix on 99.99% Al, at the same temperature. This can be observed in Figure 4.3. This difference could be due, in part, to

Table 4.2  
Summary of Results for Activation Energy  
and the Stress Sensitivity Coefficient

Aluminum	n	$Q_c$ (eV/at.)	$H_{sd}$ (eV/at.)	$H_c$ (eV/at.)	Reference
99.99	-	1.54			Lytton et al. (129)
99.99	-	1.63			Lee et al. (130)
99.99*	4.6	1.56			Weertman (131)
99.99*	4.3	1.40			Mishlyaev (47)
99.93	4.9	1.40			"
99.99	4.9	1.40			Tobolova & Cadek (132)
99.999			1.43		Norwick (133)
99.999			1.43		Lundy & Murdock (5)
99.999			1.39		Federighi (134)
99.9999			1.25		Fradin & Rowland (135)
99.999	4.6	1.43		1.41	This Study

\*data obtained using aluminum single crystal

$Q_c$  apparent activation energy for creep

$H_c$  apparent enthalpy for creep

$H_{sd}$  enthalpy for self-diffusion in aluminum

n stress sensitivity coefficient for the steady state strain rate

the different degrees of purity of the specimens used in this investigation and those used by Ahlquist and Nix (122).

#### 4.2.3 Stress Dependence of the Subgrain Size

During the course of this investigation, an attempt was made to use Transmission Electron Microscopy (TEM) for subgrain size determinations. Data was obtained which was in good agreement with the data reported by Orlova et al. (63), but the fine substructure was localized in certain regions of the foil. The morphology of this substructure was questioned by Ajaja (128). Subsequently, very careful TEM specimen preparation revealed a much larger subgrain structure which had the characteristic dislocation configuration usually associated with subgrains formed during high temperature creep deformation. The size observed in the electron microscope was so large that at the lowest magnification of the microscope only one to three subgrains were visible on the screen. A photomontage could be made but, in general, the thin areas produced usually accommodated no more than four subgrains. The use of TEM would therefore require preparation of a large number of foils for observations if statistically significant results were desired. Thus, it was decided to concentrate on data collected using optical microscopy even though the optical techniques have been criticized because it is difficult to distinguish the smaller subgrains (67).

In Figure 4.4 the subgrain structures observed by electron and optical microscopy in the same specimen are shown. The value  $\sim 20$  micrometers obtained by TEM is smaller than the value  $26 \pm 3 \mu\text{m}$  obtained by optical microscopy. This apparent discrepancy can be explained by considering that only a very small area of the specimen is being analysed in the TEM observation. Other areas selected randomly during observation at the electron microscope showed a larger subgrain size. Large statistical errors are certainly associated with this TEM observation. In the optical observations, statistics were improved by counting a large number of intercepts in several randomly selected areas.

To verify the behavior of the subgrain size as a function of strain, three tests were performed at  $300^{\circ}\text{C}$  and an applied stress of 8.35 MPa. The tests were interrupted at predetermined strains during the steady state stage and the specimens were quenched under load. The results obtained for the subgrain size at the interruption are shown in Table 4.3.

Table 4.3  
Values of Subgrain Size for Different Strains  
in the Steady State Region

TEST	STRAIN	SUBGRAIN SIZE ( $\mu\text{m}$ )
88	.11	36 + 4
75	.16	31 + 3
78	.25	35 + 4



Figure 4.4 (a) Transmission electron micrograph of a sample deformed at 573 K and 9.01 MPa to a true strain of 0.16. An illustration of the typical subgrain structure observed. The sample was quenched at room temperature under load to maintain the high temperature structure. Magnification = 3500 X

These results show that the subgrain size does not seem to vary with strain during the steady state stage.

To determine the stress dependence of the subgrain size, creep tests were performed at several stresses at 573 K. Samples were strained to a true strain of 0.16 which, as shown in the previous chapter, corresponds to steady state behavior for the stresses used. At this strain, each test was interrupted and the specimen water quenched to room temperature under the applied stress. The values obtained for the subgrain size are shown in Table 4.1.

To determine the correlation between  $\lambda$  and the applied stress, Equation 2.12 is used. A log-log plot of the subgrain size versus the applied stress yields both the values of B and m. This procedure is applied to the data in Table 4.1 and the resulting curve is shown in Figure 4.5. Included in the figure are results obtained by McLean and Farmer (52) and Servi et al. (136) to permit a comparison. As can be seen, the data obtained in this study are in very good agreement with data found in the literature. A best fit of the experimental points by a straight line yields the values:

$$m = 1.1 \pm 0.1 \text{ and } B = 3.65 \times 10^2 \text{ N/m}^2.$$



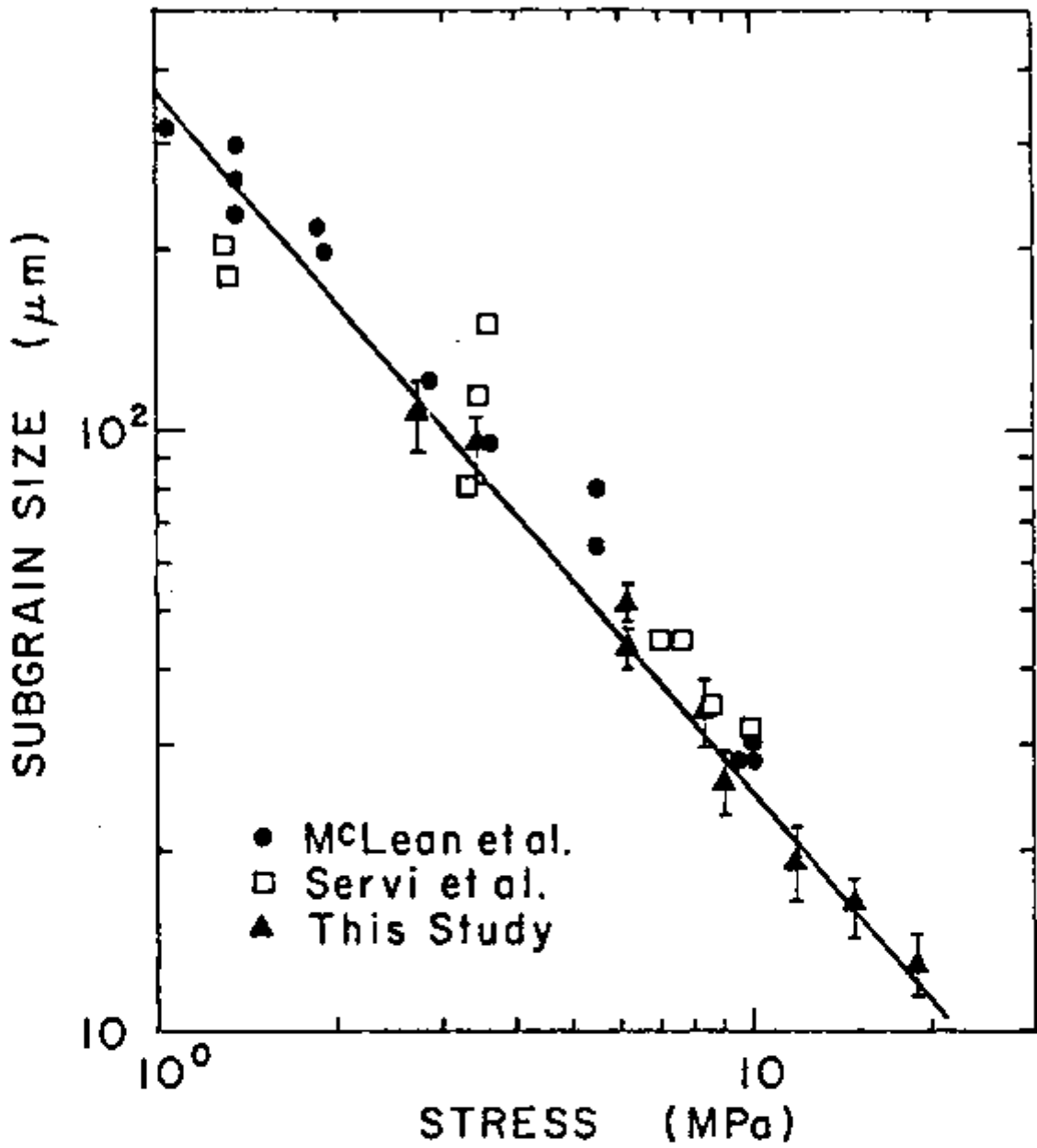


Figure 4.5 The variation of subgrain size in the steady state stage as a function of applied stress. The error bars shown for the data obtained in this study indicate 95% confidence limits.

### 4.3 Summary and Conclusions

In this chapter, the steady state creep parameters for high purity aluminum were analysed in terms of the applied stress and temperature. For applied stresses such that  $\dot{\epsilon}_s / D < 10^9 \text{ cm}^{-2}$ , the stress sensitivity coefficient obtained was  $n = 4.6 \pm 0.2$ . An activation energy for creep  $Q_c = 1.43 \pm 0.05 \text{ eV/at.}$  was obtained. The values obtained for  $n$  and  $Q_c$  were shown to be in excellent agreement with reported values for aluminum. No significant variation of these parameters was observed that could be related to the purity of the aluminum used.

A study of the stress and strain dependence of the subgrain size developed during the secondary creep stage was also performed. No measurable variation of the subgrain size during the secondary stage was observed. The stress dependence of the subgrain size obtained,  $m = 1.1 \pm 0.1$ , was seen to be in excellent agreement with reported values for aluminum of lower purity.

The magnitude of the transient strain in the primary stage increased with an increase in the applied stress. A strain of 0.16 was chosen as the strain at which reductions in stress were to be performed (refer to Chapters 5 and 6). This strain corresponds to steady state behavior for all stresses used in this study.

## CHAPTER V

### TRANSIENT CREEP EXPERIMENTS

#### 5.1 Introduction

The behavior of the creep strain versus time following a reduction in stress is a matter of controversy in recent literature. The reason for this controversy is the lack of substructural observations following the stress reduction. For example, the assumption is usually made that the subgrains grow after a stress change, but very few experiments proving the validity of this have been reported.

In this chapter, the influence of subgrain size on creep rate is analysed using results obtained in stress reduction tests. Constant stress tests, performed at a certain initial applied stress, are used to introduce a subgrain structure in the specimen. At a true creep strain of 0.16, the applied stress is reduced and the strain, strain rate and subgrain size are analysed as a function of time after the stress reduction. The influence of the initial and reduced stresses is discussed.

#### 5.2 Results and Discussion

Constant stress creep tests were conducted by deforming similar samples at 573 K and initial applied stresses,  $\sigma_I$ , of 15 MPa, 8.35 MPa, and 6.23 MPa to a true creep strain of 0.16. As shown in the previous chapter, a strain of 0.16 corresponds to steady state

creep conditions for all initial stresses used. At this strain of 0.16, the stress was reduced to 3.44 MPa by rapidly removing a portion of the applied load, as described in Chapter 3.

A typical strain time curve obtained after stress reduction from 6.23 MPa to 3.44 MPa is shown in Figure 5.1. As shown in this example, the creep strain rate decreases from an initial value  $\dot{\epsilon}_1$ , obtained immediately following a reduction in stress, to a minimum value  $\dot{\epsilon}_2$  for a brief interval of time. Thereafter, the creep rate increases and if the reduced stress is maintained sufficiently long, the steady state creep rate for the reduced stress is reached. The form of the creep curves obtained after stress reduction coincides, in general, with that described by Raymond et al. (137).

Figure 5.2 shows the total transient creep curves obtained after stress reductions from 15, 8.35, and 6.23 MPa to 3.44 MPa. The strain rates as a function of time after the stress reduction determined by measuring the slopes of the strain-time curves, are shown in Figure 5.3. As can be seen, the strain rate immediately after the stress reduction first decreases, then gradually increases, approaching the steady state value which would be obtained at the reduced stress. Also, the initial interval of time in which  $\dot{\epsilon}$  decreases is increased when the initial applied stress is increased. Several photographs of the specimen taken at various stages of the experiment are shown in Figure 5.4. As can be seen, no necking was visible for total true strains below 0.28, but at strains of this magnitude the sample surface was rough and uneven, making it extremely difficult to deter-

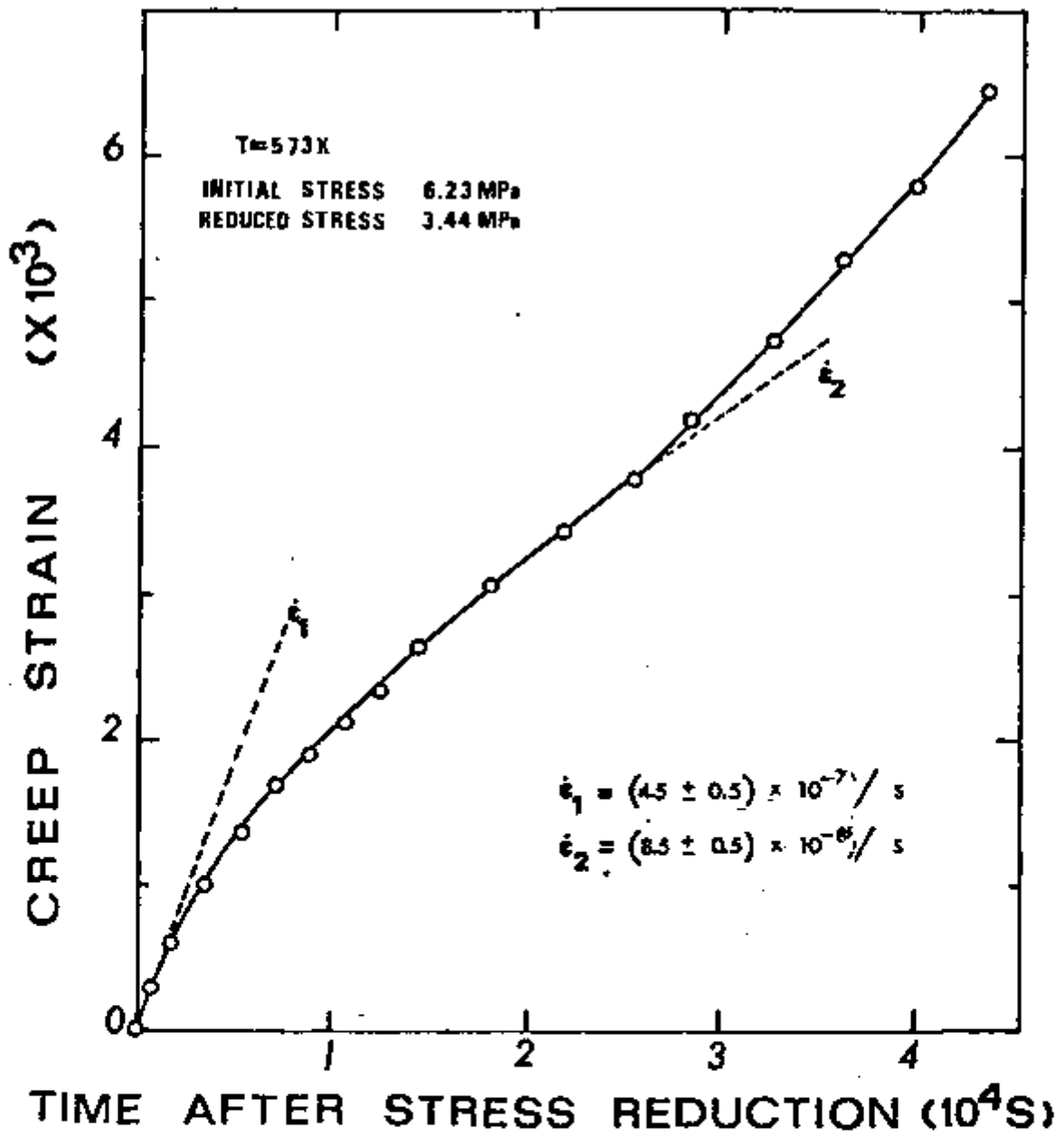
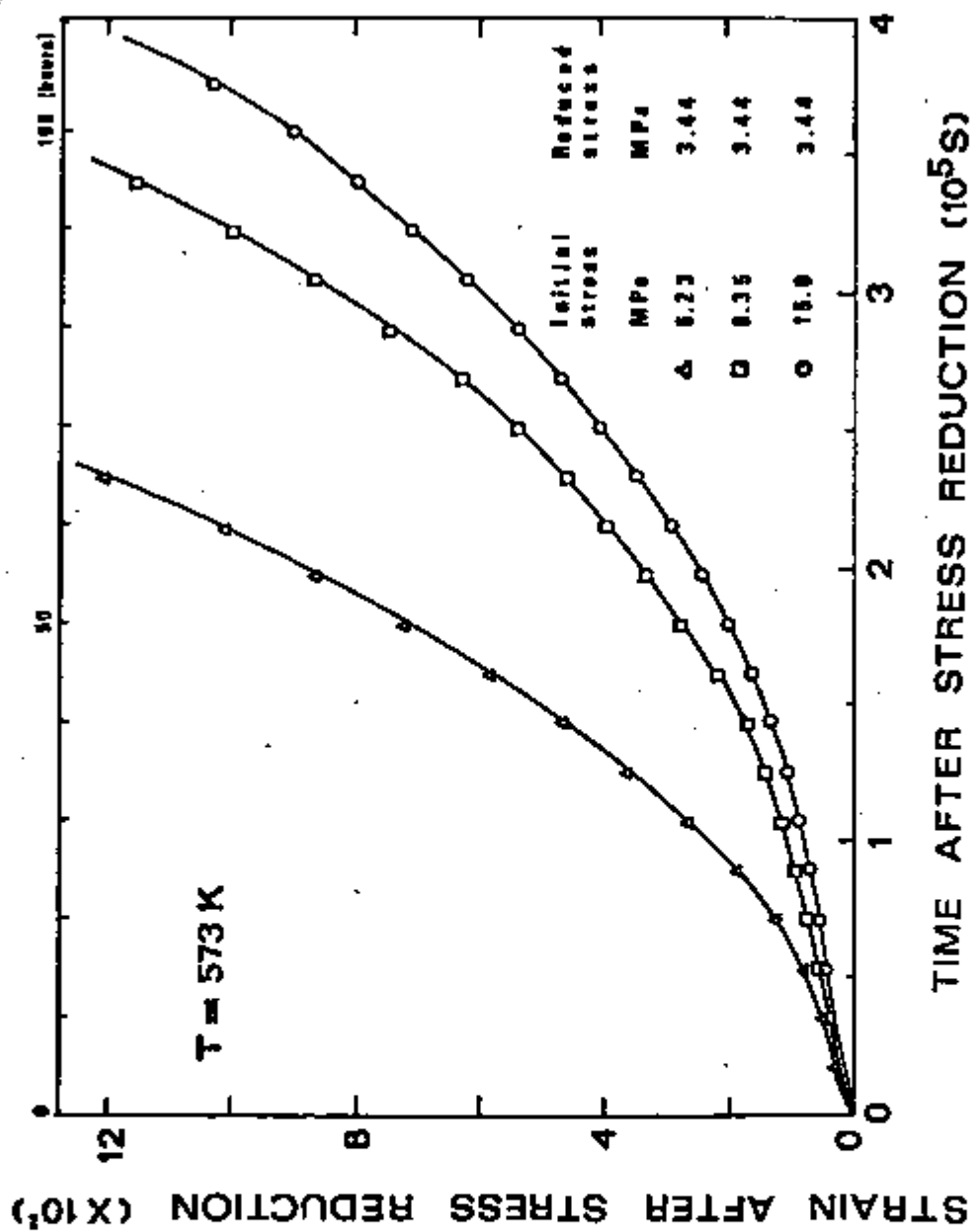


Figure 5.1 Typical creep transient curve obtained at 573 K after a stress reduction from 6.23 MPa to 3.44 MPa



**TIME AFTER STRESS REDUCTION ( $10^5 \text{ S}$ )**

Figure 5.2 Strain-time curves illustrating typical behavior after stress reductions from 15 MPa, 8.35 MPa and 6.23 MPa to 3.44 MPa. The stress was reduced at a true strain of .16 in each case.

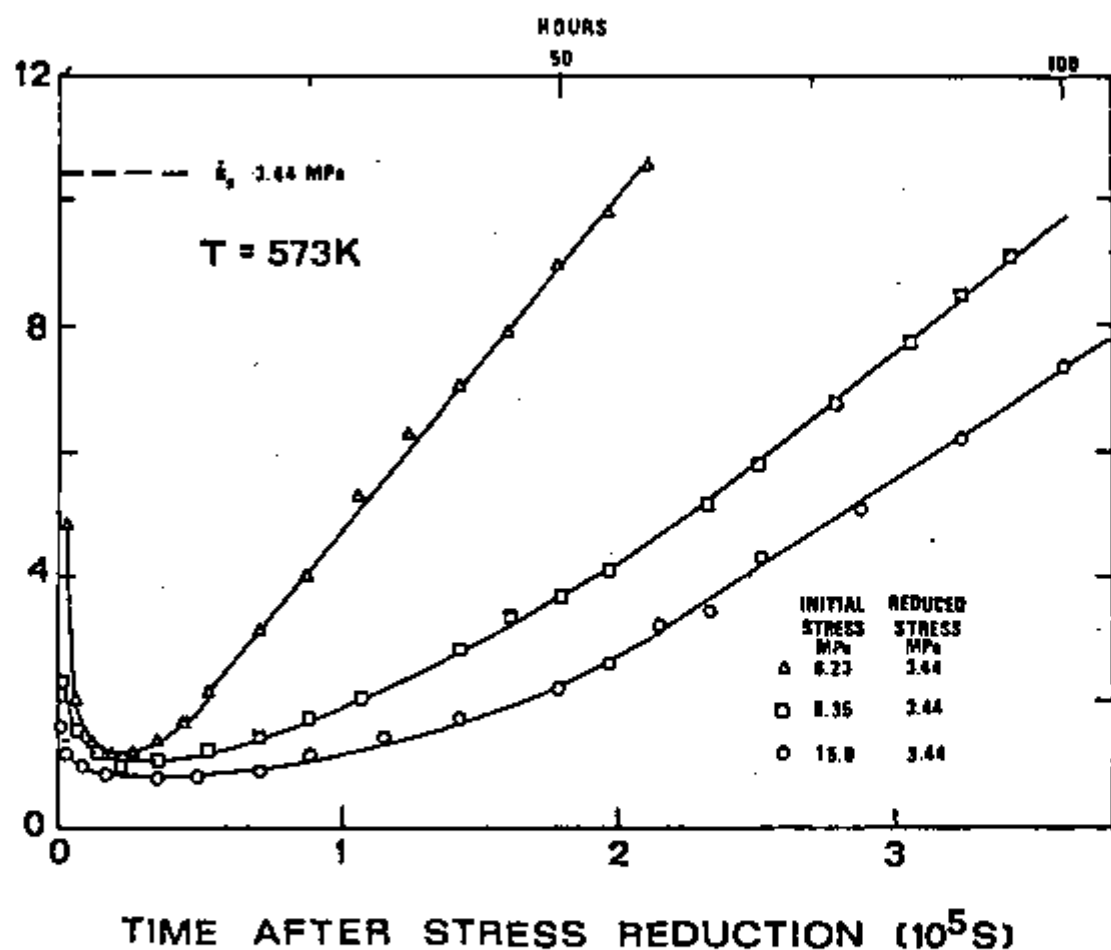
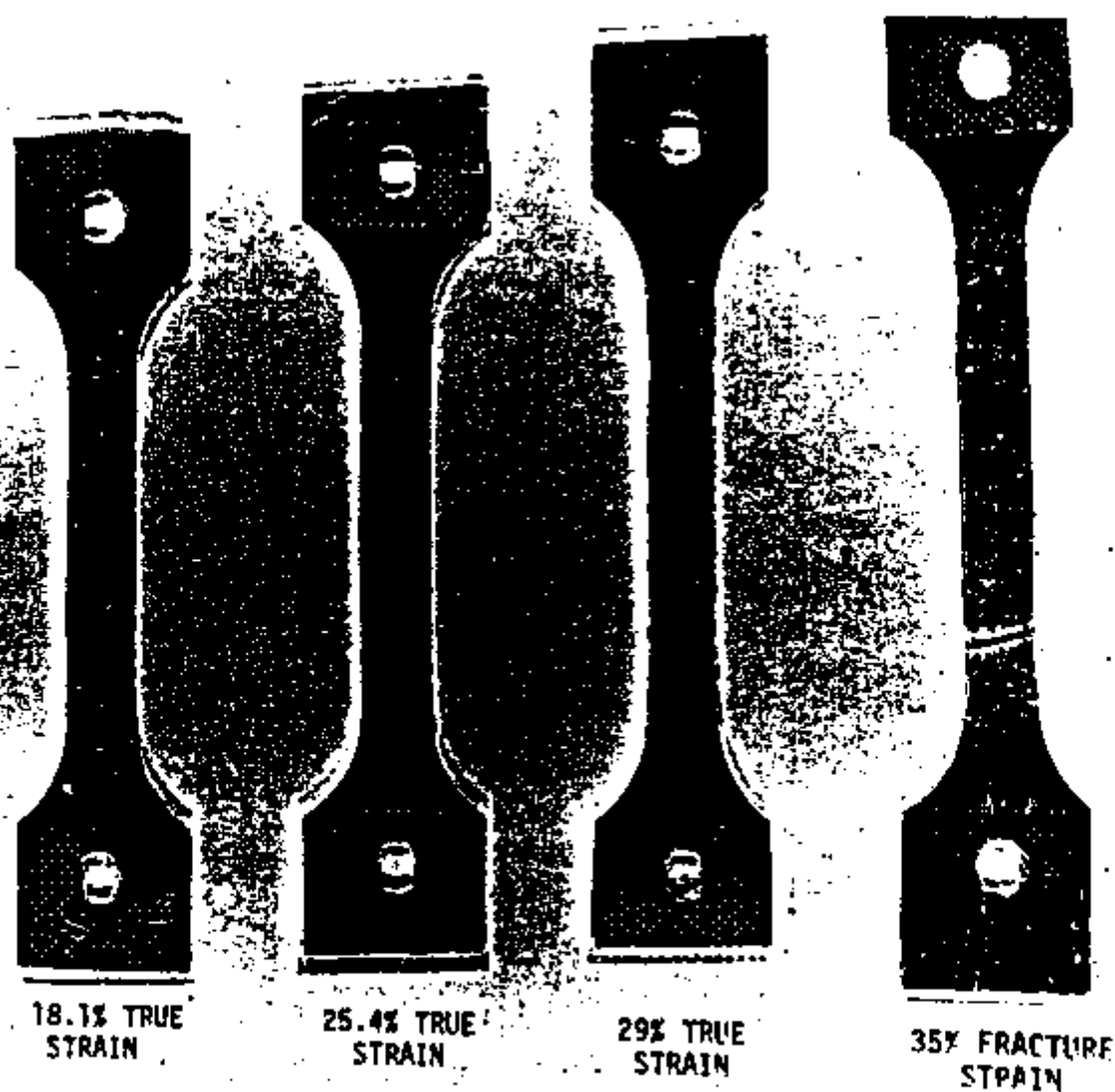


Figure 5.3 The variation in strain rate as a function of time after a stress reduction for initial stresses of 15 MPa, 8.35 MPa and 6.23 MPa reduced to 3.44 MPa at a true strain of 0.16 in each case.



5.4 Macrophotograph of the specimens at several stages of creep strain



mine when necking occurred. For total true strains greater than 0.28, the measured strain rates at 3.44 MPa were higher than the steady state strain rate at 3.44 MPa, but necking was clearly observed in these samples.

The variation in subgrain size as a function of time following stress reductions is shown in Figure 5.5. These data clearly show that the subgrain size increases after stress reductions, approaching the subgrain size that would be obtained during steady state deformation at 3.44 MPa. This increase in subgrain size is accompanied by an increase in creep rate. This effect is clearly illustrated in Figure 5.6, which shows log strain rate vs log subgrain size for samples which have been held at the test temperature for increasingly longer times after the stress reduction. This figure also shows that, except for the period of time in which the strain rate decreases, the instantaneous creep rate can be correlated to the subgrain size in the specimen by the equation

$$\dot{\epsilon}(t) \Big|_{\sigma, T} = A \lambda^p(t) \quad (5.1)$$

in which  $A$  is a function of the reduced stress and temperature and  $p$  is a constant. The values of  $A$  and  $p$ , determined by a straight line best fit of the experimental points are:  $A = 1.36 \times 10^2 \text{ s}^{-1} \text{ m}^{-2}$  and  $p = 2$ .

These experiments clearly show that the subgrain size in high purity aluminum increases after a stress reduction. This supports

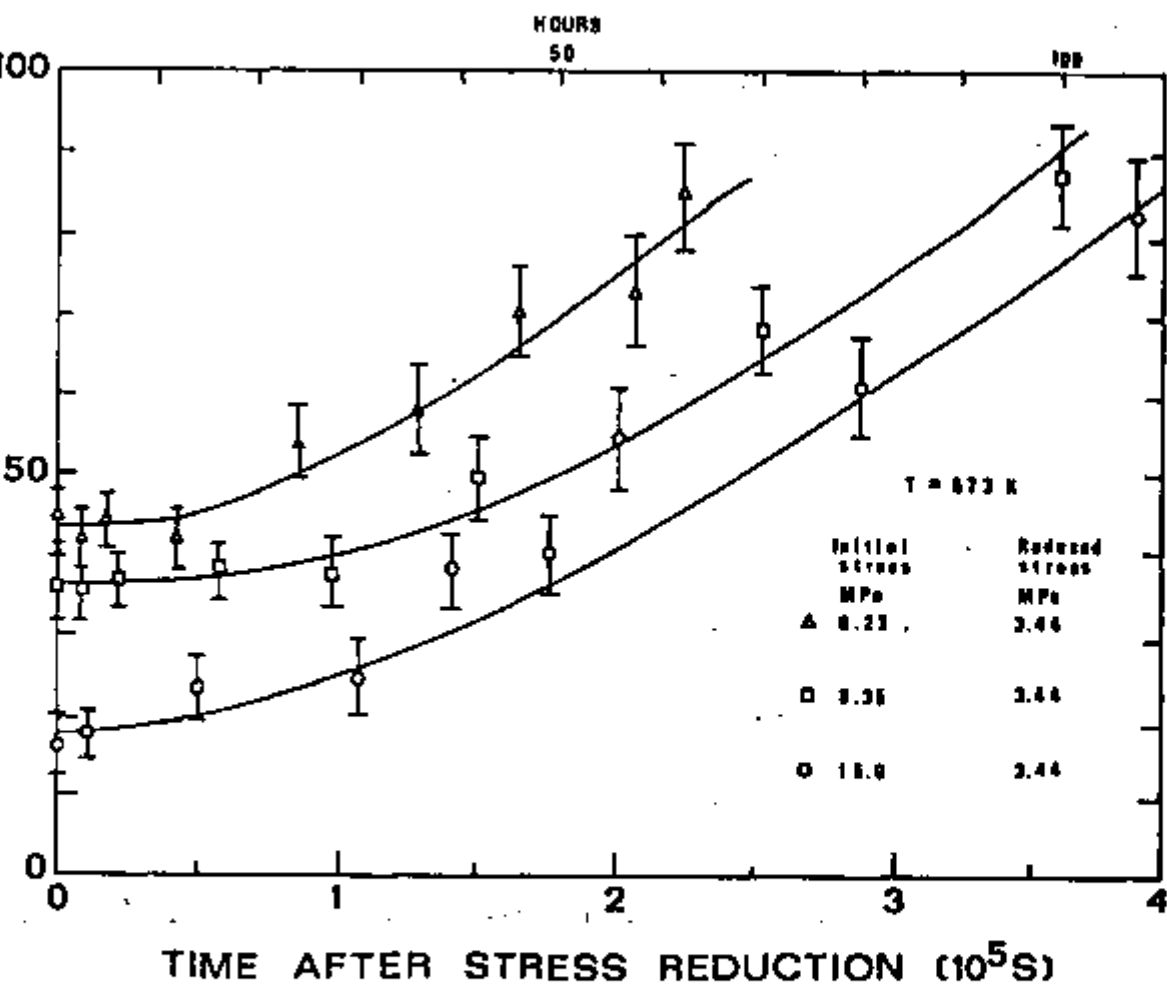


Figure 5.5 The variation of subgrain size as a function of time for initial stresses of 15 MPa, 8.35 MPa and 6.23 MPa reduced to 3.44 MPa at a true strain of 0.16. The error bars indicate 95% confidence limits

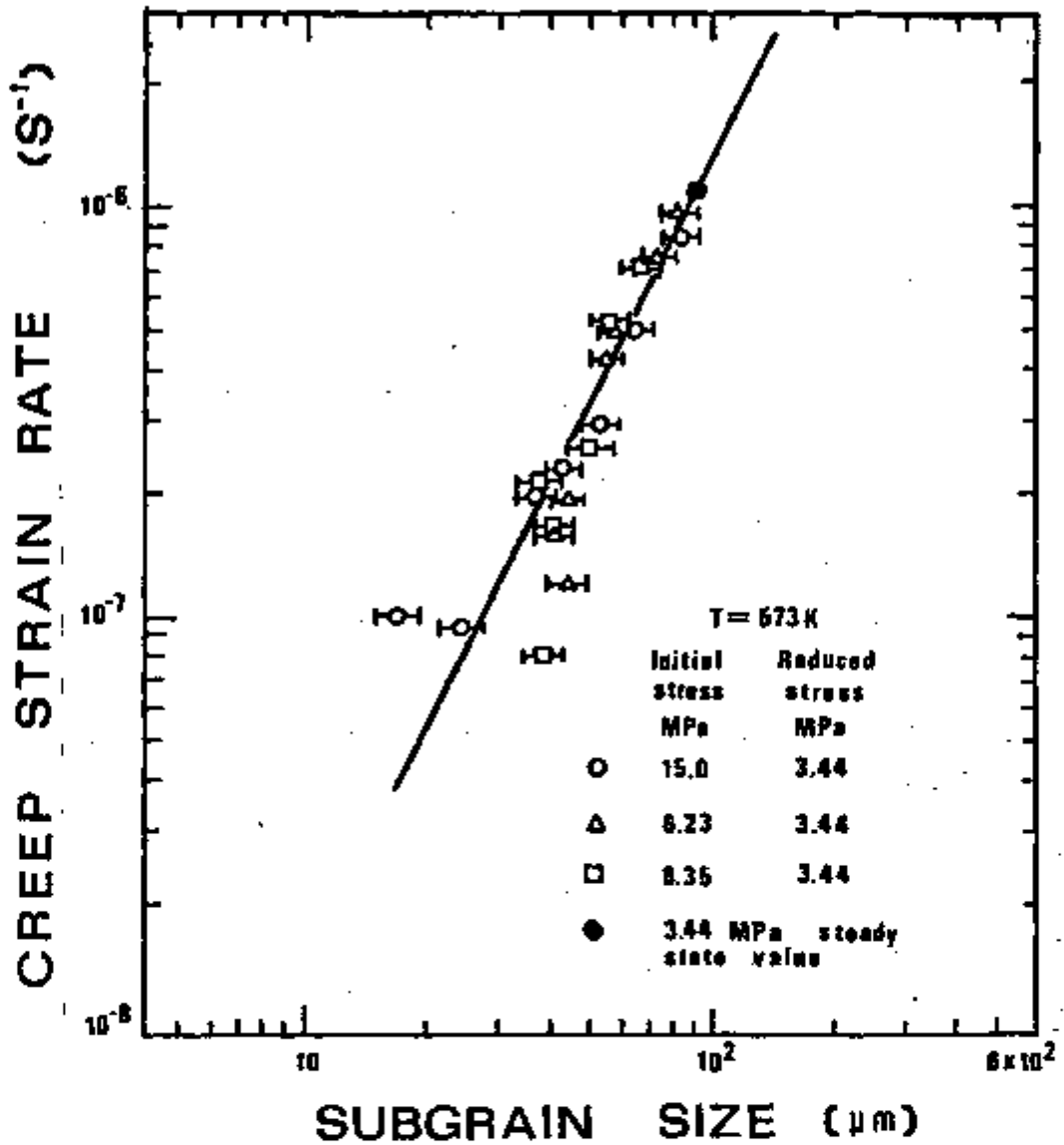


Figure 5.6 Strain rate vs subgrain size for samples which have been subjected to a stress reduction from 15 MPa, 8.35 MPa and 6.23 MPa to 3.44 MPa and allowed to deform at the reduced stress for differing time intervals. The strain rate is measured just before the test is interrupted for subgrain size measurements. The data for a sample deformed well into the steady state region at 3.44 MPa and not subjected to a stress reduction is shown for comparison.

the assumptions made by Sherby and his coworkers (1,2,3) and expressed in Equations 2.28 and 2.31, but is in disagreement with the observations of Pontikis and Poirier (108) and of Parker and Wilshire (109). This study also shows that a significant amount of strain after the stress reduction is required for the subgrain size readjustment, thus confirming the suggestion by Miller et al. (138); in a recent publication these authors analysed the data published by Pontikis and Poirier (108) and Parker and Wilshire (109) and suggested that large strains after the stress reduction would be required for subgrain growth to be observed. The data published by Parker and Wilshire indicates that the strain-time-subgrain size measurements were conducted for approximately 3600 sec. after the stress reduction, which corresponds to a strain after stress drop of 0.5%. This study clearly shows that no change in subgrain size in pure aluminum would be observed after a strain of 0.5%, as obtained by Parker and Wilshire after the stress reduction.

The data published by Pontikis and Poirier (108) indicates that they studied the strain-time subgrain size behavior under load, after reductions in stress, for approximately 50 hours and did not observe a change in subgrain size even though the strain rate increased. The lack of structure variation in the experiments of Pontikis and Poirier is confusing for the following reasons. First, it is difficult to rationalize the large amount of plastic flow, which occurred at the reduced stress, without a change in structure. Second, a criticism may be made concerning the technique of sequential stress

changes on a single sample used in the tests by Pontikis and Poirier. The initial steady state creep rate and hence structure are not allowed to re-establish before each stress change. Instead, the stress reductions were performed from an increased stress level without allowing sufficient time for the steady state structures and rates to develop. This makes it difficult or even dubious for a comparison of creep rates after the stress reductions of Pontikis and Poirier with creep rates obtained after the stress reduction from the same original structural conditions. This might also be the reason why the final creep rate obtained by Pontikis and Poirier, after the stress reduction, was lower than the creep rate observed in a continuous test performed at the reduced stress (refer to Figure 2 of reference 108). Third, the fact that ionic solids behave in a different fashion than metallic solids cannot be completely rejected. In ionic crystals, creep anomalies associated with bonding and charge neutrality often occur:

- 1) The stress dependence of the subgrain size is observed to be very low, for example, Streb (139) obtained data which show  $\lambda \propto \sigma^{-1/2}$ ;
- 2) A strong temperature dependence of the subgrain size is observed and is unexplained (139). It seems thus more reasonable to view the lack of subgrain growth in the experiments of Pontikis and Poirier as either the result of anomalies in creep behavior or the effects of the complex thermomechanical history of the sample than to reject the ideas of Sherby and coworkers (1,2,3).

One conclusion that can be drawn from these experiments is that the deformation at a higher stress definitely strengthens high purity

aluminum as the stress is reduced. This can be understood if it is noted that the creep rates after the stress reductions are much smaller than the steady state creep rate at the reduced stress. Only subgrain coarsening can increase the creep rate.

It appears very reasonable at this point to continue this investigation on the lines suggested by Equation 2.31. According to this equation, when temperature and stress are maintained constant, the instantaneous creep rate must be a function exclusively of the subgrain size. This is shown to be true by the excellent correlation obtained in Equation 5.1. The same reasoning can be utilized if the temperature and subgrain size are maintained constant. In this case, Equation 2.31 reduced to

$$\dot{\epsilon} \Big|_{\lambda, T} = A \sigma_R^N \quad (5.2)$$

where A is a constant at  $\lambda$  and T constants,  $N = 7$ . One way to check Equation 5.2 is to perform a series of stress reductions to various reduced stresses, correlating the results obtained for each reduced stress by Equation 5.2. If coherent results are obtained, i.e., if correlation 5.1 continues to exist, it is possible to cross-plot the data at constant subgrain size to determine the stress dependence at constant subgrain size. This investigation follows.

To eliminate the influence of the initial stress, all specimens were initially deformed at a constant temperature of 573 K and at the same applied stress of 15 MPa. Each stress reduction was performed at a strain of 0.16 to safely maintain the same initial

structure in the specimens. The stress was reduced to 6.23 MPa and 8.35 MPa and the strain rate-time-subgrain size relationship analysed. The strain-time curves obtained after these stress reductions are shown in Figure 5.7. The strain rates as a function of time, determined by measuring the slopes of the strain-time curves, are shown in Figure 5.8. The same general behavior, i.e., the instantaneous creep rate following the stress reduction, decreases at first, then continuously increases toward the steady state strain rate at the reduced stress. The period of time in which the instantaneous creep rate decreases becomes smaller when the reduced stress is increased. A series of micrographs of the structure obtained is shown in Figure 5.9 to illustrate the subgrain-strain behavior following a stress reduction. The corresponding variation in subgrain size as a function of time following the stress reductions is shown in Figure 5.10. In Figure 5.11, the correlation obtained between the instantaneous creep rate and subgrain size is shown. The same strain-rate-subgrain dependence is obtained, that is,  $p = 2$  for all reduced stress levels. The results of cross plotting the values of the instantaneous creep rate at constant subgrain size versus the reduced stress is shown in Figure 5.12. For the various subgrain sizes selected, a correlation of the form of equation 5.2 is obtained in which  $N = 6.8 \pm 0.2$ . If the following values:

$$D(573 \text{ K}) = 8.82 \times 10^{-18} \text{ m}^2/\text{s} \quad (5)$$

$$E(573 \text{ K}) = 5.698 \times 10^{10} \text{ N/m}^2 \quad (4)$$

$$b = 2.86 \times 10^{-10} \text{ m (Room Temperature)}$$

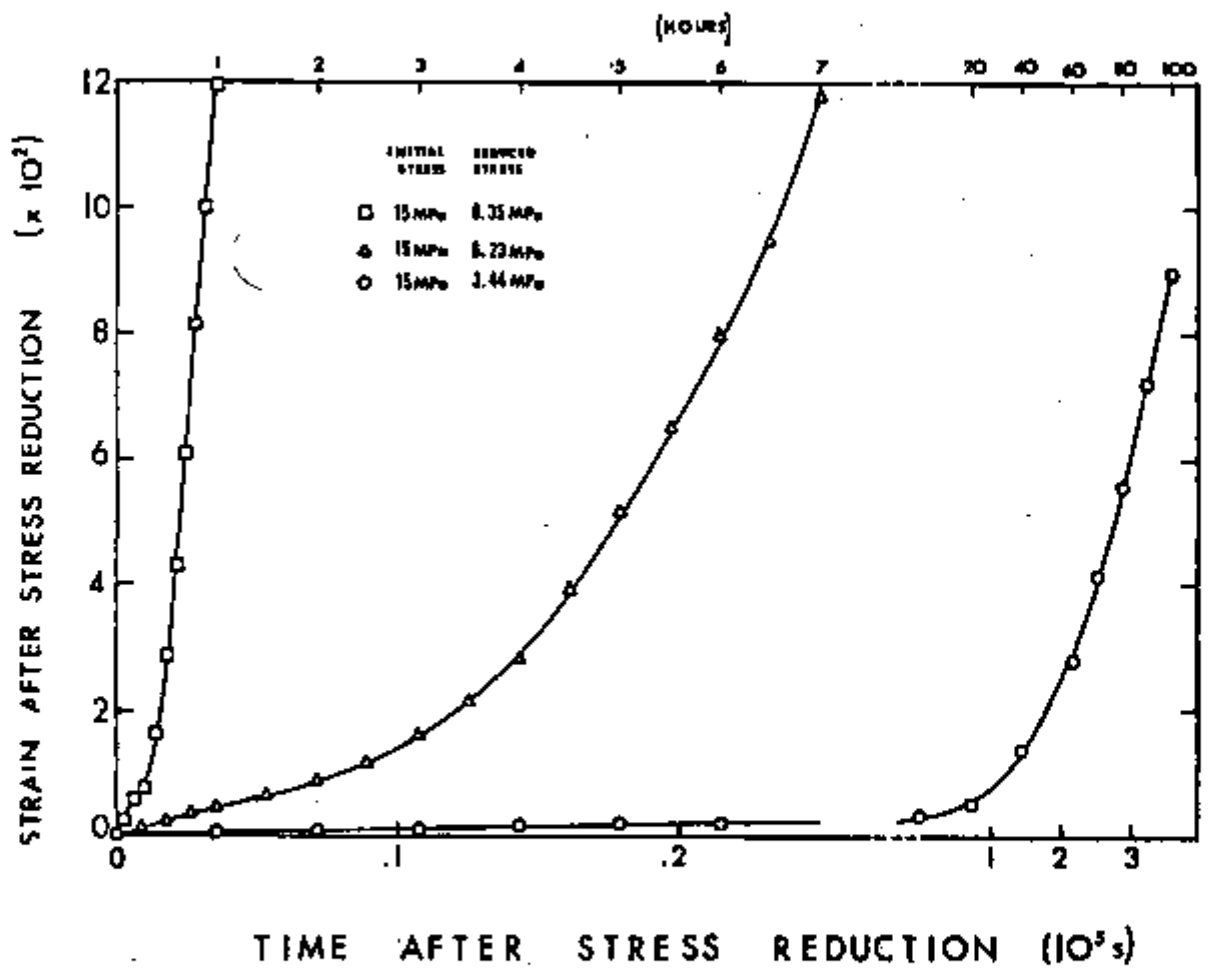


Figure 5.7 Strain-time curves illustrating typical behavior after stress reduction for an initial stress of 15 MPa and reduced stresses of 8.35 MPa, 6.23 MPa and 3.44 MPa at 573 K.



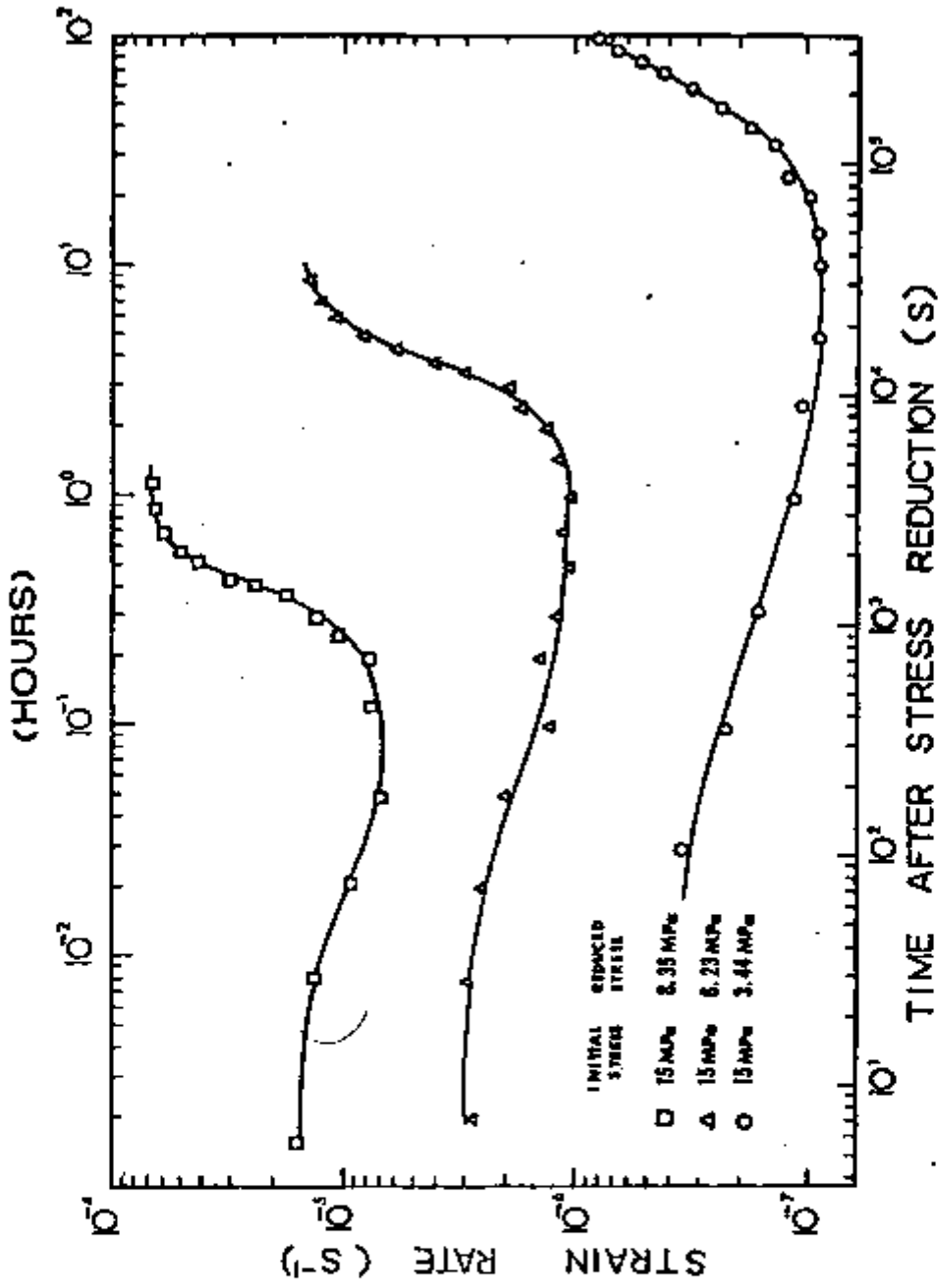


Figure 5.8 The variation of strain rate as a function of time after stress reduction for an initial stress of 15 MPa and reduced stresses of 8.35 MPa, 6.23 MPa and 3.44 MPa.



Figure 5.9 (b) Magnification = 240 X

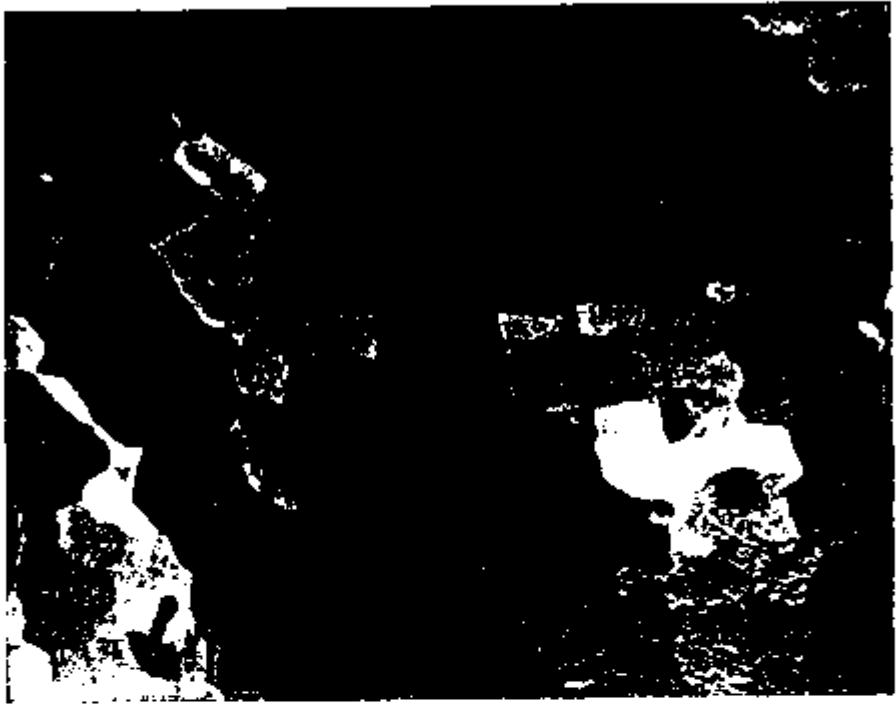


Figure 5.9 (b) - Mag. = 240 X

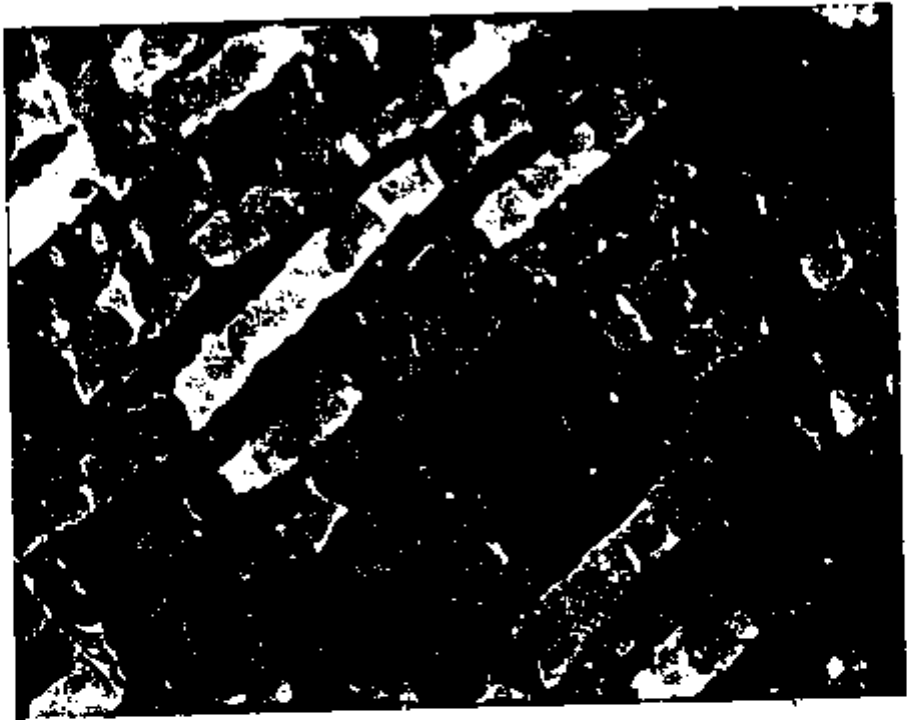


Figure 5.9 (c)      Mag. = 147 X

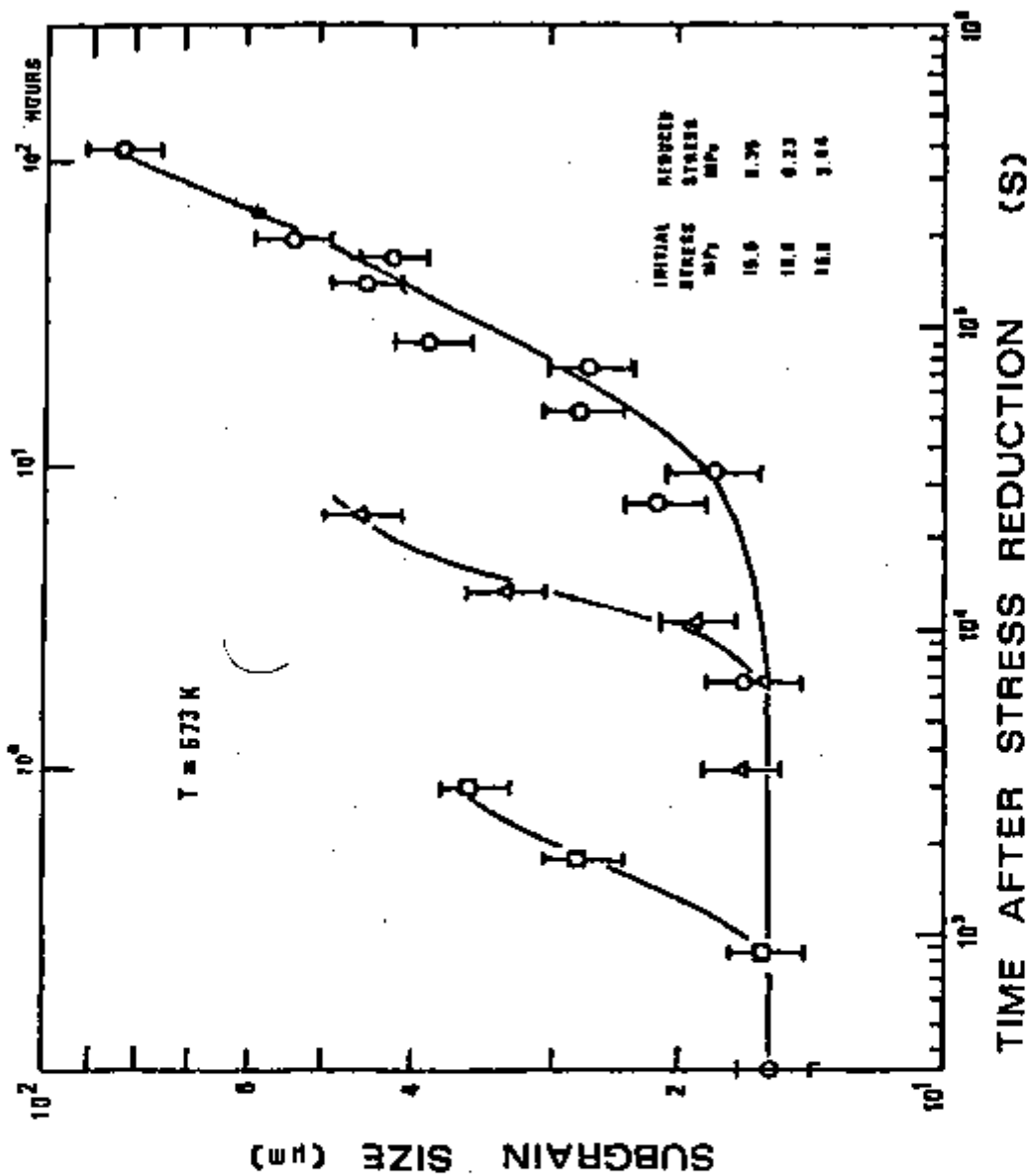


Figure 5.10 The variation of the subgrain size as a function of time after stress reduction for an initial stress of 15 MPa reduced to 8.35 MPa, 6.23 MPa at a true strain of 0.16. The error bars indicate 95% confidence limits.

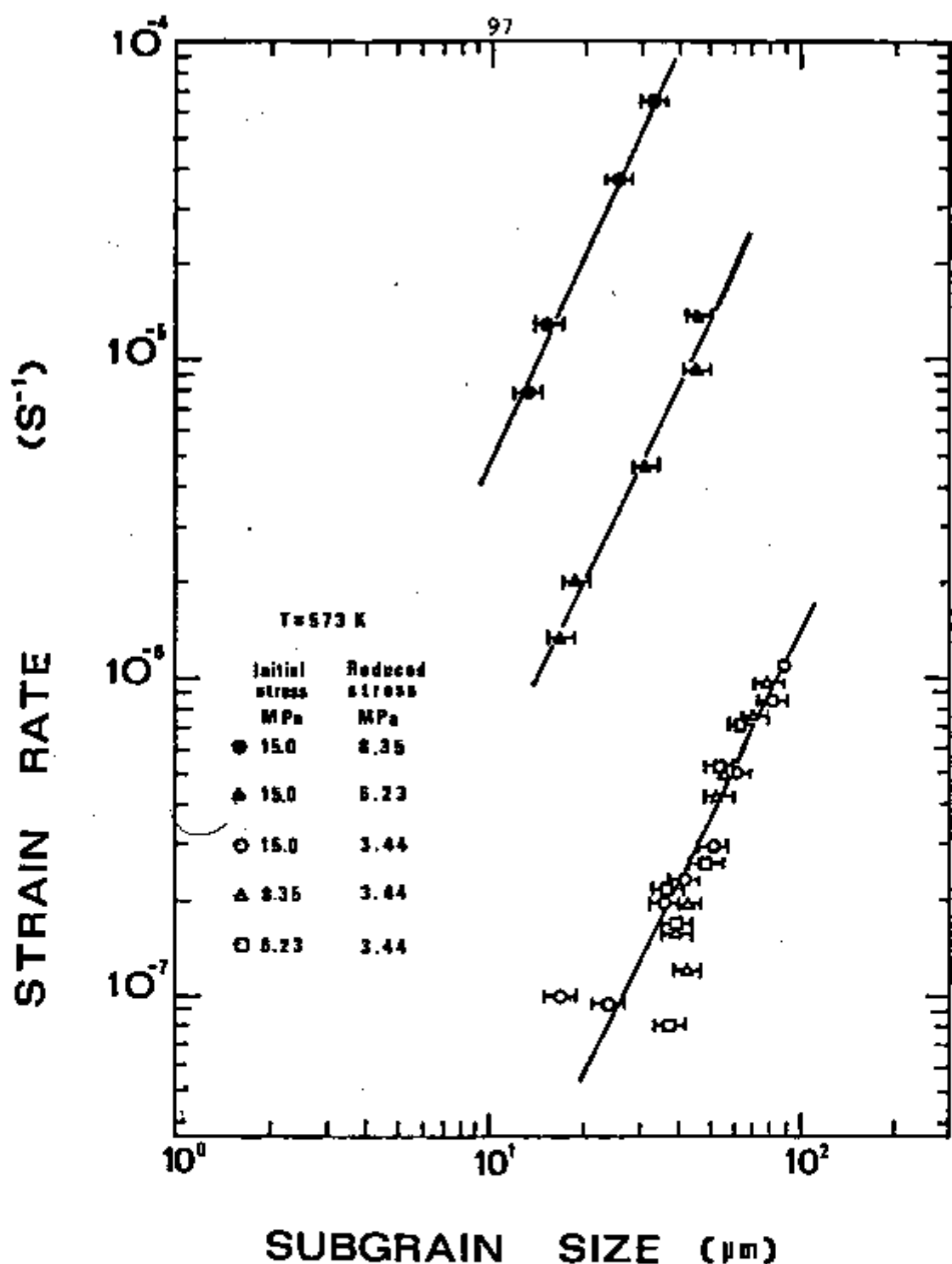


Figure 5.11 Strain rate vs subgrain size for samples which have been subjected to a stress reduction from a certain initial stress to a reduced stress and allowed to deform at the reduced stress for differing time intervals.

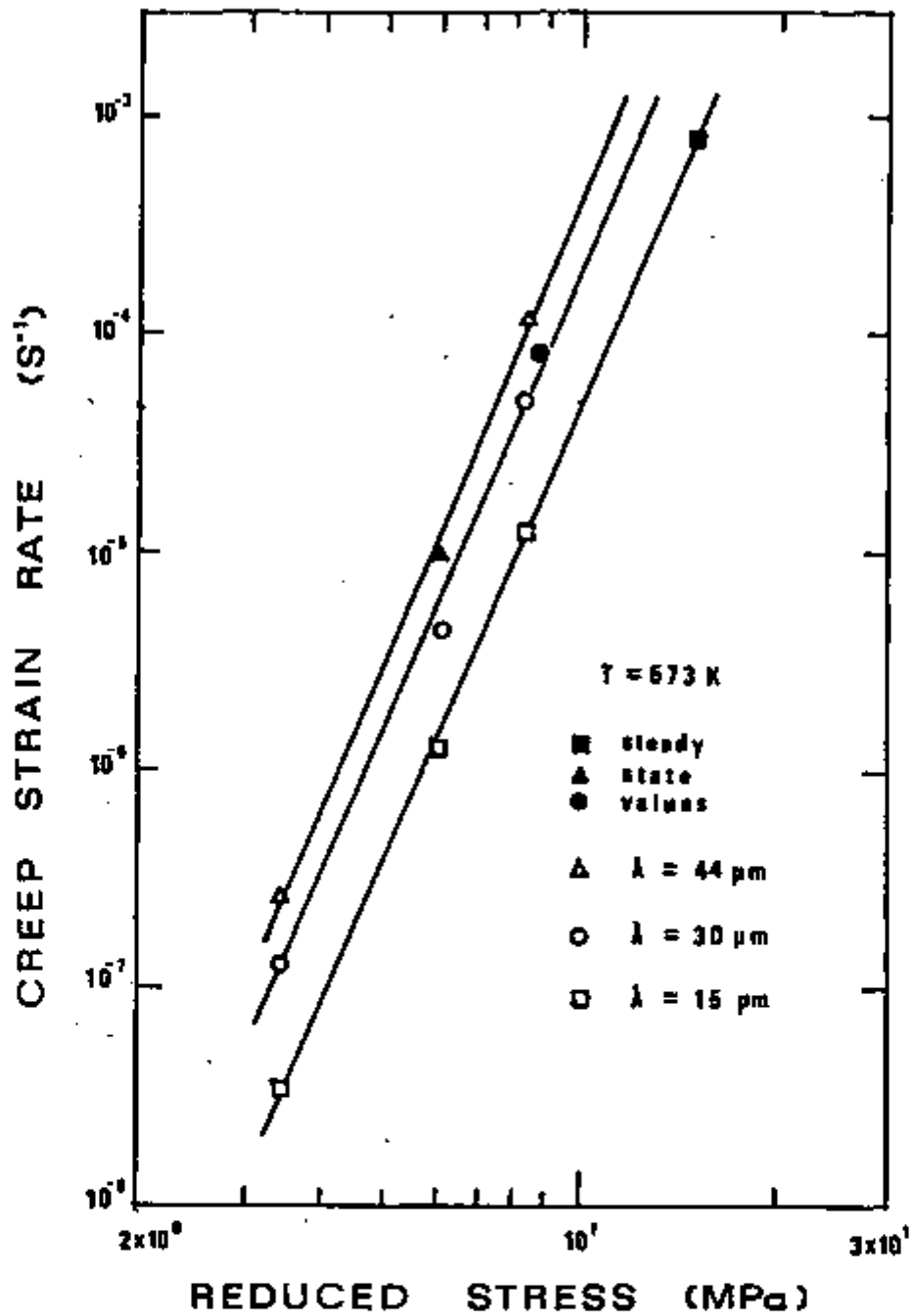


Figure 5.12 Creep strain rate vs the reduced stress at constant subgrain size  $\lambda$

are used, the data in this study may be described by the equation:

$$\dot{\epsilon} = 1.1 \times 10^9 (D/b^2) (\lambda/b)^2 (\sigma/E)^{6.8 \pm 0.2} \quad (5.3)$$

Equation 5.3 reduces to Equation 2.5 when the stress dependence of the subgrain size during the steady state stage is used, that is, Equation 2.12 with  $m = 1.1 \pm 0.1$ , and  $n = N - p = 4.6$ .

The fact that the values  $N = 7$  and  $q = 2$ , found in this investigation, differ from the values  $N = 8$  and  $q = 3$  reported by Sherby, Klundt and Miller (3), requires additional comment. To obtain the values of  $N$  and  $q$ , Sherby, Klundt and Miller utilized strain rate and subgrain size data reported by several authors on 99.99% Al. The approach used involves the correlation of the strain rate, measured immediately after a stress reduction (constant structure test), and the subgrain size. Since the data used were obtained at various stresses and temperatures, a normalization of the data was necessary; the strain rate data were normalized to a common temperature of 530 K by multiplying the creep rate by  $D(530 \text{ K})/D(\text{Test})$  and the stress data were normalized for the modulus variation with temperature by multiplying the stresses by  $E(530 \text{ K})/E(\text{Test})$ . In this study, a different approach is adopted, that is, the instantaneous creep rate during the transient period following a stress reduction is correlated to the subgrain size present in the specimen. All subgrain size data and strain rate data are obtained utilizing the same material (99.999% Al) under identical experimental conditions.



In the S-K-M study, variables such as grain size of the specimens, strain at which the stress reduction is performed, apparatus sensitivity and the specimens themselves may have influenced the final results.

### 5.3 Theoretical Analyses of the $\lambda^2$ and $\sigma^7$ Terms

At this point, an attempt is made to identify the  $\lambda^2$  strain rate-subgrain size dependence observed in this study using existing theoretical models. A number of models of high temperature creep in pure metals will be briefly considered in this section. Models have been presented on the basis of climb of edge dislocations generated by Frank-Read sources (25,28,96), the glide of jogged screw dislocations (26), the growth and stability of a three-dimensional Frank network of dislocations (88,89,90) and others. As discussed in Chapter II, these models generally do not explicitly include the subgrain size or subgrain boundaries in the formulation of a rate equation. However, the excellent correlation obtained in this study, between the instantaneous creep rate and the subgrain size during transient creep clearly shows that the subgrains do play an important role during the creep process.

A first approach to understanding the  $\lambda^2$  term would associate it with a slip plane area. In the 1955 and 1957 theories proposed by Weertman and in a later modification of the previous models (80), the author describes the creep rate as  $\dot{\epsilon} = R\lambda b$ , where  $R$  is the rate of generation of dislocations,  $A$  is the slip plane area swept out by a dislocation from generation to annihilation or immobilization,

M is the density of Frank-Read sources and  $b$  is the Burgers' vector for the dislocation generated. The approach being used would imply the association of  $\lambda^2$  with the A term, since both have the same dimension. In the 1955 model, the A term is expressed by the product of  $LL'$ , where  $L$  is the grain size and  $L'$  is the average subgrain size at the applied stress; thus, the A term in this model does not have the same character as  $\lambda^2$ . In the 1957 model, the creep rate obtained is proportional to  $L^2$ ,  $L$  being now the width of a dislocation pile-up group. However,  $L$  is not explicitly identified with subgrain dimensions in this case. In a later model, Weertman (80) describes the creep rate as proportional to  $L/\log L$  where  $L$  now is the radius of a dislocation pillbox, with radius  $L$  and thickness  $d$ , in which a single dislocation source is operating; this dependence also cannot be associated with  $\lambda^2$ . In the jogged screw dislocation model, the creep rate is proportional to  $L^2/\log L$  where  $L$  is now the subgrain size, but in this case the subgrain size term varies more slowly than  $L^2$  due to the  $\log L$  divisor.

The effect of subgrains on the creep rate has also been examined theoretically by Weertman. Applying the Nabarro-Herring analyses to idealized subgrains, the author obtains a strain rate proportional to  $D/L^2$ . Although this prediction is normal for N-H creep, that is, creep at very high temperature and low stresses, the stress dependence and subgrain size dependence are not consistent with the findings of this study.

In a model proposed by Ivanov and Yanushkevich (84), the subgrain boundaries are assumed to work as sinks for dislocations generated in the subgrain interior. The creep rate is expressed by the product

$$\dot{\epsilon} = L^2 t^{-1} b (L/h) L^{-3} \eta \quad (5.4)$$

where  $\eta$  is an orientation factor,  $L^2$  is the area swept out by a dislocation loop that expands to the subgrain boundary,  $b$  is the Burgers vector,  $t$  is the time required to annihilate a dislocation loop segment that enters the boundary,  $L/h$  is the number of annihilating dislocation segments of length  $L$  in a subgrain boundary, and  $L^{-3}$  is the number of subgrains per unit volume. In this model, the area swept by the dislocation is identified as the square of the subgrain size. The model has a remarkable point, that is, the subgrain size  $L$  actually drops out of the final equation. However, the expression gives only a power of three for the steady state creep rate stress dependence. In a modification of Ivanov and Yanushkevich creep analyses, Weertman (86) considers the subgrain boundaries to act as barriers and sinks to a group of piled up dislocations. Again the area swept by a dislocation is identified with the square of the subgrain size. The model gives a final expression for the strain rate

$$\dot{\epsilon} = K (D/b^2) (L/b)^3 (\sigma/E)^6 \quad (5.5)$$

where  $L$  is now the subgrain size. This equation resembles Equation 5.3 found in this study, i.e., at constant stress the strain rate is a power function of the subgrain size and at constant subgrain size, a higher stress dependence is obtained. The approach presents some difficulties:

- a) pile-ups of dislocations are not observed in experiments
- b) at steady state, the equation gives a power of three for the stress dependence.

Weertman discusses these two points and gives reasons for the fact that pile-ups are not observed experimentally. He concludes that to improve the model a subgrain wall thickness has to be included in the treatment. This requires a further assumption, not based on experimental findings, that the subgrain wall thickness is not stress dependent (85).

A second possibility is that the area term associated with  $\lambda^2$  is not a slip plane area, but an interface area such as the subgrain surface area. This treatment would lead to a different line of reasoning, involving the role of subgrain surface as source and or sinks of dislocations. In a model recently proposed by Ilchner (16), the subgrain boundaries are considered to be strong obstacles to dislocation movement (impenetrable wall). Dislocation generation is assumed to occur mainly by dislocation interactions within the subgrains (volume reaction) and dislocation annihilation assumed to occur mainly by reaction with subgrain walls (surface reaction). Although an analytical expression for the strain rate is not given,

it is suggested that the strain rate is proportional to the rate of dislocation annihilation. This implies that the creep rate is proportional to the area of subgrains. In this model, the structural adjustment following a stress change is understood to occur through an increase in subgrain size. The  $\lambda^2$  term would then correspond to the effect of an alteration of the normal sink/source action.

We must conclude that, at the present stage of creep theories, two possible ways of interpreting the  $\lambda^2$  term are possible. Perhaps the analysis made by Weertman (86) is closer to reality, since an equation similar to Equation 5.3 is obtained. However, a number of refinements are necessary.

#### 5.4 Summary and Conclusions

Data has been presented in this chapter to show that, contrary to the assumptions of the majority of creep theories, the subgrain size developed during high temperature creep of pure materials may be an important variable in the rate controlling mechanisms. The following conclusions can be reached:

1. The subgrain size developed during the steady state stage increases during the transient period following a stress reduction. It is also observed that large creep strains are required for the readjustment of the subgrain size. The results of Pontikis and Poirier (107) and Parker and Wilshire (109) are critically analysed in terms of the findings of this study. It is concluded that, at least for high purity aluminum, the assumption made by Sherby, Klundt

and Miller (3) and by Robinson and Sherby (1) in their development of a phenomenological equation based on subgrain strengthening is correct.

2. A correlation between the transient creep rate and the subgrain size in the specimen, at constant stress, is obtained:  $\dot{\epsilon} \propto \lambda^2$ . The creep rate at constant subgrain size depends on the applied stress. The stress sensitivity exponent obtained at constant subgrain size is  $6.8 \pm 0.2$  and the exponent obtained from normal isostress steady state creep tests is  $4.6 \pm 0.1$ . The difference in stress exponents obtained by the two testing procedures is shown to be consistent with the strain rate - subgrain size dependence.

3. Using a different approach from the one by Robinson and Sherby (1) and Sherby, Klundt and Miller (3), a phenomenological equation for the creep rate at 530 K is developed which describes the steady state strain rate and, except for a short period of time, the instantaneous rates after the stress reduction. This equation is written

$$\dot{\epsilon} = 1.1 \times 10^9 (D/b^2) (\lambda/b)^2 (\sigma/E)^{6.8 \pm 0.2}$$

where  $D$  is the diffusion coefficient,  $b$  is the Burgers' vector,  $E$  is Young's modulus of elasticity,  $\lambda$  is the subgrain size and  $\sigma$  is the applied stress. The equation, however, cannot be used to describe the decreasing creep rate observed in the initial period following the stress reduction, i.e., before any subgrain growth occurs. Another mechanism is probably operating during this period.

4. The theoretical background for the subgrain size dependence term  $\lambda^2$  and for the high stress sensitivity coefficient  $N \approx 7$  is discussed. It is concluded that at the present stage of the creep theories,  $\lambda^2$  can be interpreted either as a slip plane area or as surface area of the subgrain. The  $\lambda^2$  term may be identified with parameters in the model of high temperature creep presented by Weertman (86) but refinements of the theory to allow for a higher stress dependence are necessary.

## CHAPTER VI

### TRANSIENT CREEP - INCUBATION PERIOD

#### 6.1 Introduction

The precise measurement of transient deformation after a rapid change in stress between the preceding and the new steady state of deformation should be of great value in the understanding of the creep phenomena. However, the results available in the literature to date and their interpretation are the subject of considerable controversy. This controversy concerns the existence of an incubation period following reductions in stress, in which the creep rate is zero. One group of experimenters (31,32,88,140) always observe an incubation period. They explain the transient behavior in terms of the network recovery theory (88). Another group of experimenters (35,122,132,141,142) observe an incubation period only after a characteristic stress reduction and explain the transient behavior using the internal stress theory of Ahlquist, Gasca-Neri and Nix (95).

In the preceding chapter, it was concluded that part of the transient behavior following a stress reduction is due to the coarsening of the subgrain structure. A correlation between the instantaneous creep rate and the subgrain size was obtained which is valid only for the period in which the creep rate increases. An explanation for the observed initial decrease in creep rate was not attempted.



In this chapter, attention will be directed to the decreasing creep rate, that is, to the initial period following the stress reduction. Data is presented to evaluate the effects of temperature, initial stress and reduced stress on the transient behavior after the stress reduction. The existence of an incubation period is analysed and the data is discussed in terms of the network and internal stress theories.

## 6.2 Results

### 6.2.1 Influence of temperature and stress

A series of experiments was performed to test the influence of temperature on the behavior of the creep strain after the reduction in stress. The specimens were deformed at the temperatures 523 K, 547 K, 573 K and 623 K and at an applied stress of 6.23 MPa, until a strain of 0.16 was reached. At the 0.16 true strain, the stress was rapidly reduced to 3.44 MPa and the creep strain recorded as a function of time. The results obtained in these experiments are shown in Figure 6.1 in a log-log plot. The figure shows that:

- For strains smaller than  $4 \times 10^{-3}$ , the creep rate decreases slightly as a function of time ( $\dot{\epsilon} \propto t^{0.666}$ ).
- For strains larger than approximately  $4 \times 10^{-3}$ , the creep rate increases as a function of time ( $\dot{\epsilon} \propto t^2$ ).

Figure 6.1 also shows that a change in temperature does not alter the shape of the creep curves after a stress reduction. However, an increase in temperature translates the curves to shorter times. This effect of temperature on the creep strain after a reduction

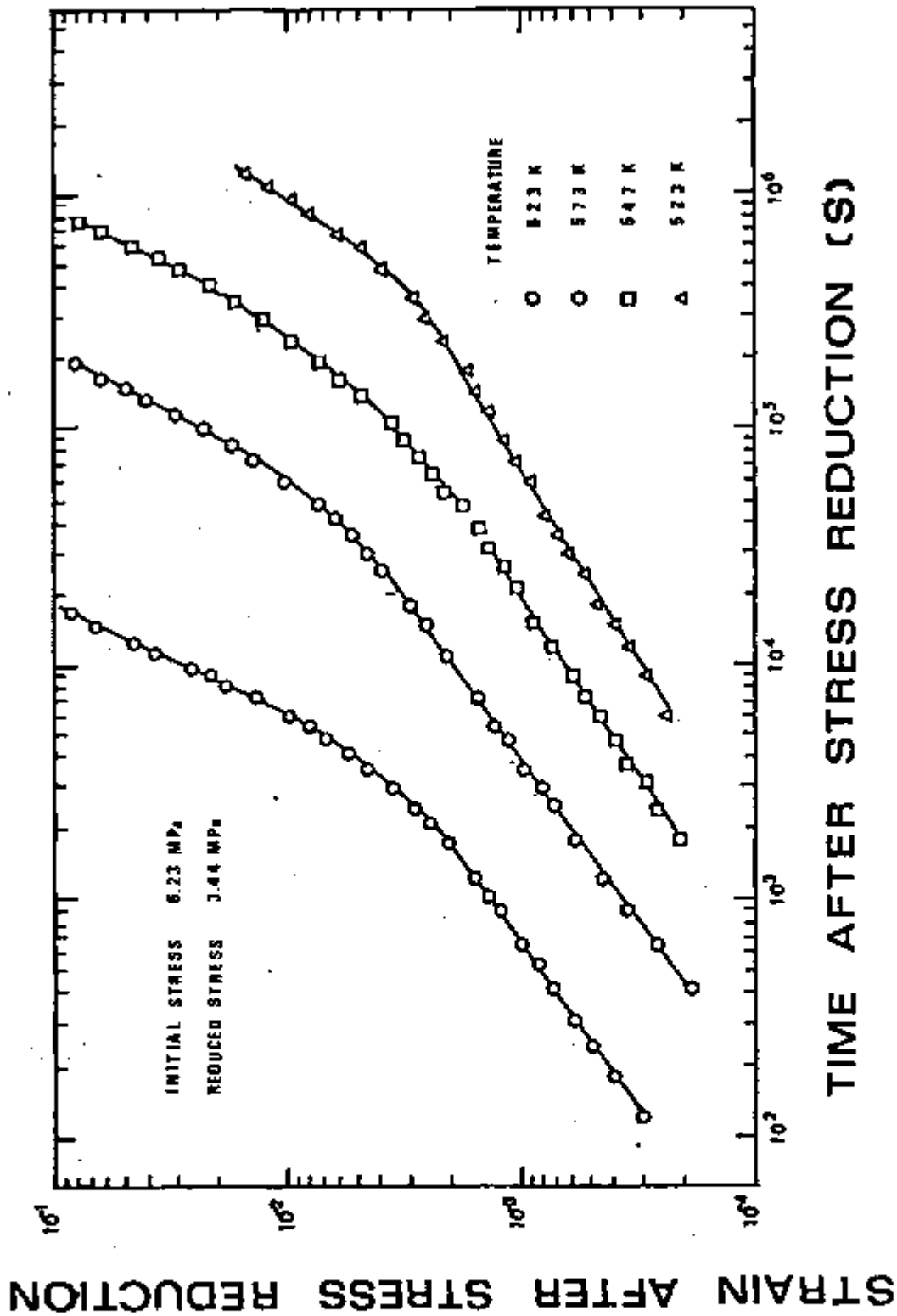


Figure 6.1 Strain time curves illustrating the effect of temperature. The stress was reduced at a true strain of .16 in each case.

in stress is similar to the effect of temperature on creep strain in a normal creep test at constant stress (137).

Dorn (143) proposed a method to analyse the effect of temperature on the creep strain. In his analysis, the effect of temperature on strain is described by the following equation

$$\epsilon = F \left[ t' \exp\left(\frac{-Q_c}{kT}\right) \right] = F(\theta_c) \quad (6.1)$$

where

$\epsilon$  = the total true tensile creep strain for a given applied stress

$t'$  = duration of the test

$T$  = the absolute temperature

$Q_c$  = the apparent activation energy for creep, which is independent of the stress

$F$  = a function of  $\theta_c = t \exp(-Q_c/kT)$  and of the stress.

The Dorn analysis can also be applied to the data shown in Figure 6.1 (12). A similar expression can be written for the creep strain obtained after the reduction in stress, i.e.:

$$\epsilon = F(t \exp(-Q/kT)) = F(\theta) \quad (6.2)$$

at constant reduced stress  $\sigma_R$ , where  $t$  is the time elapsed after the reduction in stress,  $Q$  is the apparent activation energy for the process or processes operating following a change in stress.

Equation 6.2 shows that, for a constant transient creep strain, i.e.,  $\theta$  constant, the time  $t$  is related to temperature by the equation

$$t = \theta \exp(+Q/k T) \quad (6.3)$$

The activation energy  $Q$  can be determined by plotting the logarithm of  $t$  versus  $1/T$  at constant strain. This procedure is used in Figure 6.2 for several values of strain or  $\theta$ . A set of parallel straight lines is obtained indicating that the activation energy  $Q$  is not dependent on the transient strain. The value obtained for  $Q$ , determined from the slope of the straight lines in Figure 6.2, is equal to  $1.44 \pm 0.05$  eV/at. This value of  $Q$  is about equal to the value of the apparent activation energy for creep previously discussed in Chapter IV, before the correction for the temperature dependence of the modulus of elasticity, that is,  $1.43 \pm 0.05$  eV/at.

The influence of stress in the transient behavior can be analysed using the data presented in Figures 5.2 and 5.7. These data are replotted using a log-log scale and the resulting curves are shown in Figures 6.3 and 6.4. A comparison of Figures 6.1, 6.3 and 6.4 permits the following observations:

1. The shape of the strain-time curves is the same, independent of temperature, initial stress and reduced stress;
2. The transient creep curves consist of two parts: a part in which the creep rate decreases as a function of time ( $\dot{\epsilon} \propto t^{0.66}$ ) and a part in which the creep rate increases as a function of time ( $\dot{\epsilon} \propto t^2$ );

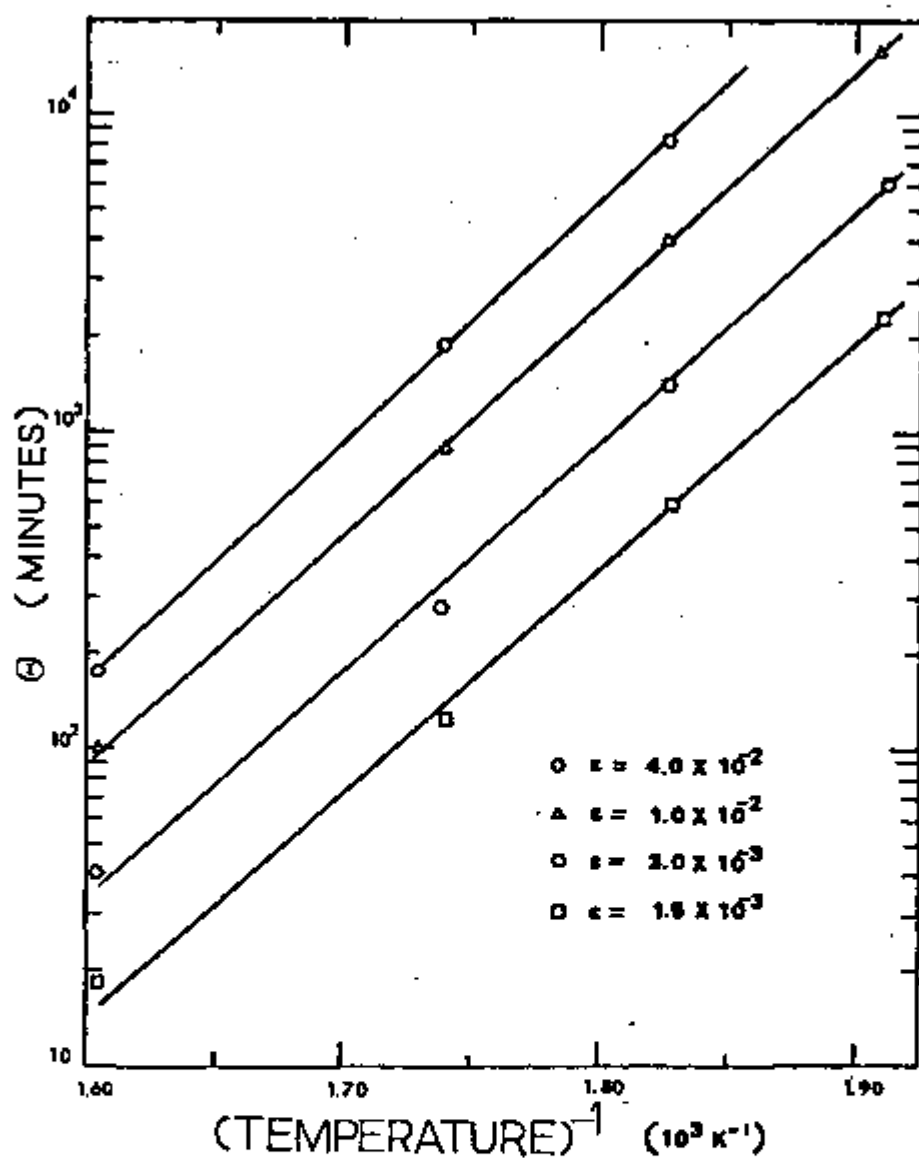


Figure 6.2 The effect of temperature on the time  $\theta$  required to reach the transient strain  $\epsilon$ . The stress is reduced from 6.23 MPa to 3.44 MPa at a true strain of .16.

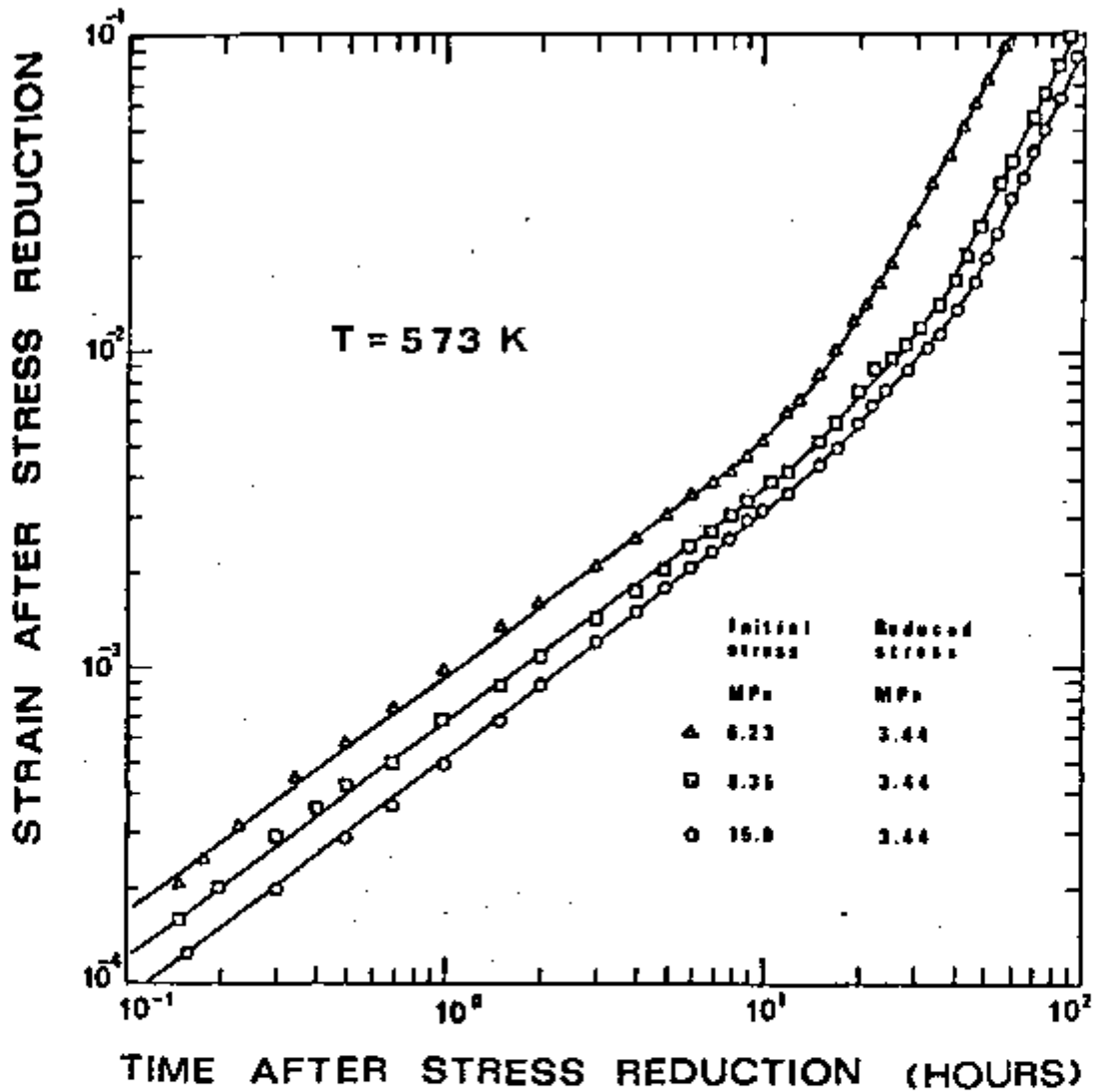


Figure 6.3 Strain-time curves illustrating typical behavior after stress reductions from 15 MPa, 8.35 MPa and 6.23 MPa to 3.44 MPa. The stress was reduced at a true strain of .16 in each case.

# STRAIN AFTER STRESS REDUCTION

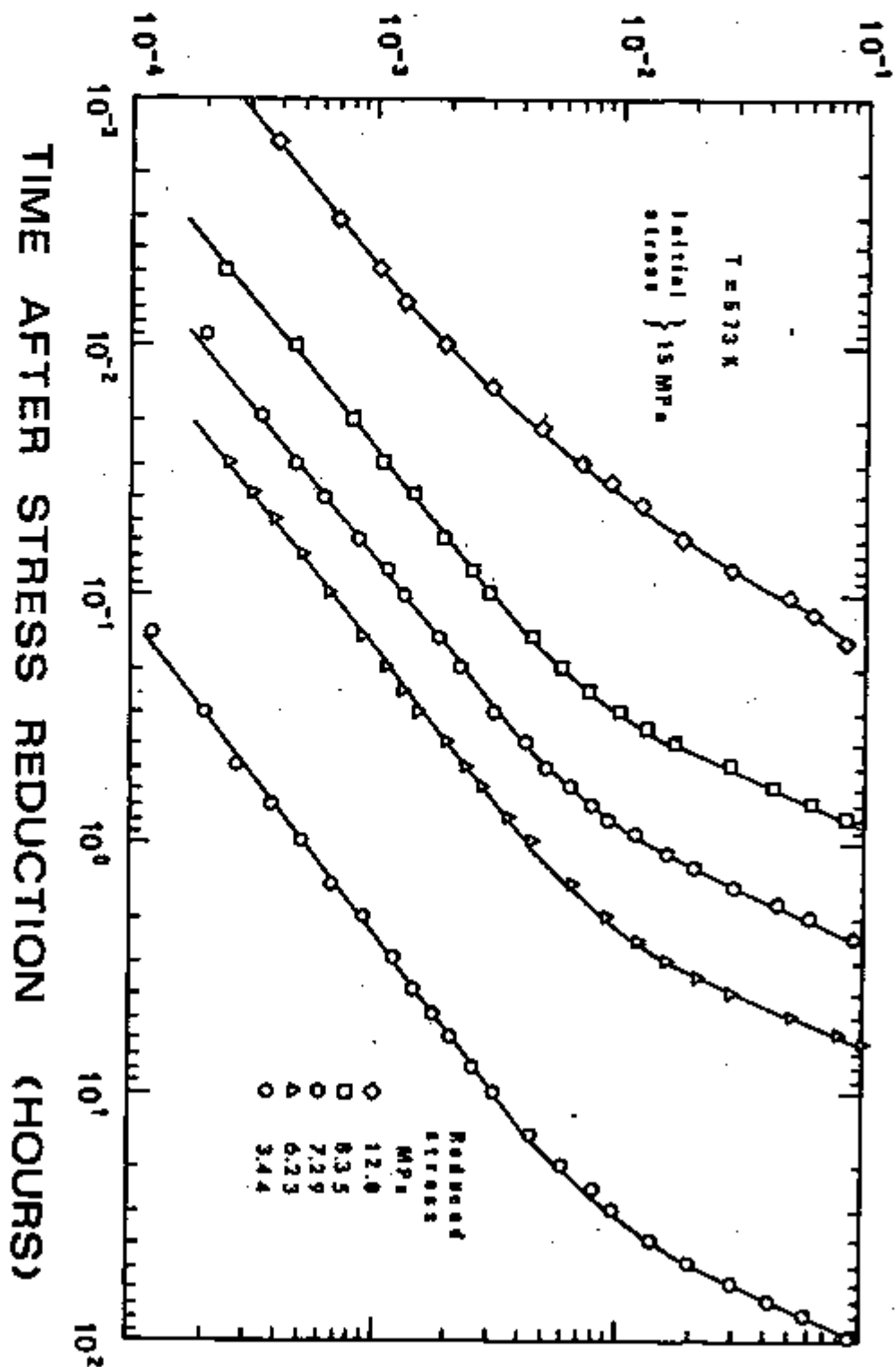


Figure 6.4 Strain-time curves illustrating typical behavior after stress reductions from 15 MPa to several reduced stresses.

3. The break in the curves is translated to shorter times whenever:

- a) the test temperature is increased and  $T$  and  $\sigma_I$  are maintained fixed
- b)  $\sigma_R$  is increased and  $T$  and  $\sigma_I$  are maintained fixed
- c)  $\sigma_I$  is decreased and  $T$  and  $\sigma_R$  are maintained fixed.

To simplify the analysis, the transient creep curves after the reduction in stress will be divided into two stages:

Stage I: Creep behavior corresponding to the time interval in which the creep rate decreases (strains smaller than  $4 \times 10^{-3}$ )

Stage II: Creep behavior corresponding to the time interval in which the creep rate increases (strains in excess of  $4 \times 10^{-3}$ ).

The influence of the reduced stress on the interval of time  $\Delta t_I$ , involved in Stage I, is shown in Figure 6.5. It can be seen that

$$\Delta t_I = A \exp(B(\sigma_I - \sigma_R)/G) \quad (6.4)$$

where  $A = 1.13$  s.,  $B = 2.01 \times 10^4$  and  $G$  is the shear modulus. This equation will be used later, when comparison of the data with theories is made.

### 6.2.2 Recovery of the Transient Strain after Stress Reduction

Recovery of the transient strain after the stress reduction was studied in a series of experiments in which the specimens were allowed to recover at the reduced stress. After a certain period of time, the total stress was reapplied and the creep transient recorded. Figure 6.6 shows examples of transient creep after steady



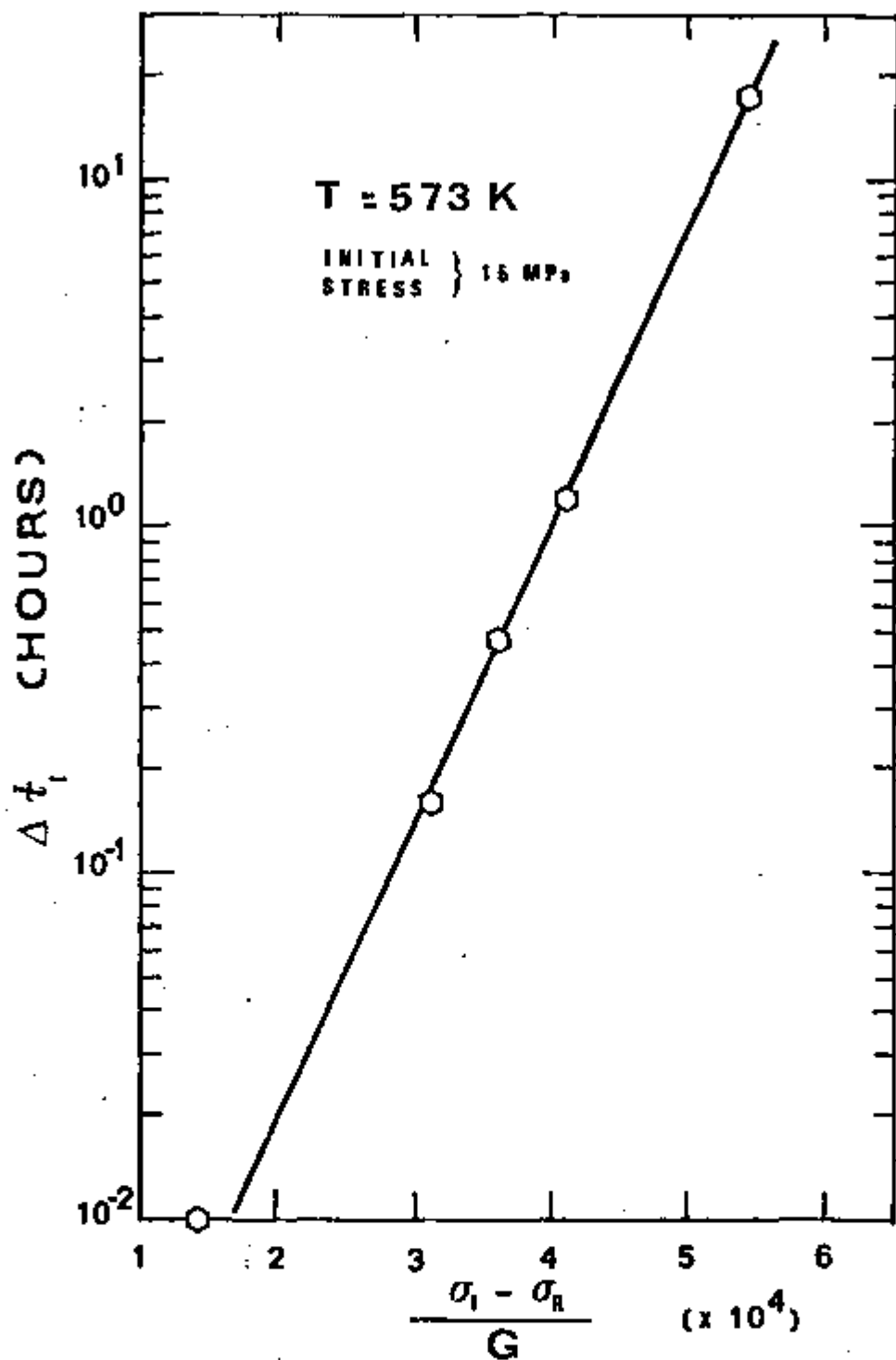


Figure 6.5 The variation of the interval of time  $t_I$  involved in stage I, as a function of  $(\sigma_I - \sigma_R)/G$ . ( $\sigma_I$  = initial stress,  $\sigma_R$  = reduced stress,  $G$  shear modulus)

state deformation at 8.35 MPa and at various recovery times at a reduced stress of 3.44 MPa. In spite of the short time at the reduced stress, the specimen exhibits a marked range of transient creep on reloading. In Figure 6.7, the length  $\Delta\epsilon$  of the transient strain determined from curves similar to that in Figure 6.6 is plotted on a log-log scale as a function of time after stress reduction. After a long stay at zero reduced stress, one might expect  $\Delta\epsilon$  to be of the order or slightly smaller than the initial transient obtained in the primary stage, in a continuous test at 6.23 MPa and 8.35 MPa. This transient strain is of the order of 10%, as can be seen in Figure 4.1. Figure 6.7 shows that  $\Delta\epsilon$  increases as a function of time, but is always smaller than 10%.

The reduced stress applied to the specimen prior to reloading does not seem to influence the recovery of  $\Delta\epsilon$  during Stage I as seen in Figure 6.7. However, in Stage II, the recovery of  $\Delta\epsilon$  is sensitive to the level of reduced stress. If the stress is reduced to zero, the  $\Delta\epsilon$  obtained after reloading during Stage II are nearly constant even after times  $\sim 60$  hours. But, when the stress is reduced to 3.44 MPa, the  $\Delta\epsilon$  obtained after reloading increase slowly during Stage II. This behavior of  $\Delta\epsilon$  during Stage II at a reduced stress of 3.44 MPa seems to be related to subgrain growth. To investigate this point, a specimen was deformed at 573 K to a true strain of 0.16, at an applied stress of 6.23 MPa. At this true strain, the test was interrupted and the specimen quenched, under load, to room temperature. Subsequently, the subgrain size present in the

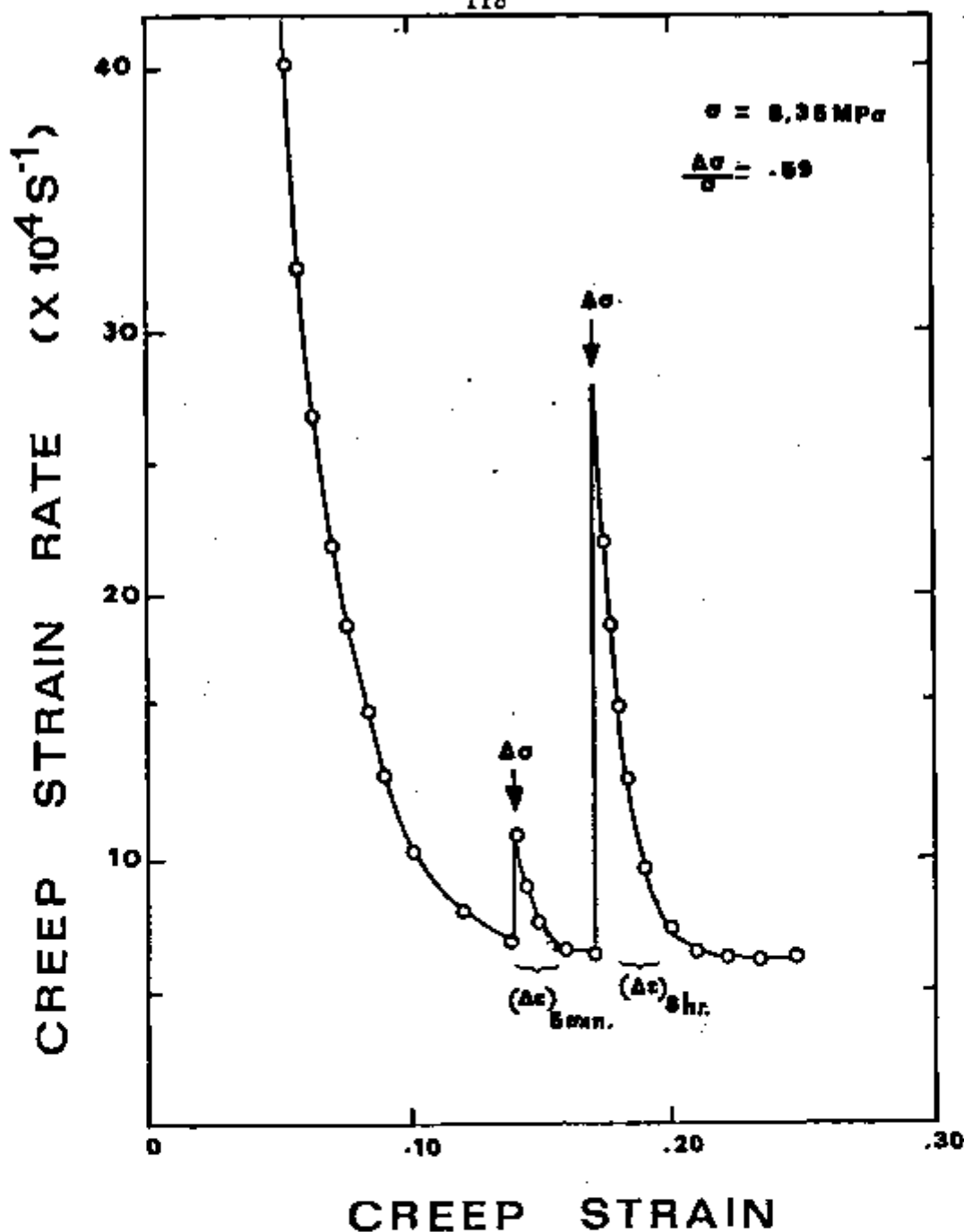


Figure 6.6 Examples of transient creep obtained on reloading, after steady state deformation at 8.35 MPa and at 5 min. and 8 hours at a reduced stress of 3.44 MPa.

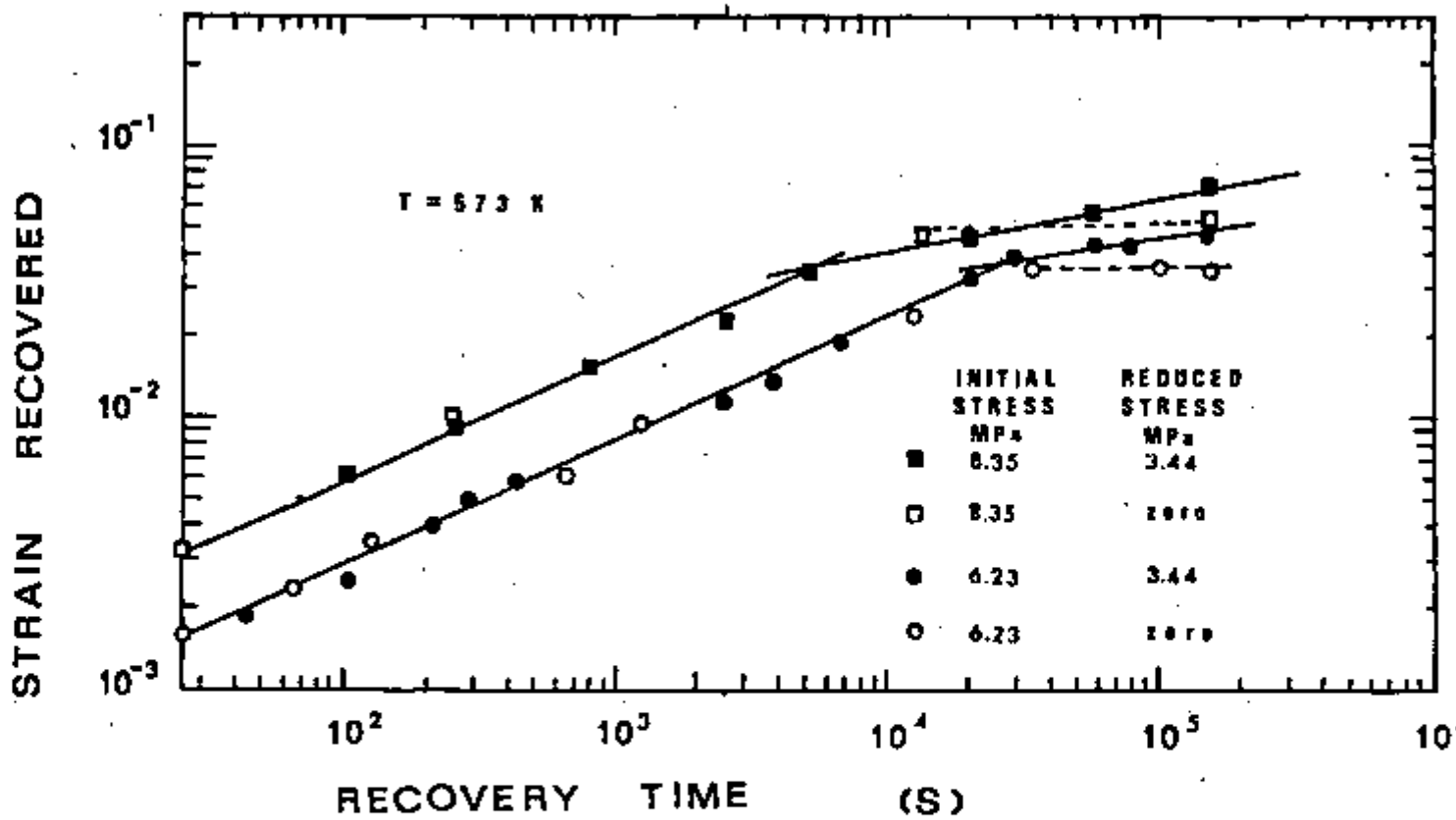


Figure 6.7 Transient strain recovered as a function of the time the specimen is allowed to recover at the reduced stress.

specimen was measured and the value  $53 \pm 5 \mu\text{m}$  was obtained, in agreement with the data reported in Figure 4.5. Following this procedure, the specimen was heat treated at 573 K in the absence of a load, for 169 hours (-one week). After this heat treatment, the subgrain size was measured again and the value  $48 \pm 5 \mu\text{m}$  was obtained. This experiment clearly shows that, if the stress is reduced to zero, the growth of the subgrain is drastically restrained.

### 6.2.3 Dislocation Density Measurements

The behavior of the dislocation density within subgrains following the reduction in stress was analysed by performing substructural observations at several strains in the transient region. The dislocation density inside the subgrains was measured for a test performed at 573 K and an initial applied stress of 8.35 MPa, in which the stress was reduced to 3.44 MPa.

The measurement of the dislocation densities in high purity aluminum requires some discussion. Due to the lack of a strong pinning mechanism in high purity aluminum, dislocations are lost during foil preparation and during observation in the microscope. It was observed in this study that very thin areas of the foil (usually areas close to the border of a hole on the foil) possessed very few dislocations. These dislocations moved out of the foil during observation in the TEM. However, in thicker areas of the foil the dislocation structure seemed to be very stable during observation. As described in Chapter III, only those areas with a thickness larger

than 200 nanometers were used for dislocation density measurement. It is believed that the presence of a subgrain structure aids in dislocation retention in areas thicker than 200 nm (119). Dislocations were probably lost during the thinning process used in this investigation. It will be assumed that the length of dislocation line lost is the same for all specimens.

The results obtained for the dislocation density within subgrains are shown in Figure 6.8. Also included in Figure 6.8 are the values obtained for the creep rate following the stress reduction. The absolute value of  $\rho$  obtained at  $t = 0$ ,  $\rho = 6.2 \times 10^8 \text{ cm}^{-2}$  is one order of magnitude larger than the value  $6.10^7 \text{ cm}^{-2}$  obtained by an extrapolation of data reported by Daily and Ahlquist (65) to the stress  $\sigma = 8.35 \text{ MPa}$ . However, the data of Daily and Ahlquist was obtained by etch pitting single crystals of high purity aluminum deformed in tension at 619 K to the steady state flow stress using an Instron machine. In a study of Fe-3% Si, Barrett, Nix and Sherby (37) have observed that the dislocation densities obtained using transmission electron microscopy were about a factor of four larger than those obtained using etch pitting techniques. They suggested that the etch pit densities are lower because some dislocations do not produce etch pits and also because, in some instances, one etch pit may correspond to a group of closely spaced dislocations. Also, there is evidence that the dislocation density inside subgrains during steady state creep decreases slightly with increases in test temperature (28,63). These observations indicate that the

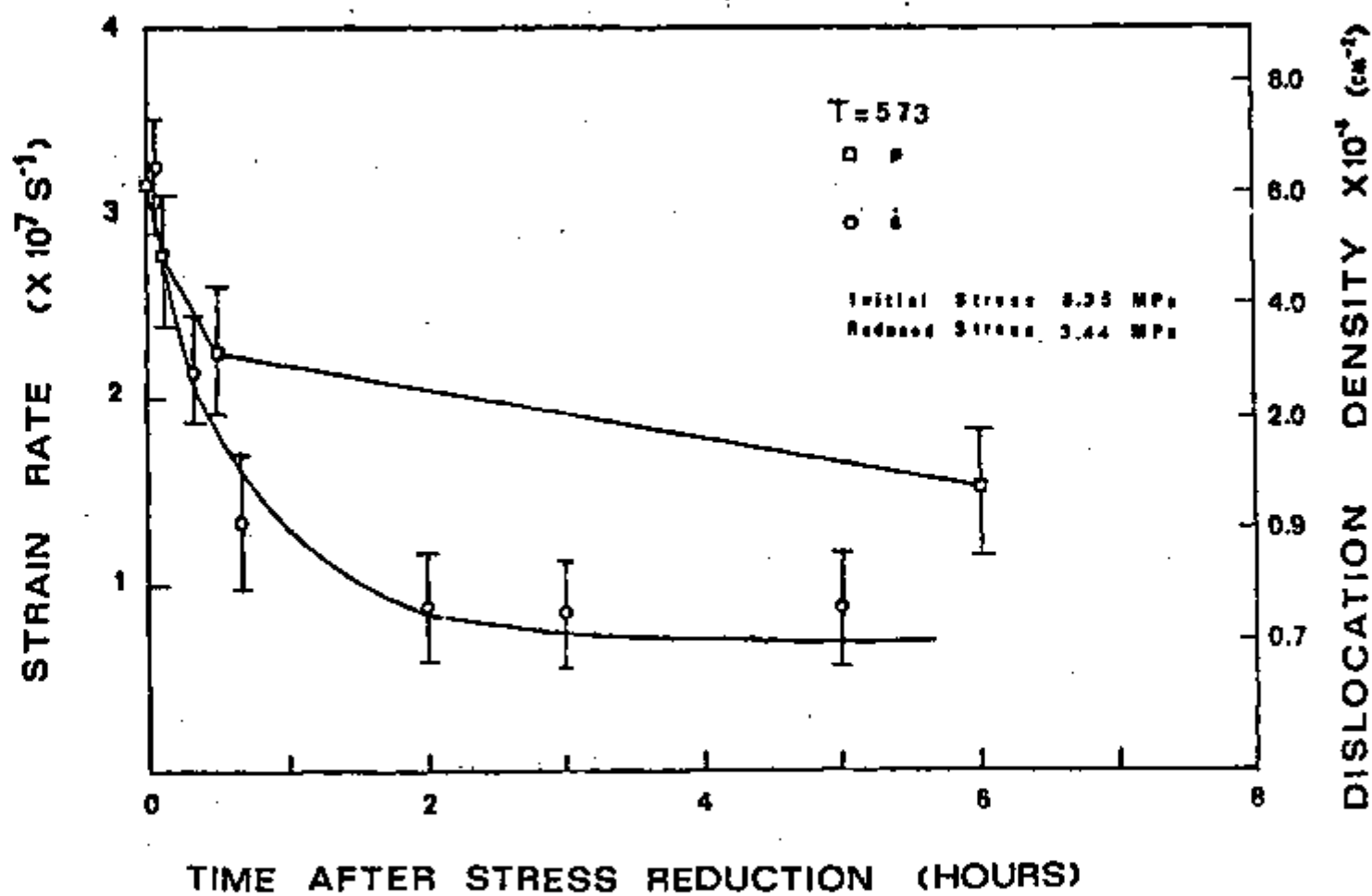


Figure 6.8 Strain rate and dislocation density as a function of time after a stress reduction for initial stress of 8.35 MPa reduced to 3.44 MPa

dislocation density obtained in this investigation is in reasonable agreement with those obtained by Daily and Ahlquist. The results presented in Figure 6.8 clearly show that the dislocation density tends to decrease during Stage I in the same manner as the creep rate, that is, the dislocation density decreases approximately 60% and the creep rate decreases 75% in equivalent time intervals.

### 6.3 Discussion

The data presented in this section shows that a reduction in stress, performed in the steady state region, is always accompanied by a transient creep behavior. It is easily seen that this transient deformation can be separated into two stages: Stage I, in which the creep rate decreases as a function of time; and Stage II, in which the creep rate accelerates to the steady state value obtained at the reduced stress. Stage I is characterized by a nearly constant subgrain size and by a large decrease in the dislocation density within subgrains. Stage II is generally characterized by coarsening of the subgrain structure. The activation energies determined for Stages I and II were found to equal the apparent activation energy for steady state creep, that is, 1.43 eV.

The data presented failed to show any time interval in which the creep rate is zero, i.e., no incubation period was detected. Before any discussion of the existence of an incubation period, it is interesting to refer to the original paper by Mitra and McLean (88) in which this idea was first introduced.



The transient creep curve reported by these authors is reproduced in Figure 6.9 to illustrate this discussion. Mitra and McLean (88) performed stress reductions in aluminum and nickel, in an attempt to determine the rate of recovery. In these experiments, the creep rate was measured using a transducer attached to the specimen shoulders. The authors did not comment on the sensitivity of the strain measuring device.

When the transient creep curve shown in Figure 6.9 is compared with the transient creep curves obtained in this study and shown in Figures 6.3 and 6.5, it becomes apparent that there are two cases which must be discussed:

1. The incubation period in Mitra and McLean's experiments would correspond to the region called Stage I in this investigation. The association of Stage I with the incubation period is suggested by the observations that:

- a) The time interval  $\Delta t_1$ , involved in Stage I increases when  $\Delta\sigma$  is increased in agreement with the observations by Mitra and McLean (83);
- b) A very small strain (3 to 4  $\times 10^{-3}$ ) occurs during Stage I. If the sensitivity of the apparatus used by Mitra and McLean was, for example,  $10^{-3}$ , Stage I would appear to the experimenters as a period of zero creep rate.

2. Another way to view the experimental results obtained in this study would be to neglect the correspondence assumed above and imagine the existence of an incubation period that could not be detected in this study. In this case, the incubation time  $\Delta t$  must

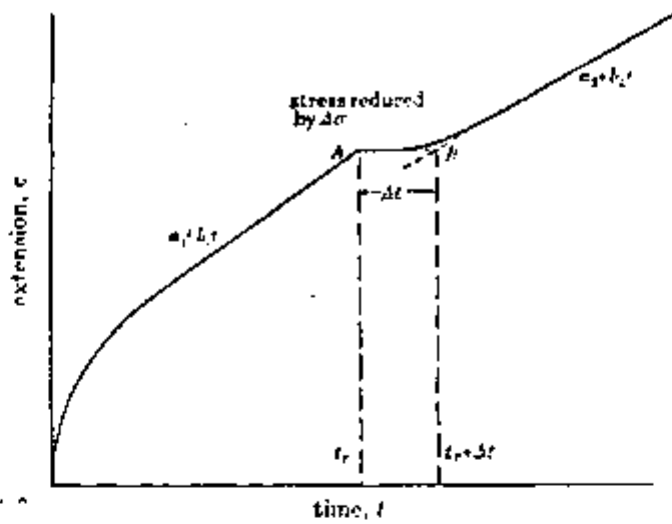


Figure 6.9 (a) Schematic diagram showing the measurement of recovery time.

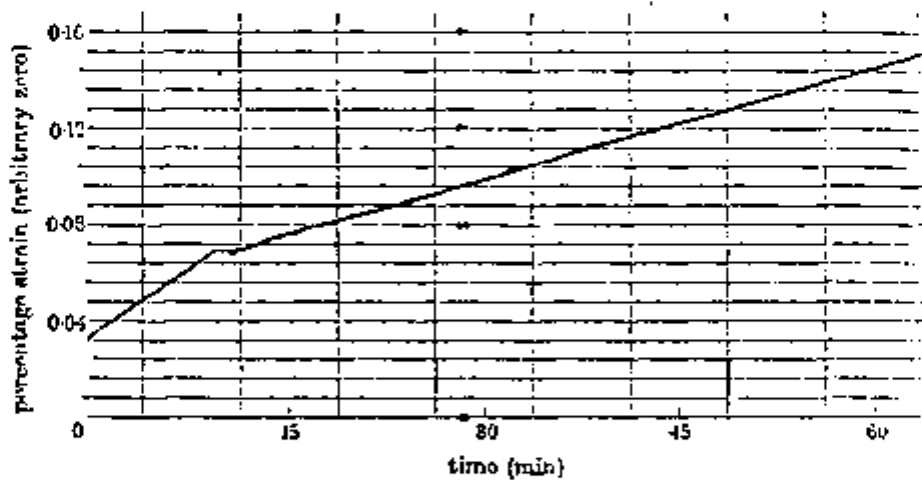


Figure 6.9 (b) Reproduction of chart trace showing effect of stress reduction for nickel  $650^{\circ}\text{C}$ ;  
 initial stress  $10.55 \text{ Kg/mm}^2$ ;  
 stress reduction  $0.45 \text{ Kg/mm}^2$  (88).

be smaller than the mean time,  $\Delta t_m$ , of the intervals of time after the stress change, during which the magnitude of the creep rate cannot be clearly established due to limitations in the apparatus.

To discuss these two conflicting ideas, it is necessary to estimate the incubation period from theory. Two calculations of  $\Delta t$  are available in the literature: one by Stang et al. (7) and another by Burton (34).

Stang et al. (7) calculated the time  $\Delta t$  required for dislocation structure adjustment after a reduction in stress. The incubation period was calculated for the process of dislocation network coarsening. In their calculation, it was assumed that the internal stress is approximately equal the applied stress, i.e.,  $\sigma_i \sim \sigma$ , and that no additional deformation or strain-hardening takes place during recovery of dislocations (static recovery). The network growth was treated as a dislocation-climb controlled process and use was made of the rate of network coarsening proposed by Hirth and Lothe (44),

$$\frac{dL}{dt} = \frac{D b^3 G}{k T L} \quad \text{where } L \text{ is the average link length of the network.}$$

The expression obtained for  $\Delta t$  after this procedure is

$$\Delta t_{SBN} = \frac{\alpha^2 G k T}{2 D b^3} \left( \frac{1}{\sigma_R^2} - \frac{1}{\sigma_I^2} \right) \quad (6.5)$$

where  $\alpha$  is a constant,  $\sigma_I$  is the initial applied stress,  $\sigma_R$  is the reduced stress and the other quantities have the previously cited meaning.

The calculation by Burton (34) involved the same general assumptions as made by Stang et al. (7), but differs only in the assumption used to calculate  $dL/dt$ . Burton considered the rate of climb of lines of the network to be controlled by the rate of emission of vacancies by jogs in the dislocation lines and used the equation suggested by Friedel (145) for this process

$$\frac{dL}{dt} = \frac{DGb^3}{kTL} \exp(U_j/kT) \quad (6.6)$$

where  $U_j$  is the energy of formation of jogs in the dislocation line. Thus, the exponential term in Equation 6.6 is related to the concentration of jogs on the dislocation line. The final equation obtained by Burton for the incubation period is

$$\Delta t_B = \frac{\alpha^2 GkT}{2Db} \exp(U_j/kT) \left( \frac{1}{\sigma_R^2} - \frac{1}{\sigma_I^2} \right) \quad (6.7)$$

The value of  $U_j$  given by Friedel (145) for aluminum is  $U_j = 0.1 G b^3$ . At 573 K the exponential term is  $\exp(U_j/kT) = 1$ .

The equations obtained by Stang et al. (7) and Burton (34) for the incubation period lead to the same values of  $\Delta t$  at high temperature. Both equations predict  $\Delta t \approx 1/\sigma_r^2$ .

The values for  $\Delta t$  can now be calculated for the stress reduction experiments described in this chapter. Use is made of the following values of the parameters:

$$T = 573 \text{ K}$$

$$D = 8.81 \times 10^{-18} \text{ m}^2/\text{s}$$

$$\alpha = 0.5$$

$$b = 2.86 \times 10^{-10} \text{ m}$$

$$G = 2.13 \times 10^{10} \text{ N/m}^2 \text{ at } 573 \text{ K}$$

$$k = 1.38 \times 10^{-23} \text{ J/K}$$

The result of this calculation is shown in Table 6.1.

TABLE 6.1

Summary of Results for  $\Delta t_{th}$ ,  $\Delta t_I$ ,  $\Delta t_m$ ,  $h_m$ ,  $h_m/G$   
from Stress Reduction Tests During Steady State

initial stress (MPa)	reduced stress (MPa)	$\dot{\epsilon}_s$ ( $\text{s}^{-1}$ )	$\Delta \sigma$ (MPa)	$\Delta t_{th}$ (s)	$\Delta t_I$ (s)	$\Delta t_m$ (s)	$h_m$ (Pa)	$h_m/G$
15	12	$3 \cdot 10^{-3}$	3.0	21	40	3	$3.33 \times 10^8$	0.02
15	8.35	"	6.65	83	360	3	$7.39 \times 10^8$	0.03
15	7.29	"	7.71	120	1440	3	$8.57 \times 10^8$	0.04
15	6.23	"	8.77	178	3600	5	$5.85 \times 10^8$	0.03
15	3.44	"	11.56	668	36000	5	$7.71 \times 10^8$	0.04
8.35	3.44	$7.5 \cdot 10^{-5}$	4.96	586	43000	5	$1.33 \times 10^{10}$	0.62
6.23	3.44	$1.5 \cdot 10^{-5}$	2.79	490	21600	5	$3.72 \times 10^{10}$	1.75

The calculated values of  $\Delta t$  have the same order of magnitude of  $\Delta t_I$  only for small reductions in stress. As shown in Table 6.1, the time interval involved in Stage I can be one to two orders of magnitude larger than  $\Delta t$  calculated from theory. This disagreement was expected since  $\Delta t_I \propto \exp(-\sigma_R)$  and the theories predict  $\Delta t \propto 1/\sigma_R^2$ . Therefore, if the association of the Stage I with the incubation period is assumed, the network theory will not explain this discordance at large  $\sigma_R$ .

If an incubation period which is too short to be detected in this study (case 2) is assumed, it will be shown that this approach will not help in explaining the results in terms of the network theory. It is possible to estimate the rate of strain hardening that would be obtained if an incubation period of this magnitude exists ( $\Delta t \leq \Delta t_m$ ). Mitra and McLean (88) and Davies et al. (31) have shown that the rate of recovery,  $r$ , can be determined from incubation period as

$$r = \lim_{t \rightarrow 0} \frac{\Delta \sigma}{\Delta t} \quad (6.8)$$

where  $\Delta \sigma$  is the magnitude of stress reduced and  $\Delta t$  is the incubation period. If reference is made to the variation of the incubation period  $\Delta t$  with the degree of stress reduction, reported by Davies et al. (31) in copper, one expects that

$$r > \frac{\Delta \sigma}{\Delta t} \quad (6.9)$$

Combining equation 6.9 with the Bailey Orowan equation (Equation 2.24) it is possible to estimate the coefficient of strain hardening by

$$h > h_{\min} = \frac{\Delta \sigma}{\dot{\epsilon}_s \Delta t_m} \quad (6.10)$$

where  $\dot{\epsilon}_s$  is the steady state creep rate at the initial applied stress.

The estimated minimum values for  $h$  can now be calculated using the values for  $\dot{\epsilon}_s$  and  $\Delta t_m$  found experimentally. The result of this calculation is shown in Table 6.1. From this table, it is seen that  $h_{\min}$  ranges from values around 0.03 G at 15 MPa to values of 1.8 G at 6.23 MPa. These values may be compared to the coefficient of strain hardening during Stage II of fcc metals:  $h = \frac{d\sigma}{d\epsilon} = M^2 \frac{d\tau}{d\epsilon}$  ( $\tau$  shear stress,  $\gamma$  shear strain and  $M$  = Taylor coefficient), which is about 0.03 G (127). Thus, the minimum value obtained for the coefficient of strain hardening would be higher than 0.03. Barrett et al. (146), Nordstrom and Barrett (147), and Blum et al. (127) have already shown that the values of  $h$  calculated from the Bailey-Orowan equation in connection with  $r$  are often higher than can be justified by the theories of strain hardening. Obviously, the same criticism applies to the values of  $h_m$  derived above. Furthermore, if an incubation period of this magnitude exists, the network theory would not explain the decreasing creep rate observed during Stage I.

The network theory predicts that following the incubation period, the creep rate is a continuously increasing function of time due to the continuous increase in the dislocation link length.

It has to be concluded that neither approach 1 nor approach 2 can lead to an explanation of the results obtained in this study in terms of the network recovery theories.

In the following, an attempt is made to interpret the results in terms of the internal stress theory proposed by Ahlquist, Gasca-Neri and Nix (95). This theory explains the steady state creep rate in terms of the existence of an equilibrium internal stress. The primary stage of creep is explained by the increase in the internal stress. Measurements of internal stress by Ahlquist and Nix (122), Tobolova et al. (132) and by Konig et al. (141), show that the internal stress decreases when the applied stress is decreased. Assuming that the internal stress does not change instantaneously after a change in stress, it is expected at  $t = 0$ , immediately after the reduction in stress, that the internal stress present in the specimen has the equilibrium value consistent with the initial applied stress, that is,  $(\sigma_i)_0$ . Therefore, immediately after the stress reduction, the system is in a non-equilibrium state. The internal stress will then decrease, by recovery, to the value compatible with the new reduced stress. The expected behavior of the internal stress, following the reduction in stress, is shown schematically in Figure 6.10. Depending on the level of the reduced stress, the effective stress,  $\sigma^* = \sigma - \sigma_i$ , can be positive, negative, or zero. A decrease



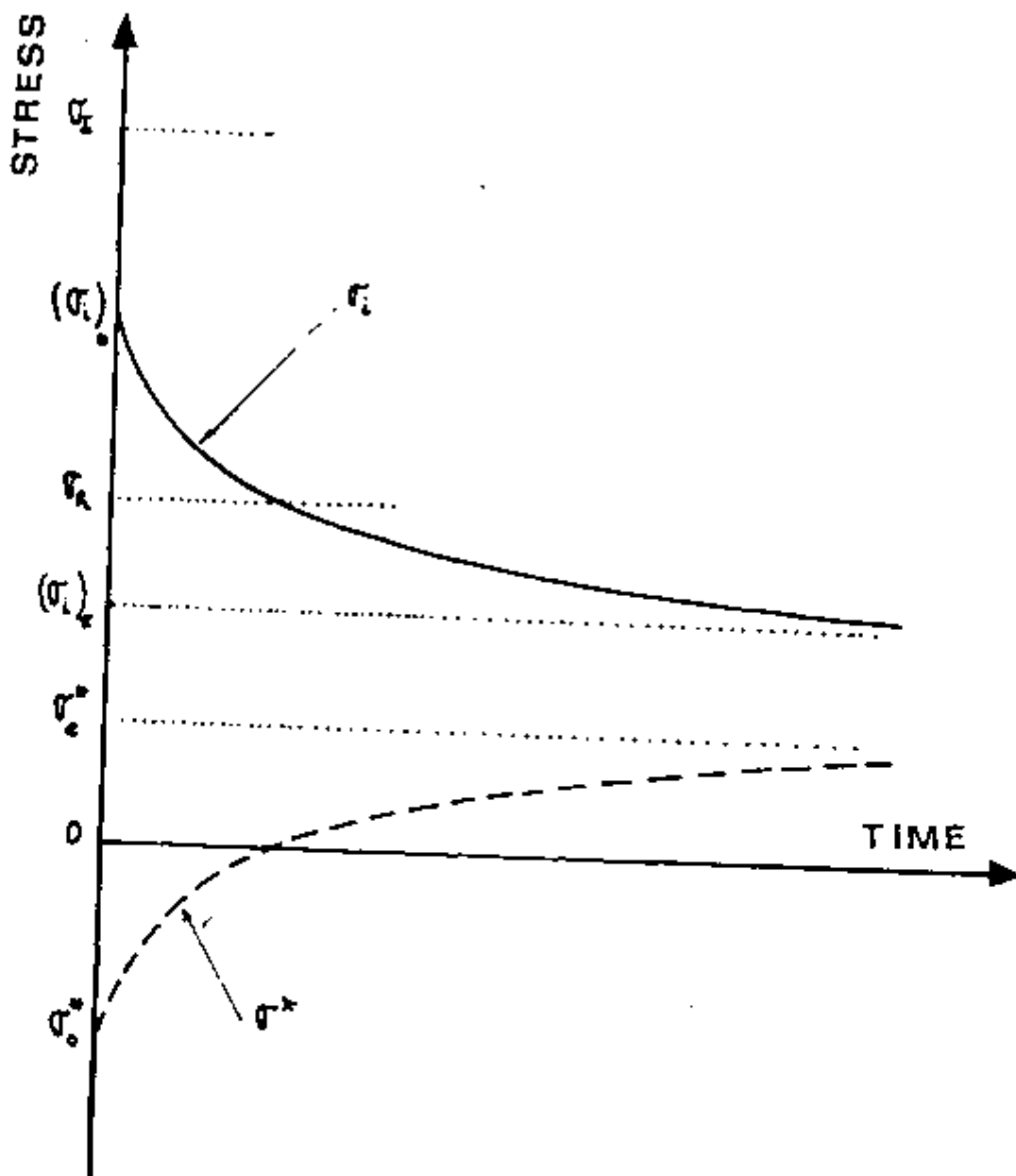


Figure 6.10 Schematic variation of the interval and effective stresses as a function of time after the stress reduction

in internal stress is thus accompanied by an increase in effective stress. At any instant of time after the stress reduction, the equation  $\sigma = \sigma_i + \sigma^*$  is valid.

The instantaneous creep rate following the reduction in stress can be expressed by the equation

$$\dot{\epsilon} = \alpha \rho_m v \quad (6.11)$$

where  $\alpha$  is a constant,  $\rho_m$  is the density of mobile dislocations and  $v$  is the dislocation glide velocity.

The velocity of dislocations can be expressed in terms of the effective stress by (148)

$$v = v_0 \exp(-H_0/kT) \exp(bA\sigma^*/kT) \quad (6.12)$$

where  $v_0$  is a constant,  $H_0$  is the activation enthalpy,  $A$  is the activation area for creep and the other quantities are as previously defined. Making use of Equations 6.11 and 6.12, the instantaneous creep rate following a reduction in stress can be expressed at constant temperature by

$$\dot{\epsilon} \Big|_T = K \exp(bA\sigma^*/kT) \rho_m \quad (6.13)$$

where  $K$  is a constant.

The dependence of the activation area on stress is not well known. It will be assumed that following a reduction in stress the activation area does not change. This assumption is usually made by most glide theories.

It has been observed in the experiments involving the recovery of  $\Delta \epsilon$  that the recovery of the transient strain is not dependent on the level of the reduced stress during Stage I. Since the recovery of  $\Delta \epsilon$  reflects the decrease in internal stress (122), then the assumption can be made that the decrease in the dislocation density after the stress reduction is not dependent on the level of reduced stress. This has been observed experimentally by Hausselt and Blum (150) following stress reductions performed in Al-11% Zn alloys.

If the additional assumption that the mobile dislocation density  $\rho_m$  is a constant fraction of the dislocation inside the subgrains, that is,  $\rho_m \propto \rho$ , the instantaneous creep rate can be written

$$\dot{\epsilon} \Big|_T = K \exp(bA\sigma^*T)/kT) \rho \quad (6.14)$$

The assumptions made above imply that the time required for the strain rate to decrease to its minimum value (end of Stage I) will be dependent on the inverse of the dislocation velocity, since the influence of the decrease of  $\rho$ , as assumed, is the same for all levels of reduced stress. Therefore,

$$\Delta t_I \propto 1/V \propto \exp(-\sigma^*_T) \quad (6.15)$$

It has been observed (132) that  $\sigma^* = \alpha\sigma$  where  $\alpha = 0.6$ . Thus, it is possible to write

$$\Delta t_1 \propto \exp(-\sigma^*) \propto \exp(-\sigma_r) \quad (6.16)$$

Equation 6.16 could explain the behavior observed experimentally for  $\Delta t_1$  and shown in Figure 6.5. This simple explanation, however, is not free from criticism since it involves a large number of very general assumptions.

When the stress is reduced from 15 MPa to 12 MPa at 573 K, Stage I occurs in a very short period of time (10 sec.). Also, the strain involved in Stage I for this particular stress reduction is smaller than the value  $4 \times 10^{-3}$  usually found for very large stress reductions. This observation would probably be due to the fact that Stage I is occurring simultaneously with the reduction in stress. It is expected then that the creep rate, following a reduction of the applied stress to values larger than 12 MPa would be a continuous and increasing function of time, i.e., no Stage I will be detected experimentally (Stage I would be occurring simultaneously with the reduction in stress and would not be detected). This type of behavior has been reported by Hausselt and Blum (149) in a Al-11% Zn alloy. It is interesting to point out that 12 MPa is approximately equal to the maximum internal stress present in the specimen prior to the reduction in stress, as estimated from values reported by Tobolova and Cadek for aluminum (132). Therefore, when the stress is reduced to values larger than 12 MPa, the effective stress in

the specimen, immediately after the stress reduction, is positive. The creep rate after the stress reduction would be positive and continuously increasing. Since an increasing creep rate reflects growth of the subgrains, this fact suggested that a positive effective stress is required for subgrain growth to occur.

For large stress reductions,  $\sigma_r > 12$  MPa, the effective stress present in the specimen after the stress reduction is negative. According to Hausselt and Blum (149), recovery of dislocations can occur even if the effective stress is negative. The dislocation density decreases, increasing the effective stress. When the effective stress is positive, subgrain growth starts to take place. This interpretation is consistent with the observation that at zero reduced stress, the subgrain size does not grow.

#### 6.4 Summary and Conclusions

1. The data presented in this chapter show that a reduction in stress, performed in the steady state region, is always accompanied by transient creep behavior. The transient creep deformation can be separated into two stages: Stage I for strains smaller than  $4 \times 10^{-3}$ , and Stage II for strains greater than  $4 \times 10^{-3}$ . During Stage I, the creep rate decreases as a function of time, and during Stage II, the creep rate accelerates to the steady state value at the reduced stress.
2. The activation energy determined for Stages I and II is  $1.43 \pm 0.05$  eV/at. and is equal to the apparent activation energy for

steady state creep. This suggests that the recovery processes following stress reductions are controlled by self diffusion and have the same character as those responsible for steady state creep.

3. During Stage I, the dislocation density inside the subgrains decreases rapidly. The decrease in dislocation density within subgrains is paralleled by the decrease in creep rate in Stage I. This suggests that Stage I is controlled by recovery of dislocations inside the subgrains. The processes responsible for Stage II seem to be the growth of the subgrain size.

4. The results are analysed in terms of the network theory. Two possible cases for incubation period are discussed. It is shown that the network recovery theories cannot explain the results obtained in this study.

5. The results are analysed in terms of the internal stress theory. Based on the internal stress theory, it is suggested that a critical value of effective stress exists, above which subgrain growth can occur.

## CHAPTER VII

### SUMMARY OF RESULTS AND CONCLUSIONS

During this study, a number of results and conclusions have been drawn concerning the steady state and transient creep behavior of high purity aluminum deformed at temperatures near  $0.5 T_m$ .

The major results and conclusions drawn from the experiments performed include

1. That the apparent activation energy for steady state creep is  $1.43 \pm 0.05$  eV/at. and the coefficient  $n$  describing the stress sensitivity of the steady state creep rate is  $4.6 \pm 0.2$ . These parameters are not strongly sensitive to purity of the sample (Chapter IV).
2. That a correlation between strain rate,  $\dot{\epsilon}$ , subgrain size,  $\lambda$ , diffusion coefficient,  $D$ , and the applied stress,  $\sigma$ , which describes the steady state and transient creep behavior, exists. This correlation is expressed by the equation

$$\dot{\epsilon} = 1.1 \times 10^9 (D/b^2) \cdot (\lambda/b)^2 \cdot (\sigma/E)^{6.8 \pm 0.2}$$

where  $b$  is the Burgers' vector and  $E$  is the elastic modulus (Chapter V).

3. That the transient creep following a stress reduction can be separated into two states: Stage I, in which the creep rate decreases as a function of time, and Stage II, in which the creep rate increases as a function of time (Chapter VI).

4. That Stage I is characterized by a rapid decrease in the dislocation density within subgrains and a nearly constant subgrain size (Chapters V and VI).
5. That Stage II is characterized by the growth of the subgrain size (Chapters V and VI).
6. That a certain creep strain is required for subgrain growth to occur (Chapter V).
7. That the activation energies for the processes responsible for Stages I and II are the same and are equal to the apparent activation energy for steady state creep.



## CHAPTER VIII

### SUGGESTIONS FOR FURTHER WORK

The results obtained during the development of this study have led to some very interesting conclusions. However, as in any scientific study, this research program leaves several unanswered questions. To help in advancing the understanding of the rate controlling creep mechanisms, a number of studies can be suggested, including:

1. A study of the behavior of the subgrain size and dislocation density within subgrains following increases in the applied stress, performed in the steady state region.
2. A study of subgrain boundary structure and of the average subgrain misorientation during transient creep.
3. A study of the kinetics of subgrain growth at temperatures above the test temperature in a zero stress condition.
4. A study of the behavior of the average internal stress during transient creep.
5. A study of the behavior of the subgrain size under cycled stress conditions.

## BIBLIOGRAPHY

1. S.L. Robinson and O.D. Sherby, Acta Metall., 17 (1969) 109.
2. C.M. Young, S.L. Robinson and O.D. Sherby, Acta Metall., 23 (1974) 633.
3. O.D. Sherby, R.H. Klundt and A.K. Miller, Metall. Trans., 8A (1977) 843.
4. M.E. Fine, Rev. Sci. Instrum., 28 (1957) 643.
5. T.S. Lundy and J.F. Murdock, J. Appl. Phys., 33 (1962) 1671.
6. A. Seeger, D. Wolf and H. Mehrer, Phys. Stat. Sol. b, 48 (1971) 481.
7. R.G. Stang, W.D. Nix, C.R. Barrett, Met Trans., 6A (1975) 2065.
8. R.R. Vander Voort, Met. Trans., 1 (1970) 857.
9. A.H. Cottrell and V. Aytakin, J. Inst. Metals, 77 (1950) 389.
10. H. Conrad and W.D. Robertson, Trans. AIME, 212 (1958) 536.
11. P. Haasen, B. Reppich and B. Ilchner, Acta Metall., 12 (1964) 1283.
12. T. Hazegawa, Y. Ikeuchi and S. Karashima, Metal Sci. J., 6 (1972) 78.
13. W.A. Coghlan, R.A. Menezes and W.D. Nix, Phil. Mag., 23 (1971) 1515.
14. T.H. Hazlett and R. Hansen, Trans. ASM, 47 (1954) 508.
15. B. Ancker, T.H. Hazlett and E.R. Parker, Trans. AIME, 27 (1956) 333.
16. B. Ilchner in "Constitutive Equations in Plasticity," ed. A.S. Argon, MIT Press, Cambridge (1975) 467.
17. F. Garofalo, "Fundamentals of Creep and Creep Rupture in Metals," New York, McMillan, 1 (1965).
18. O.D. Sherby and P.M. Burke, Progress in Mat. Scie., 13 (1968) 325.

19. O.D. Sherby, J.L. Robbins and A. Golberg, J. Appl. Phys., 41 (1970) 3961.
20. F.R. Nabarro, report of a Conference of the Strength of Solids, Bristol, England, The Physical Society, 75 (1948).
21. C. Herring, J. Appl. Physics, 21 (1950) 437.
22. J.E. Bird, A.K. Mukherjee and J.E. Dorn in "Quantitative Relations Between Properties and Microstructure," ed. D.G. Brandon and A. Rosen (Israel University Press: Jerusalem, 1969) 255.
23. S.N. Zurkov and T.P. Sanfirova, Zh. Tech. Fiz., 28 (1958) 1719.
24. F. Garofalo, Trans. AIME, 227 (1963) 351.
25. J. Weertman, J. Appl. Phys., 27 (1955) 1213.
26. C.R. Barrett and W.D. Nix, Acta Metall., 13 (1965) 247.
27. O.D. Sherby, Acta Metall., 10 (1962) 135.
28. S. Takeuchi and A.S. Argon, J. Mat. Sci., 11 (1976) 1541.
29. A.K. Mukherjee, "Treatise on Material Sci and Technology," ed. R.J. Arsenault, Academic Press, N.Y., Vol. 6 (1975) 163.
30. C.R. Barrett and O.D. Sherby, Trans. AIME, 230 (1964) 1322.
31. P.W. Davies, G. Nelves, K.R. Williams and B. Wilshire, Metal Sci. J., 7 (1973) 87.
32. J.D. Parker and B. Wilshire, Metal Sci., 9 (1975) 248.
33. G. Nelves and B. Wilshire, Scripta Metall., 10 (1976) 697.
34. B. Burton, Metal Sci., 9 (1975) 297.
35. J.C. Gibeling and W.D. Nix, Metal Sci., 11 (1977) 453.
36. R. Lagneborg, Int. Metall. Reviews, 17 (1972) 130.
37. C.R. Barrett, W.D. Nix and O.D. Sherby, Trans. ASM, 59 (1966) 3.
38. C.H.M. Jenkins and G.A. Mellor, J. Iron Steel Inst., 132 (1935) 693.

39. G.R. Wilms and W.A. Wood, J. Inst. Metals, 76 (1946 - 1950) 237.
40. W.A. Wood, G.R. Wilms and W.A. Rachinger, J. Inst. Metals, 79, (1951) 159.
41. W.A. Wood and W.A. Rachinger, J. Inst. Metals, 76 (1946 - 1950) 237.
42. S. Karashima, H. Oikawa and T. Watanabe, Trans AIME, 242 (1968) 1073.
43. R. Horiuchi and M. Otsuka, Trans Japan Inst. Metals, 13 (1972) 284.
44. J.L. Lytton, C.R. Barrett and O.D. Sherby, Trans AIME, 233, (1965) 116.
45. T. Hasegawa, R. Hasegawa and S. Karashima, Trans Japan Inst. Metals, 11 (1970) 101.
46. A.H. Clauer, R.A. Wilcox and J.P. Hirth, Acta Metall., 18 (1970) 381.
47. M.M. Myshlyaev, Proc. 4th Int. Conf. on Strength of Metals and Alloys, Nancy, 3 (1976) 1037.
48. D. McLena, J. Inst. Metals, 81 (1952 - 1953) 133; 81 (1952 - 1953) 287.
49. F. Garofalo, W.F. Domis and F. von Geminger, Trans AIME, 230, (1964) 1460.
50. W.R. Johnson, PhD Thesis, Stanford University, 1969.
51. R.B. Jones and J.E. Harris, Joint Int. Conf. on Creep, p. iii, Inst. of Mech. Eng., London (1963).
52. D. McLean and M.H. Farmer, J. Inst. Metals, 85 (1956 - 1957) 41.
53. H. Conrad, Mechanical Behavior of Materials at Elevated Temperatures, ed. J.E. Dorn, New York: McGraw Hill (1961) 164.
54. A. Franks and D. McLean, Phil. Mag., 1 (1956) 101.
55. R.C. Gifkins, J. Inst. Metals, 82 (1953 - 1954) 39.
56. H.J. McQueen and J.E. Hockett, Metall. Trans., 1 (1970) 2997.

57. P. Feltham and R.A. Sinclair, J. Inst. Metals, 91 (1962 - 1963) 235.
58. T. Hasegawa, H. Sata and S. Karashima, Metall. Trans., 1 (1970) 231.
59. C.R. Barrett, Acta Metall., 13 (1968) 1088.
60. L.J. Cuddy, Metall. Trans., 1 (1970) 395.
61. D.J. Mitchell, J. Moteff and A.J. Lowel, Acta Metall., 21 (1973) 1269.
62. S. Karashima, T. Iikubo and H. Oikawa, Trans. Japan Inst. Metals, 13 (1972) 176.
63. A. Orlova, Z. Tobolova and J. Cadek, Phil. Mag., 26 (1972) 1263.
64. K. Challenger and J. Moteff, Metall. Trans., 4 (1973) 749.
65. S. Daily and C.N. Ahlquist, Scr. Metall., 6 (1972) 95.
66. A. Thompson, Metall. Trans., 8A (1977).
67. J.J. Jonas, C.M. Sellars and W.J. McG. Tegart, Metall. Rev., 14 (1969) 1.
68. C.M. Young and O.D. Sherby, J. Iron Steel Inst., 211 (1973) 640.
69. V.K. Sikka, H. Hahn and J. Moteff, Mat. Sci. Eng., 20 (1975) 55.
70. H.M. Miekkoja and V.K. Lindroos, in "Constitutive Equations in Plasticity," ed. A.S. Argon, MIT Press, Cambridge, 1975, p. 327.
71. D. McLean, J. Inst. Metals, 80 (1951 - 1952) 507.
72. B. Fazan, O.D. Sherby and J.E. Dorn, Trans. AIME, 200 (1954) 919.
73. H. Brunner and N.J. Grant, J. Inst. Metals, 85 (1956 - 1957) 77.
74. J.G. Harper, L.A. Shepard and J.E. Dorn, Acta Metall., 6 (1958) 509.

75. J.A. Martin, M. Herman and N. Brown, Trans AIME, 209 (1957) 78.
76. R.C. Gifkins, Fracture, New York: John Wiley and Sons, Inc., (1959) 579.
77. R.W. Bailey, J. Inst. Metals, 35 (1926) 27.
78. E. Orowan, J. West Scotland Iron Steel Inst., 54 (1946 - 1947) 45.
79. J. Weertman, J. App. Phys., 28 (1957) 362.
80. J. Weertman, Trans. ASM, 61 (1968) 680.
81. P.M. Hazledine, J. Physica, 27, Supp. C3 (1967) 210; Canad J. Physics, 45 (1967) 765.
82. F.R.N. Nabarro, Phil. Mag., 16 (1967) 231.
83. J.M. Dupoy, Phil. Mag., 22 (1970) 205.
84. L.I. Ivanov and V.A. Yanushkevich, Phys. Metals and Metallography, 17 (1964) 102.
85. W. Blum, Phys. Stat. Sol. (b), 45 (1971) 561.
86. J. Weertman, presented at J.E. Dorn Memorial Symposium, Cleveland, Ohio, Oct. 17, 1972.
87. S.F. Exell and D.H. Warrington, Phil. Mag., 26 (1972) 1121.
88. S.K. Mitra and D. McLean, Proc. R. Soc., London, 295 A (1966) 288.
89. D. McLean, Trans AIME, 242 (1968) 1193.
90. P.W. Davies and B. Wilshire, Scr. Metall., 5 (1971) 475.
91. P. Hirsch and D. Warrington, Phil. Mag., 6 (1961) 735.
92. N.F. Mott, Phil. Mag., 43 (1952) 1151.
93. J.E. Dorn and D.E. Mote in "High Temperature Structure and Materials", eds. A.M. Freudenthal, B.A. Boley, and H. Liebowitz, Pergamon Press, Oxford (1964) 95.
94. V.V. Levitin, Phys. Met. Metalloved, 32 (4) (1971) 190.

95. C.N. Ahlquist, R. Gasca-Neri and W.D. Nix, Acta Metall., 18 (1970) 633.
96. C.N. Ahlquist and W.D. Nix, Scr. Met., 3 (1969) 679.
97. A.A. Solomon, Rev. Scient. Instrum., 40 (1969) 1025.
98. D. McLean, "Creep and Fracture of Metals at High Temperature," HMSD, London, (1956) 73.
99. D. McLean and M.H. Farmer, J. Inst. Metals, 83 (1954 - 1955) 1.
100. D.L. Holt and W.A. Backofen, Trans AIME, 239 (1967) 264.
101. J. Grosskrewitz and P.W. Waldow, Acta Metall., 11 (1963) 1917.
102. A.V. Narlikar and D. Dew Hughes, J. Mat. Sci., 1 (1966) 317.
103. V.M. Azhaska, I.A. Gindin and Ya D. Starodubov, Fiz Met. Metalloved, 15 (1963) 119.
104. V.M. Azhaska, I.A. Gindin and Ya D. Starodubov, Fiz. Met. Metalloved, 15 (1963) 729.
105. T. Hasegawa, S. Karashima and Y. Ireuchi, Acta Metall., 21 (1973) 887.
106. O.D. Sherby, T.A. Trozera and J.E. Dorn, Proc. ASTM, 56 (1956) 784.
107. S.K. Mitra and D. McLean, Metal Sci. J., 1 (1967) 192.
108. V. Pontikis and J. Poirier, Phil. Mag., 32 (1975) 577.
109. J.D. Parker and B. Wilshire, Phil. Mag., 34 (1976) 485.
110. E.N. da C. Andrade and B. Chalmers, Proc. Royal Soc., 138 A (1932) 348.
111. M. Cook and T.L. Richards, J. Inst. Metals, 66 (1940) 1.
112. I.L. Dilamore and W.T. Roberts, Metall. Rev. 10 (1965) 272.
113. G.C. Richardson, C.M. Sellars and W.G. McTeggart, J. Inst. Metals (1966) 138.
114. P. de Lacombe and L. Beaujard, J. Inst. Metals, 74 (1948) 1
115. E.C.W. Perryman, Acta Metall., 2 (1954) 26.

116. R.K. Ham, Phil. Mag., 6 (1961) 1183.
117. P.B. Hirach, A. Howie, R.B. Nicholson, D.W. Pashley and M.J. Whelan, "Electron Microscopy of Thin Crystals," Butterworths (1965), (a) p. 422; (b) p. 417.
118. G. Thomas, "Transmission Electron Microscopy of Metals," ed. by Wiley (1970), p. 423.
119. H. Fumita, Y. Kawasaki, E. Furubaiashi, S. Kajiwara and T. Taoka, Japan J. Appl. Phys., 6 (1967) 214.
120. E. Heyn, "Short Reports from the Metallurgical Laboratory of the Royal Mechanical and Testing Institute of Charlottenburg," Metallographist MTLBB, Vol. 5 (1903) 37.
121. ASTM Designation E 122-74, Annual Book of ASTM Standards, (1974) 207.
122. C.N. Ahlquist and W.D. Nix, Acta Metall., 19 (1971) 373.
123. T.E. Volin, R.W. Baluffi, Phys. Stat. Sol., 25 (1968) 163.
124. S.L. Robinson and O.D. Sherby, Phys. Stat. Sol. Letters, 1 (1970) K119.
125. W. Blum, 2. Metallkde, 63 (1972) 757.
126. W. Blum, Phil. Mag., 28 (1973) 245.
127. W. Blum, J. Hansselt and G. Konig, Acta Metall., 24 (1976) 293.
128. O. Ajaja, Private Communication (1978).
129. J.L. Lytton, L.A. Shepard and J.E. Dorn, Trans. AIME, 212 (1958) 220.
130. E.U. Lee, H.H. Kranlein and E. Underwood, Mat. Sci. Eng., 7 (1971) 348.
131. J. Weertman, J. App. Phys., 27 (1956) 832.
132. Z. Tobolova and J. Cadek, Phil. Mag., 26 (1972) 1419.
133. A.S. Nowick, J. Appl. Phys., 22 (1951) 1182.
134. T. Federighi, Phil. Mag., 4 (1959) 502.



135. F.Y. Fradin and T.J. Rowland, Appl. Phys. Letters, 11 (1967) 207.
136. I.S. Servi, J.T. Norton and N.J. Grant, Trans. Metall. Soc. AIME, 194 (1952) 965.
137. L. Raymond, W.D. Ludemann, N. Jaffe and J.E. Dorn, Trans. ASM, 5 (1961) 111.
138. A.K. Miller, S.L. Robinson and O.D. Sherby, Phil. Mag., 36 (1977) 757.
139. G. Streb, Thesis, University of Erlangen, 1970.
140. W.J. Evans and B. Wilshire, Scripta Metall., 8 (1974) 497.
141. G. Konig and W. Blum, Acta Metall., 25 (1977) 1531.
142. A. Orlova and K. Milicka, Scrip. Metall., 12 (1978) 483.
143. J.E. Dorn, J. Mech. Phys. Solids, 3 (1954) 85.
144. J.P. Hirth and J. Lothe, "Theory of Dislocations," McGraw Hill, New York, 1968.
145. J. Friedel, "Dislocations," Addison-Wesley Pub. Co., Inc. 1967.
146. C.R. Barrett, C.N. Ahlquist and W.D. Nix, Metal Sci. J., 4 (1970) 41.
147. T.V. Nordstrom and C.R. Barrett, J. Mat. Sci., 7 (1972) 1052.
148. W. Blum, Z. Metalkunde, 68 (1977) 484.
149. J. Hausselt and Blum, Acta Metall., 24 (1976) 1027.

**VITA**

**Iris Ferreira**

**Place of Birth:** Pinhal, Estado de Sao Paulo, Brazil

**Date of Birth:** 9/18/1945

**Education:** - Instituto de Educacao Cardeal Leme  
(high school)

- Universidade de Sao Paulo  
Bachelor in Physics (1969)

- Universidade de Sao Paulo  
Master in Physics (1973)